88th annual congress of the Swiss Society of Pathology

November 9–11, 2023

Beaulieu Lausanne

Prof. Dr Laurence de Leval
Congress President, Local organizer

Prof. Dr Viktor Kölzer
Congress Vice-President

A 01
Acetone compression increases lymph node yield and enhances lymphatic metastasis detection in colorectal cancer specimens

Dr. Christina Schnoz*, Ms. Katrin Schmid, Dr. Guacimara Ortega Sanchez, Dr. Sabina, Schacher-Kaufmann, Dr. Georgios Peros, Prof. Michel Adamina, Dr. Dieter Erdin, Dr. Peter Bode

Kantonsspital Winterthur, Winterthur, Switzerland

Lymph node status is one of the most important prognostic factors in colorectal cancer, and accurate pathological nodal staging and detection of lymph node metastases is crucial for determination of postoperative management. Current guidelines, including the TNM staging system and European Society for Medical Oncology (ESMO) guidelines, recommend examination of at least 12 lymph nodes. However, identification of an adequate number of lymph nodes can be challenging, especially in the setting of neoadjuvant treatment, which may reduce nodal size.

Acetone compression is a method that involves elution with acetone and subsequent mechanical compression of adipose tissue, allowing for complete embedding of fat tissue and identification of small lymph nodes.

In this study, we retrospectively investigated 384 colorectal cancer resections that were processed at our department of pathology between January 2012 and December 2022, in which the number of detected lymph nodes was less than 12 subsequent to conventional preparation of mesocolic fat tissue. By means of acetone compression, lymph node harvest increased significantly, and the intended number of ≥12 lymph nodes was achieved in 98% of resection specimens. The number of nodal positive cases increased significantly from $n = 95$ (24.7%) before versus $n = 131$ (34.1%) after acetone compression due to additionally identified lymph node metastases. In 36 patients (9.4%) initially considered as nodal negative, acetone compression led to an up-staging to a nodal positive category and thereby drove a recommendation to offer adjuvant therapy.

In conclusion, acetone compression is a reliable and useful method implementable in routine surgical pathology for the retrieval of lymph nodes in colorectal cancer specimen, allowing for an adequate lymph node sampling and an increase in nodal staging reliability, especially after neoadjuvant radio-chemotherapy.
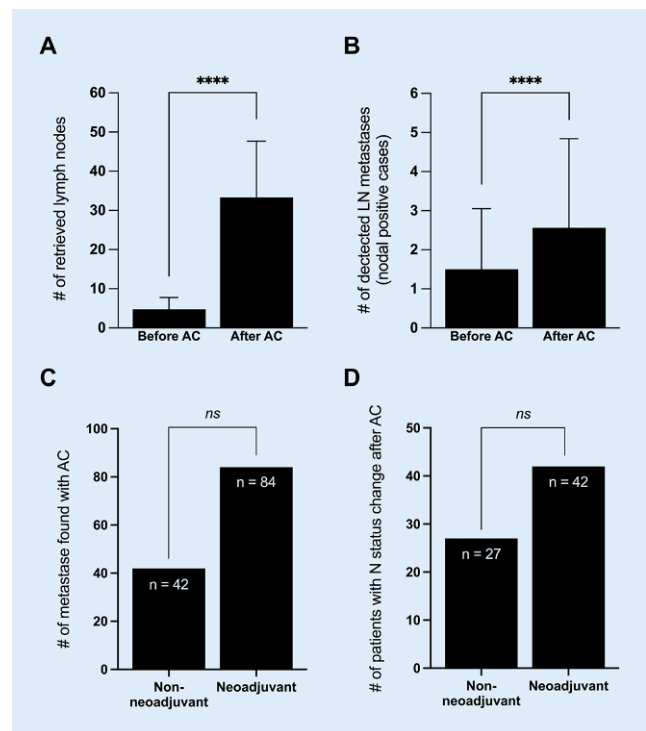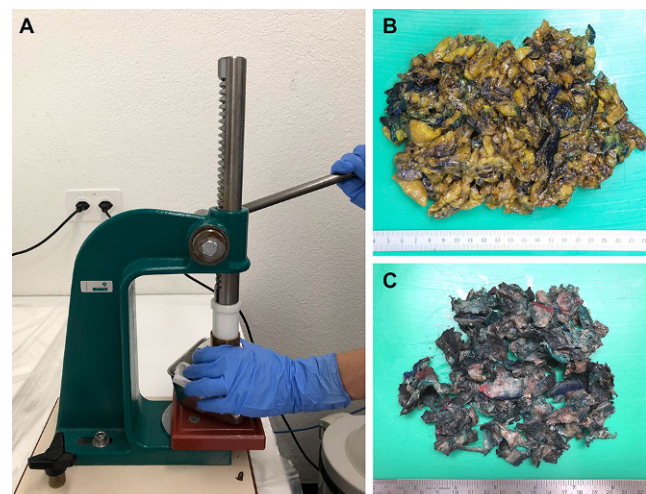
All authors marked with * are the presenting first authors.
All authors marked with ** are the presenting last authors.

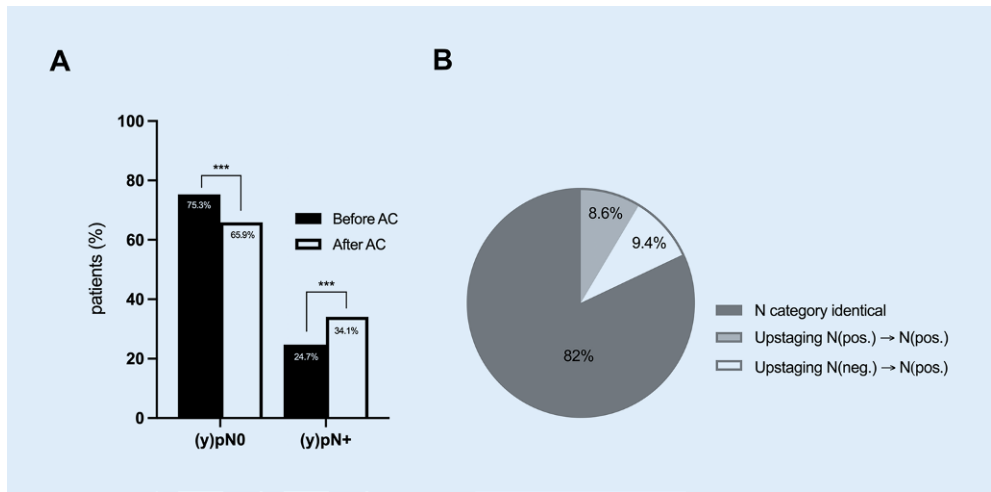**Fig. 1 | A 01 ▲**

Fig. 2 | A 01 ▲

Fig. 3 | A 01 ◄

A 02
A novel qPCR technology for direct quantification of methylation in untreated DNA from gliomas samples

Dr. Samantha Epistolio[1]*, Dr. Kamilla Adelgod Bendixen[2],
Dr. Maria Mindegaard[2], Dr. Giulia Dazio[3], Dr. Francesco Marchi[4],
Dr. Paolo Spina[5], Dr. Eva Arnspang[6], Dr. Mette Soerensen[7],
Dr. Ulf Bech Christensen[8], Dr. Milo Frattini[1], Dr. Rasmus Koefoed Petersen[8]

[1]Laboratory of Genetics and Molecular Pathology, Institute of Pathology, Ente Ospedaliero Cantonale (EOC), Locarno, Switzerland; [2]PentaBase A/S, Odense, Denmark; [3]Laboratory of Genetics and Molecular Pathology, Institute of Pathology, Ente Ospedaliero Cantonale (EOC), Locarno, Switzerland; [4]Service of Neurosurgery, Neurocenter of the Southern Switzerland, EOC, Regional Hospital of Lugano, Lugano, Switzerland; [5]Institute of Pathology, Ente Ospedaliero Cantonale (EOC), Locarno; [6]Department of Green Technology, University of Southern Denmark, Odense, Denmark; [7]Epidemiology, Biostatistics and Biodemography, Department of Public Health, University of Southern Denmark, Odense; [8]PentaBase A/S, Odense, Denmark

Background: In glioblastoma (GBM), the O^6-methylguanine-DNA methyltransferase gene (MGMT) methylation patterns have been associated with the response to temozolomide and with better survival. Until now, methylation analyses have been dependent on time consuming procedures based on pre-treatment of DNA with sodium-bisulfite. The aim of our project is to set-up and validate a new technique for assessing MGMT promoter methylation starting from untreated DNA.
Methods: We compared the methylation results obtained by two methods in 42 GBM samples: a methyl-specific PCR assay (comparator method 1) and quantitative real-time MSP Assay (comparator method 2) with a novel technology: EpiDirect® MGMT Methylation qPCR Assay (Pentabase

ApS). EpiDirect® has been designed in order to allow direct quantification of DNA methylation without any DNA pre-treatment.
Results: The sensitivity of EpiDirect®, setting the first method and the second method as a reference for comparison, was 0.82 (CI 95% [0.52; 0.95]) and 0.75 (CI 95% [0.36; 0.96]) respectively, whereas the specificity was 0.84 (CI 95% [0.41; 0.93]) and 0.76 (CI 95% [0.60; 0.88]) respectively. EpiDirect® found five additional methylated samples. With this new methodology a final result can be obtained in less than 2 h.
Conclusions: In diagnostic routine, EpiDirect® platform could be relevant in terms of time saving. In addition, it overcomes the risk of incomplete or over-conversion of the DNA during the bisulfite treatment, thus preventing false positive results. The novel platform will be tested in other assays (i. e.: MLH1 promoter).

A 03
Diagnostic whole genome sequencing: hydra of hopes and hurdles

Ms. Cassandra Litchfield[1], Dr. Ronny Nienhold[1]*, Dr. Magdalene Adamczyk[1],
Dr. Ulrich Wagner[1], Dr. Michael Schmid[1], Ms. Dagmar Seidl[1],
Dr. Domingo Aguilera[2], Prof. Viktor H. Kölzer[2], Mx. Tumor Profiler Consortium[3],
Dr. Martin Zoche[1], Dr. Jan Hendrik Rüschoff[1], Prof. Holger Moch[4],
Dr. Bettina Sobottka[2]

[1]University Hospital Zurich, Department of Pathology and Molecular Pathology, Zurich, Switzerland; [2]Department of Pathology and Molecular Pathology, University Hospital of Zurich, Zurich, Switzerland; [3]Mx. Tumor Profiler Consortium, Zurich, Switzerland; [4]Department of Pathology and Molecular Pathology, University Hospital Zurich, University of Zurich, Zurich, Switzerland
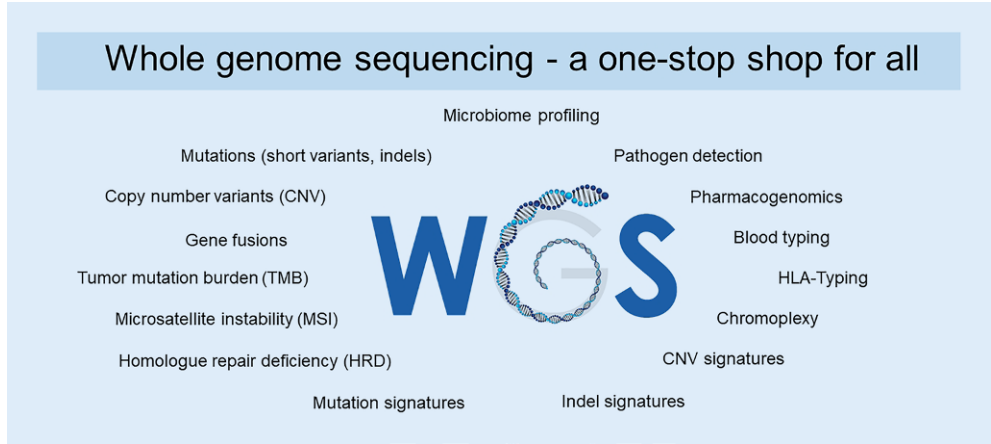

Fig. 1 | A 03 ◄

Background: The continuous advancement of next generation sequencing (NGS) has made whole genome sequencing (WGS) cost-effective and practical for clinical diagnostics. Although classical targeted NGS panels cover key markers of the most prevalent tumors, studies evaluating WGS in a clinical setting suggest improved off-label treatment options for patients with rare cancers or end-stage diseases. Therefore, the Department of Pathology and Molecular Pathology at the University Hospital Zürich aims to establish WGS for diagnostic purposes.

Methods: Total nucleic acids were extracted from the tumor and matched-control tissue. Next-generation sequencing was performed with an average coverage of 60x for tumor and 30x for normal. In-house bioinformatics pipelines have been established to analyze raw data and identified established and emerging biomarkers.

Results: Our primary objective was to compare the outcomes of WGS against a well-established gold standard of targeted NGS panel in the metastatic melanoma Tumor Profiler cohort.

The majority of SNVs reported by FoundationOne CDx were detected by WGS, and we observed a strong correlation of the variant allele fraction. Our results also showed a strong correlation for TMB and absolute CNVs. The validation of MSI, HRD and structural variants are planned following the sequencing of additional cancer entities, where these biomarkers are well represented. Furthermore, WGS enables detecting emerging biomarkers, which currently cannot be validated due to a lack of standards.

We also propose possible solutions concerning regulations for germline testing, automated variant annotation and reimbursement by health insurance companies. Lastly, we created an automated reporting engine that condenses the obtained information to the level of a conventional NGS report.

Conclusion: Based on this experience, we are planning a study employing WGS for cancer patients who have completed therapy. Here, we aim on (1) validating the clinical utility of WGS and (2) gaining additional knowledge with WGS in diagnostic routine.

A 04
## A comparison of Ki67 and gene panel testing for early breast cancer subtyping

Dr. Catherine Connolly, Dr. Barbara Padberg Sgier, Dr. Regina Masser, Dr. Juliane Friemel, Dr. Eva Karamitopoulou, Prof. Beata Bode, Prof. Marianne Tinguely

Pathologie Institut Enge, Enge, Switzerland

Background: Ki67 is a frequently used surrogate marker for gene expression tests, alongside ER, PR and HER2, for determining luminal-like subtypes as an indicator for chemotherapy in early breast cancer. This is despite ongoing controversy over the Ki67 cut-off value. The purpose of this study was to compare IHC-based subtyping against Oncotype DX® gene expression panel results, and to investigate a CE-certified artificial intelligence (AI) Ki67 image analysis system for improving subtyping accuracy.
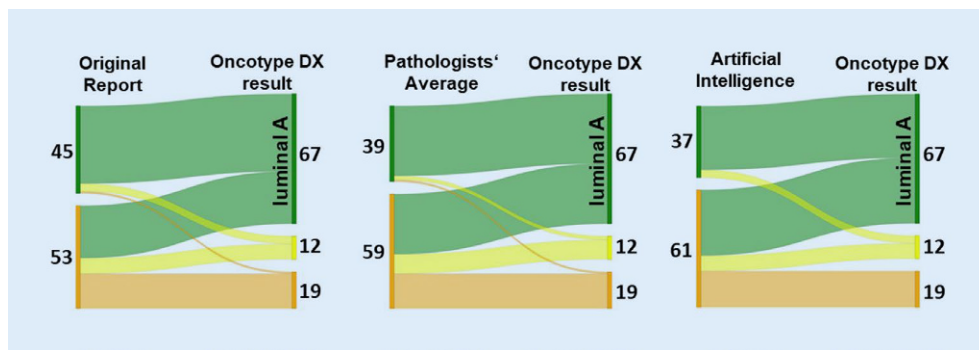
Fig. 1 | A 04 ◄ Sankey diagrams showing IHC-based surrogate luminal subtyping results using either the original report, pathologists' average or artificial intelligence, in comparison to Oncotype DX® results (luminal A = green, luminal B = orange, uncertain = yellow)
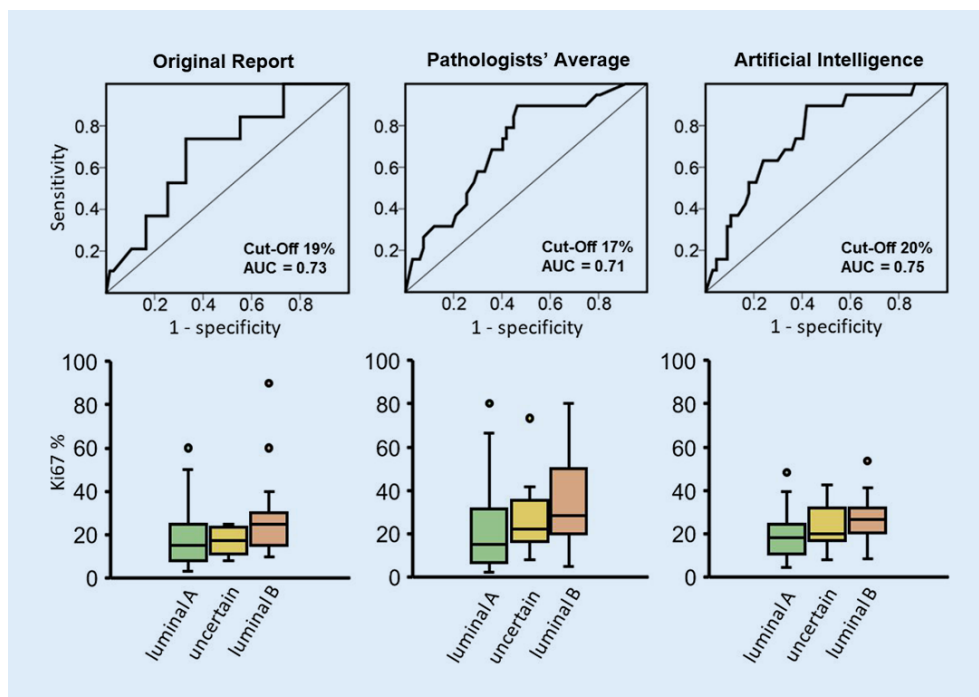
Fig. 2 | A04 ◄ ROC curves showing the performance of IHC-based surrogate luminal subtyping against results of Oncotype DX®; and corresponding distribution plots of Ki67 values for luminal A and B tumours. The maximal AUC and optimal Ki67 cut-off are shown for each method

Methods: All breast biopsies with B5b-diagnoses at our institute from 2019–2022 ($n=1736$) were evaluated, and we identified $n=104$ cases which underwent Oncotype DX® testing as per clinician requests. We performed a retrospective cohort analysis comparing the accuracy of IHC-based luminal subtyping against Oncotype DX® results, and investigated VMScope's Ki67 Quantifier (Berlin, Germany).

Results: Our Oncotype DX® cohort had an average patient age of 58 years (range 28–76) and mean tumour size of 23 mm (range 8–85 mm). We observed 100% agreement in ER status and 94.9% agreement in HER2 status with Oncotype DX® results. The distribution of cases according to Oncotype DX® results included 67 luminal A (68.4%), 12 'uncertain' (12.2%) and 19 luminal B (19.4%) tumours. The mean Ki67 for the luminal B cohort was 10.3% higher than the luminal A cohort and we detected a *moderate correlation* between Ki67 and Oncotype DX® recurrence score (RS) ($r=0.31$–0.38). Retrospective IHC-based subtyping enabled the correct classification of 43/67 (64.25) luminal A, and 16/19 (84.2%) luminal B tumours. ROC curve analyses demonstrated maximal AUC when using AI-based Ki67 scoring as compared to the original report or consensus pathologist assessments, and the optimal Ki67 cut-off was 20%.

Conclusion: Our data provides a snapshot of the real-world allocation of Oncotype DX® testing in early breast cancer in Switzerland, and demonstrates the feasibility of incorporating AI-assessment of Ki67 for maximising surrogate luminal subtyping accuracy.

A 05

Methylation-based characterization of a novel IDH2 mutation (arg172Ala) in sinonasal undifferentiated carcinoma, a case report

Dr. Simon Burgermeister[1]*, Dr. Simona Stoykova[1], Dr. Kristof Egervari[2], Prof. Ekkehard Hewer[1]

[1]Department of Laboratory Medicine and Pathology, Institute of Pathology, Lausanne University Hospital, University of Lausanne, Rue du Bugnon 25, 1011 Lausanne, Switzerland; [2]Service of Clinical Pathology, Department of Diagnostics, Geneva University Hospital, Geneva, Switzerland

Background: Mutations affecting the codon 172 of the isocitrate dehydrogenase 2 (*IDH2*) gene define a subgroup of sinonasal undifferentiated carcinoma (SNUC) with a relatively favorable prognosis. They are also recurrent (along with *IDH1* mutations) in gliomas, acute myeloid leukemia and intrahepatic cholangiocarcinoma. Common reported mutations, include Arg172Ser, Arg172Thr, Arg172Gly, or Arg172Met, all associated with aberrant *IDH2* enzymatic activity, which in turn impacts DNA methylation. We present a case of SNUC with a not previously reported *IDH2* mutation, Arg172Ala. Our report compares the methylation pattern of our sample with other cases from the GEO (Gene expression omnibus) database.

Methods: We analyzed over 850k methylation sites using Infinium MethylationEPIC BeadChip array. The profile was compared to other *IDH* mutant tumors (including SNUC) and non *IDH* mutant tumors of the sinonasal epithelium accessed from NCBI GEO. Preprocessing of methylation data was performed using R with the minfi and missMethyl packages. Clustering analysis and site identification were performed in python using Scikit-Learn.

Results: Hierarchical clustering suggests a strong association between our sample and other *IDH* mutant SNUC and a clear distinction from sino-nasal normal tissues and tumors. PCA, using 40 principal components explaining 80% of the variance, shows the position of our sample within one standard deviation (SD) of the other *IDH* mutant SNUC. Exploration of pro-
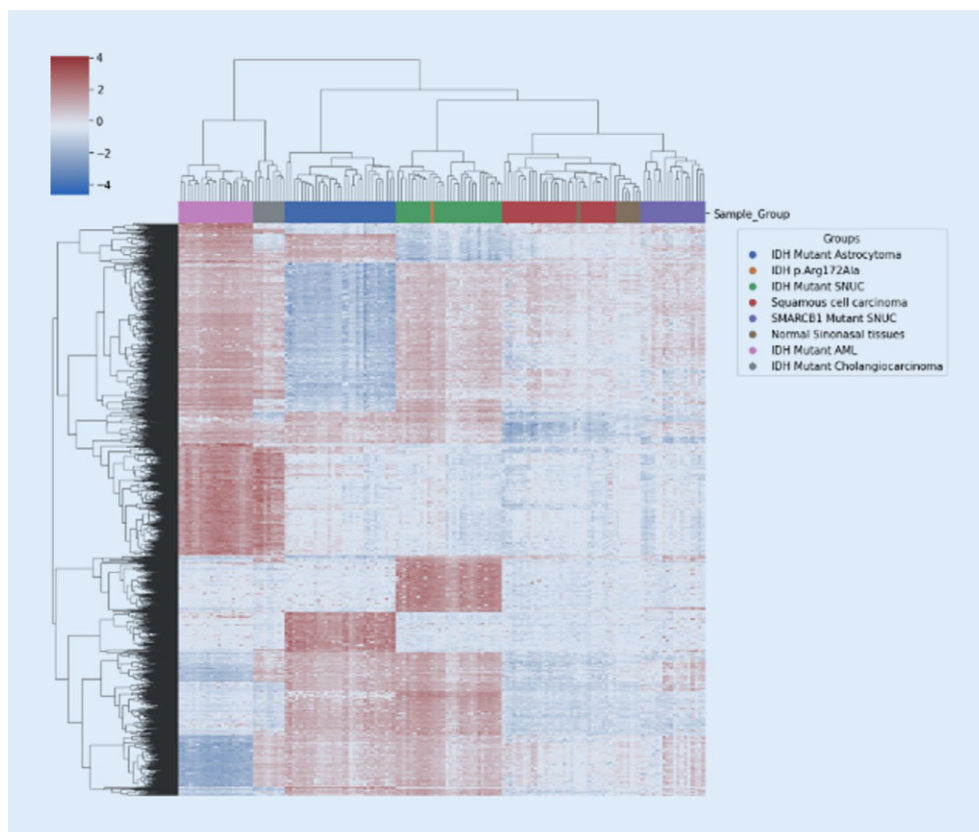
Fig. 1 | A 05 ◄ Hierarchical clustering with heatmap from the 5000 most differentially expressed probes showing clustering of our sample (orange) with other IDH mutant SNUC (green). Other sino-nasal samples (red, brown and purple) form a distinct cluster from those 1DH mutant samples
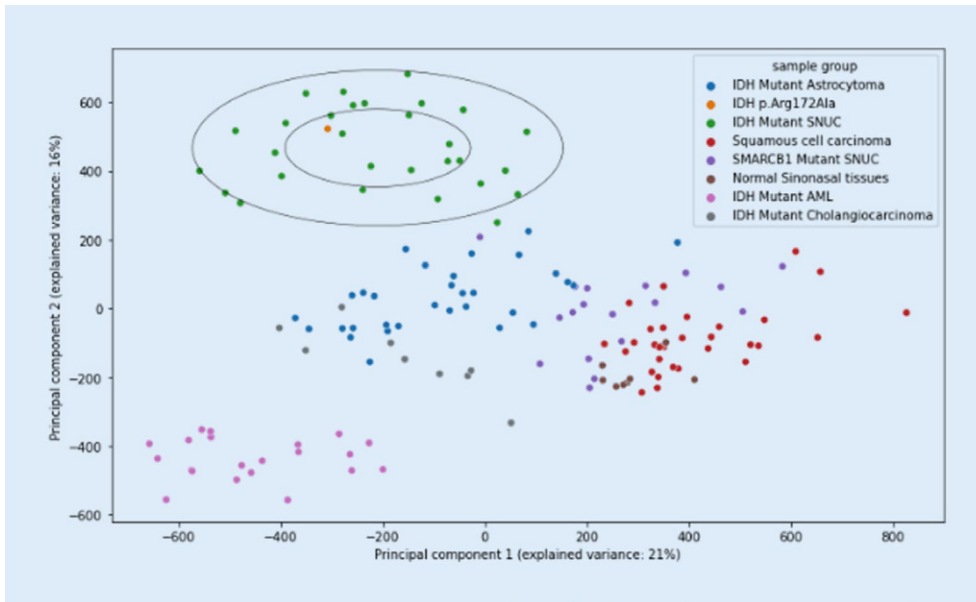
Fig. 2 | A 05 ◄ PCA representation of our data with two principal components. The black ellipsoids represent the 1st and 2nd standard deviation (SD) respectively of the IDH mutant SNUC (green dots) with our sample (orange dot) falling well under their ranges

moter regions with differential methylation status between *IDH* mutant SNUC and other sinonasal tissues shows, among others, a recurrent *CFLAR* promoter hypermethylation, also identified in our sample. Among the 10 most differentially methylated promoter associated probes between *IDH* mutant SNUC and other sino-nasal tissues, our sample shares a similar hypermethylated profile to *IDH* mutant SNUC in all of them.

Conclusion: Our preliminary findings suggest that the DNA methylation pattern associated with the mutation Arg172Ala is consistent with the already described *IDH* mutant SNUCs, forming a distinct methylation cluster.

Sample Group	Number of cases
IDH Mutant AML	21
IDH Mutant Astrocytoma	31
IDH Mutant Cholangiocarcinoma	9
IDH Mutant SNUC	29
IDH Arg172Ala SNUC	**1**
Normal Sinonasal tissues	8
SMARCB1 Mutant SNUC	18
Squamous cell carcinoma	31

Fig. 3 | A 05 ▲ Data used for s study, Our sample is in bold. The others were extracted from the Gene expressession omnibus database (GEO).

A 06*
Role of microsatellite instability in the oncogenesis of primary intestinal T-cell lymphomas

Dr. Luis Veloza[1]*, Dr. Anja Fischer[2], Dr. David Vallois[1], Mr. Vimel Rattina[1], Dr. Karine Lefort[1], Dr. Bettina Bisig[1], Prof. Philippe Gaulard[3], Dr. Reiner Siebert[2], Prof. Laurence de Leval[1], Dr. Edoardo Missiaglia[1]

[1]Institute of Pathology, Lausanne University Hospital, Lausanne University, Lausanne, Switzerland; [2]Institute of Human Genetics, Ulm University and Ulm University Medical Center, Ulm, Germany; [3]Faculty of Medicine and Health, Campus Henri Mondor, Paris-Est Créteil University, 94000 Créteil, France; Department of Pathology, Henri Mondor University Hospital, Créteil, France

Background: Primary intestinal T-cell lymphomas (ITCLs) comprising Enteropathy-associated T-cell lymphoma (EATLs) and Monomorphic epitheliotropic intestinal T-cell lymphoma (MEITL) are a group of rare and aggressive extranodal lymphomas. The clinical significance of microsatellite instability (MSI) and deficient mismatch repair (dMMR) in ITCLs is unknown to date. The objective of this study was to assess the frequency of MSI in ITCLs and possible underlying molecular mechanisms.

Methods: 63 ITCLs (37 MEITLs, 26 EATLs) were analysed by Whole Exome Sequencing (WES). MMRd/MSI status was assessed by immunohistochemistry (IHC) for MLH1, MSH2, MSH6 and PMS2 proteins in 58 tumours (42 MEITLs, 16 EATLs). PCR and fragment analysis was performed on 43 cases (28 MEITLs, 15 EATLs) using 5 well-established mononucleotide repeat markers.

Results: Of note, 3/37 MEITLs (8%) (cases 01, 30 and 54) showed MSI-associated signatures and the highest tumor mutational burden (TMB) (highest TMB: 15 mutations/Mb) based on mutational profile. Their MSI-high status was confirmed by PCR analyses in this 3 cases, while the other 40/43 MEITLs and all EATLs were microsatellite stable. Moreover, MSI cases showed complete loss of PMS2 (1/3) or MLH1&PMS2 (2/3) IHC expression. Interestingly, these cases showed either biallelic deletion of the *MLH1* locus (patients with double MLH1 and PMS2 IHC expression loss) or *PMS2* locus (patient with PMS2 expression loss). In addition, 2/42 MEITLs (5%) showed heterogeneous (partial loss or diminished intensity) expression of MLH1 or MLH1&PMS2, associated with the loss of one copy of the *MLH1* locus, not related to a MSI phenotype. At last, no case (0/63 WES) harbored *MLH1, PMS2, MSH2* or *MSH6* germline or somatic mutations.

Conclusions: MSI/dMMR plays a role in the oncogenesis of a subgroup of ITCLs, particularly MEITLs, with potential clinical implications. In our series of ITCLs, MSI/MMRd were related to *MLH1* or *PMS2* locus deletions.
*Student submission

A 07
Deep-learning enabled single-cell phenomics in application to high-throughput drug screening

Dr. Jiqing Wu[1]*, Prof. Viktor H. Kölzer[2]

[1]Department of Pathology and Molecular Pathology, University Hospital, University of Zurich, Zurich, Switzerland; [2]Department of Pathology and Molecular Pathology, University Hospital of Zurich, Zurich, Switzerland

Background: Understanding the pathological characteristics of cells in culture and identifying the efficacy of existing drugs for challenging diseases is important for medical research. High-throughput drug screening requires an in-depth analysis of phenotypic heterogeneity and dynamic transitions between physiological and pathological states. Current approaches are constrained by static-imaging-based models and consequently fail to explore the dynamic and complex changes that underlie drug-induced phenotype heterogeneity. Here, we propose to determine treatment effects by analysis of high-dimensional cellular imaging data: By measuring the eigenvalue difference between paired principal components of two collections of single-cell images, we propose a novel Generative Adversarial Nets Inversion-enabled Latent Eigenvalue Analysis (GILEA) for high-throughput cell-based drug screening.

Methods: We use cutting-edge SARS-CoV-2 drug testing datasets (RxRx19) to benchmark GILEA, where relevant cellular components and organelles including Nucleus, Endoplasmic reticulum, Actin, Nucleolus and cytoplasmic RNA, Golgi and plasma membrane are profiled with the multiplexed fluorescent cell-painting protocol. We run GILEA with ~23 million single-cell images for > 1800 drugs on SARS-CoV-2 infected VERO and HRCE cell-lines. Given four cell conditions: Infected with and without drug treatment, mock control, and irradiated control, we determine whether each drug is efficacious if it reverses the pathological state of infected cells back to the control (d_LEA).

Results: GILEA achieved a robust quantification of phenotypic changes and morphological drug effects on both cell-lines as confirmed by its positive correlation with established benchmarks (▣ **Fig. 1**). Based on deep-learning enabled phenotyping, GILEA identified Remdesivir (and the prodrug GS441524) as strongly efficacious, which was approved by FDA for the treatment of COVID-19. GILEA measurements remain consistent for all 5 cellular components and organelles (Figs. 2 and 3) and can be biologically supported by simulating dynamic phenotype transitions between physiological and pathological states in realistic video synthesis.
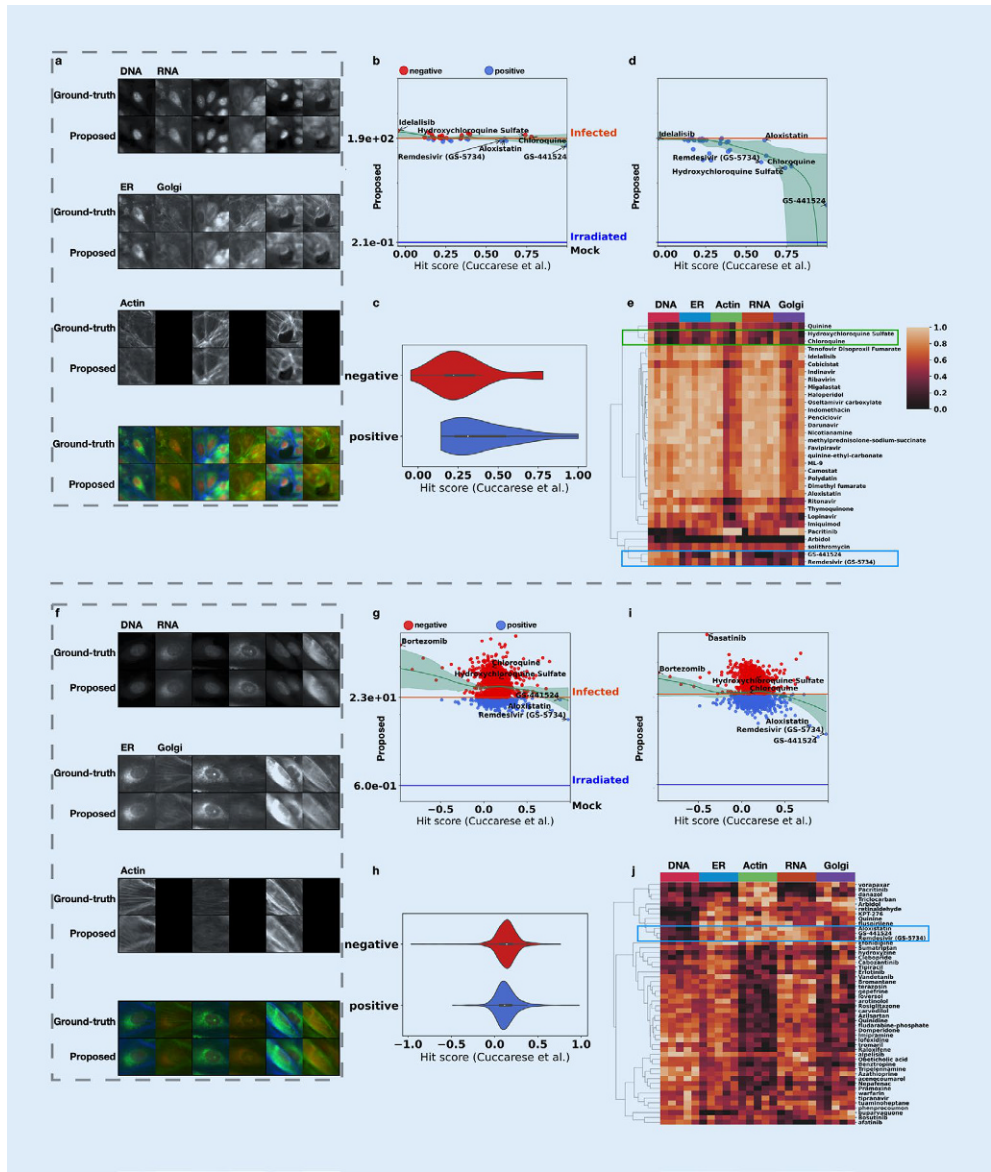

Fig. 1 | A 07 ◀ Reconstruction visualization of GILEA and quantitative comparison of drug responses between the baseline (Cuccarese et al. 5) and dLEA (Proposed). **a** (VERO) and **f** (HRCE): The reconstructed samples obtained by GILEA. **b** (VERO) and **g** (HRCE): The quantitative comparison between the hit score 5 and dLEA with the latent representations of all concentrations. **c** (VERO) and **h** (HRCE): The violin plot of overall comparison between the hit score 5 and dLEA. **d** (VERO) and **i** (HRCE): The quantitative comparison between the hit score 5 and dLEA with the latent representations of optimal drug concentration. **e** (VERO) and **j** (HRCE): The hierarchical clustering of top 50 drug compounds (if exist) w. r. t. the 5 largest eigenvalues of the latent representations of optimal drug concentration [1] (published under CC BY 4.0 international license https://creativecommons.org/licenses/by/4.0)

Conclusions: GILEA represents a broadly applicable approach for high-throughput drug screening in cell culture systems.

References

1. Jiqing Wu, Koelzer VH (2023) GILEA: -GAN Inversion-enabled latent eigenvalue analysis for phenome profiling and editing. bioRxiv. https://doi.org/10.1101/2023.02.10.528026
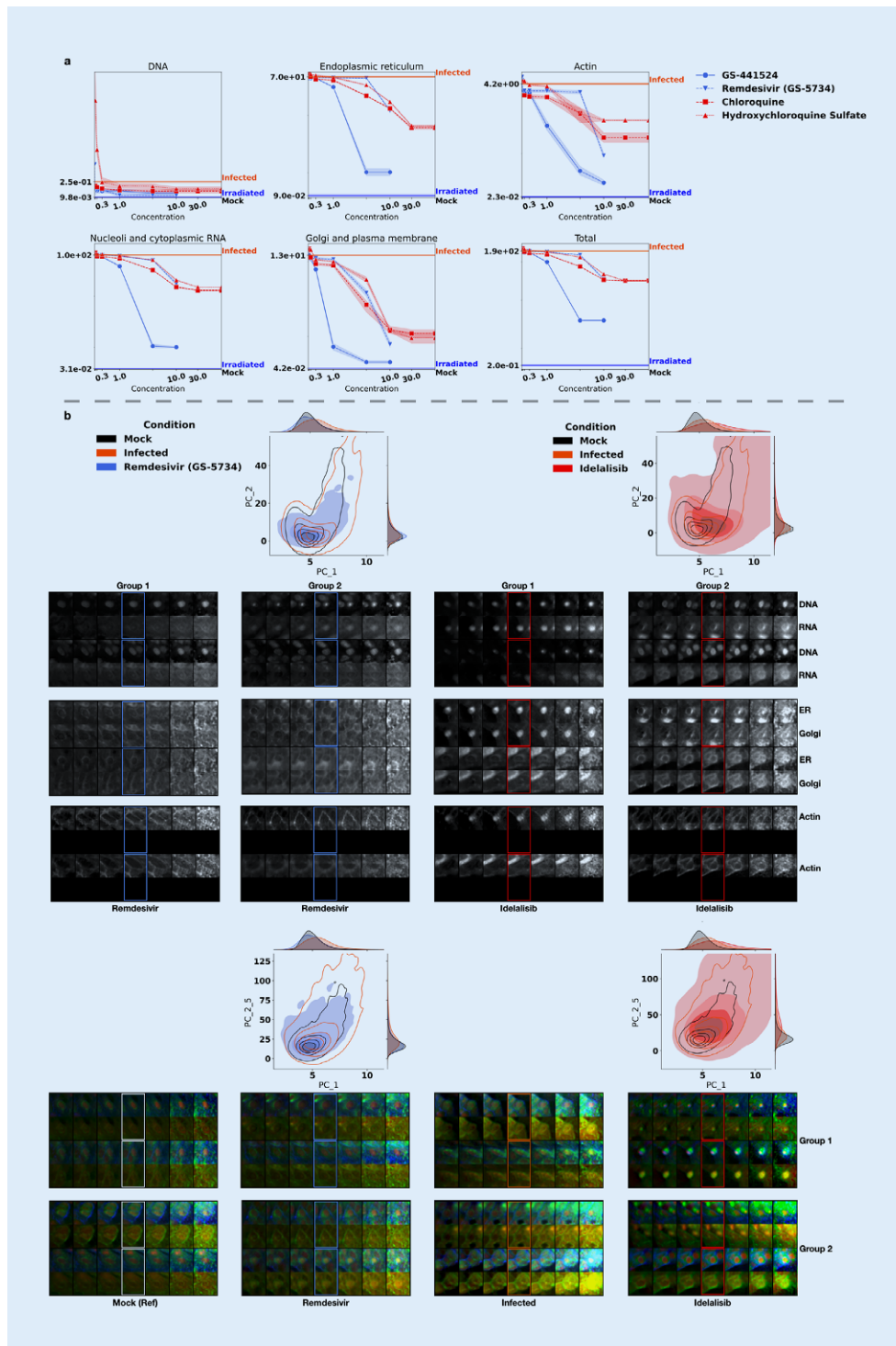
Fig. 2 | A 07 ◄ Identification of drug-concentration dependent effects and visual interpretation for key drugs of interest in the VERO cell-line. **a** The proposed dLEA of different drug concentrations for individual and all fluorescent channels. Here, we report the mean dLEA (with standard deviation) averaged on 4 randomly sampled cell collections. **b** The PCA plots and phenotypic transitions driven by manipulating the largest (top) and 5 largest (bottom) principal component(s). The bounding box indicates the reconstructed image [1]. (published under CC BY 4.0 international license https://creativecommons.org/licenses/by/4.0)
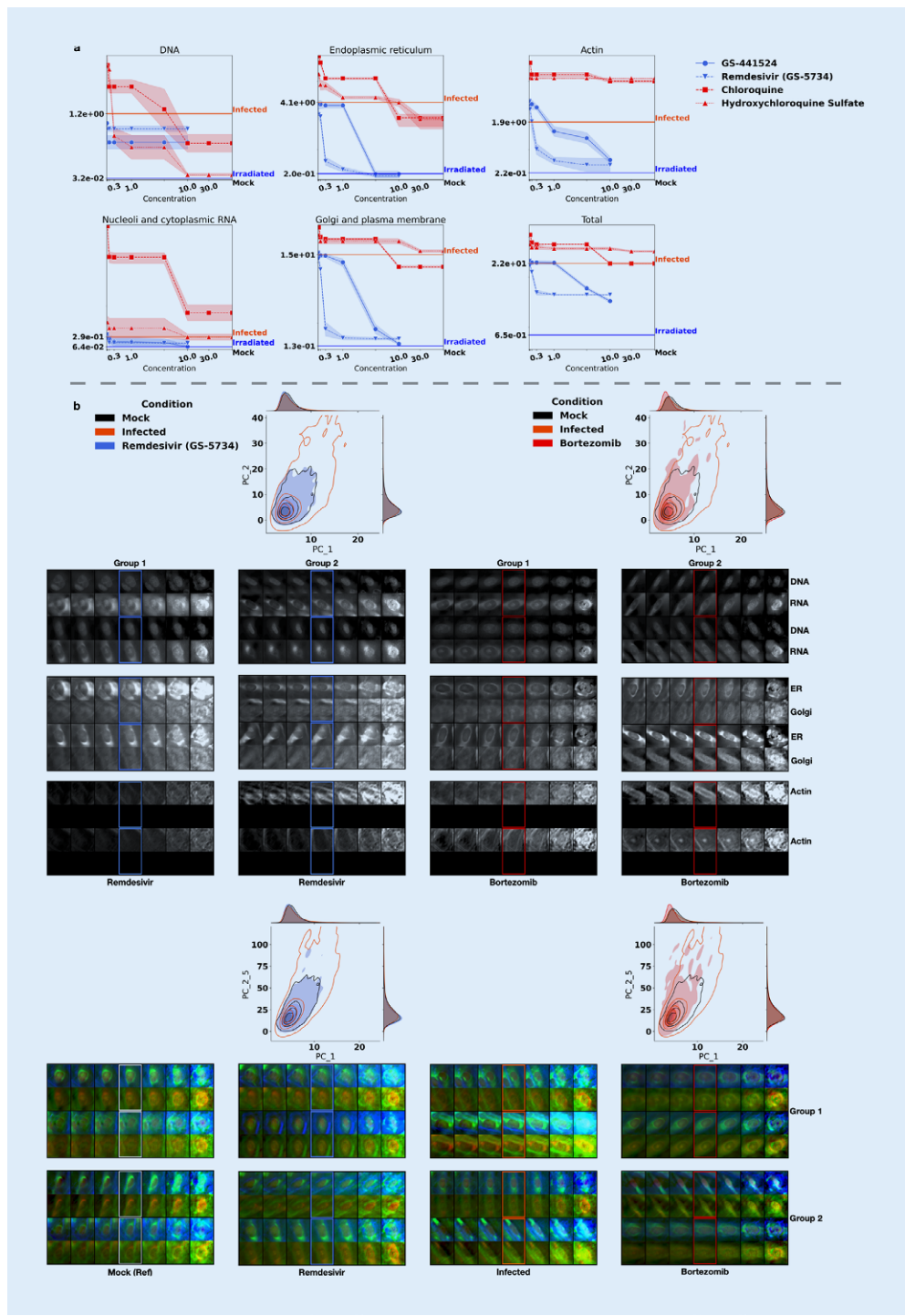
Fig. 3 | A 07 ◄ Identification of drug-concentration dependent effects and visual interpretation for key drugs of interest in the HRCE cell-line. **a** The proposed dLEA of different drug concentrations for individual and all fluorescent channels. Here, we report the mean dLEA (with standard deviation) averaged on 4 randomly sampled cell collections. **b** The PCA plots and phenotypic transitions driven by manipulating the largest (top) and 5 largest (bottom) principal component(s). The bounding box indicates the reconstructed image. [1] (published under CC BY 4.0 international license https://creativecommons.org/licenses/by/4.0)

A 08
Bone marrow hematopoiesis in patients with COVID-19

Dr. Umberto Maccio'[1]*, Dr. Ewerton Marques-Maggio[2], Dr. Alexandra Marx[3], Dr. Serena Galli[4], Dr. Nathalie Schwab[5], Dr. Angela Frank[5], Dr. Baptiste Hamelin[5], Prof. Zsuzsanna Varga[1], Prof. Cesar Nombela Arrieta[4], Prof. Kirsten Mertz[5], Dr. Alexandre Theocharides[4], Prof. Viktor H. Kölzer[1]

[1]Department of Pathology and Molecular Pathology, University Hospital of Zurich, Zurich, Switzerland; [2]Medica Pathologie Zentrum, Zurich, Switzerland; [3]Stadtspital Zurich Waid, Klinik für Innere Medizin, Zurich, Switzerland; [4]Department of Medical Oncology and Hematology, University, Hospital of Zurich, Zurich, Switzerland; [5]Institute of Pathologie, Cantonal Hospital Baselland, Liestal, Switzerland

Background: Severe acute respiratory syndrome coronavirus type 2 (SARS-CoV-2) infection broadly affects organ homeostasis, including the hematopoietic system. Autopsy studies are a crucial tool for investigation of organ-specific pathologies. Here we perform an in-depth analysis of the impact of severe coronavirus disease2019 (COVID-19) on bone marrow hematopoiesis in correlation with clinical and laboratory parameters. **Methods:** Twenty-eight autopsy cases and five control cases were included in the study. We performed a comprehensive analysis of bone marrow pathology and microenvironment features with clinical and laboratory parameters and assessed SARS-CoV-2 infection of the bone marrow by quantitative polymerase chain reaction (qPCR) analysis.

Results: In COVID-19 patients, bone marrow specimens showed a left-shifted myelopoiesis (19/28, 64%), increased myeloid-erythroid ratio (8/28, 28%), increased megakaryopoiesis (6/28, 21%) and lymphocytosis (4/28, 14%). A high proportion of COVID-19 specimens showed erythrophagocytosis (15/28, 54%) and the presence of siderophages (11/15, 73%) compared to control cases (0/5, 0%). Clinically, erythrophagocytosis correlated with lower hemoglobin levels and was more frequently observed in patients from the second wave. The stromal microenvironment showed edema (two of 28, 7%) and severe capillary congestion (one of 28, 4%) in isolated cases. No stromal fibrosis or microvascular thrombosis was found. While all cases had confirmed positive testing of SARS-CoV-2 in the respiratory system, SARS-CoV-2 was not detected in the bone marrow by high-sensitivity PCR.

Conclusions: SARS-CoV-2 infection indirectly affects the hematological compartment and the bone marrow immune environment. Erythrophagocytosis is frequent and associated with lower hemoglobin levels in patients with severe COVID-19.

A 09

Progression of pancreatic neuroendocrine tumours (PanNETs) to metastatic disease is associated with MCT4 expression and metabolic heterogeneity

Dr. Konstantin Bräutigam[1]*, Ms. Janine Straub[1], Mr. Abdulloh Kafa Bihi[1], Dr. Valentina Andreasi[2], Dr. Philipp Kirchner[1], Mr. Renaud Maire[1], Ms. Tsilla Sunier[1], Mr. Charalampos Saganas[1], Dr. Jörg Schrader[3], Prof. Stefano Partelli[2], Prof. Massimo Falconi[2], Dr. Ilaria Marinoni[1], Dr. Martin Sadowski[1], Prof. Aurel Perren[1]

[1]Institute of Tissue Medicine and Pathology, University of Bern, Bern, Switzerland; [2]Vita-Salute San Raffaele University, Milan, Italy; [3]University Medical Center Hamburg-Eppendorf, Hamburg, Germany

Background: Up to 50% of patients with PanNETs present with metastasis at time of diagnosis or relapse after surgery, with highly variable dynamics. The mechanisms driving progression from indolent disease to metastatic PanNET are largely unknown. Although having great potential for providing novel therapeutic targets, the metabolic landscape at different tumor stages is only poorly understood. Transcriptome and epigenome analyses of PanNET indicate a potential stepwise progression, which is associated with enhanced proliferation, dedifferentiation and hallmarks of hypoxia.

Methods: The aim of this study is to classify different metabolic subtypes of PanNET and investigate metabolic targets and their therapeutic potential.

Results: Immunohistochemical analysis of metabolic enzymes and assessment of microvessel density as correlate for hypoxia in two independent PanNET cohorts revealed multiple metabolic subtypes that often showed intra-tumoural heterogeneity. Based on the significant co-expression of MCT4 and CA9 which function in metabolite transport and pH homeostasis, we here report on three metabolic PanNET subtypes, MCT4neg, MCT4hom+ and MCT4het+, which showed negative, homogeneous- or heterogeneous-positive expression of one or both hypoxia markers. Low microvessel densitiy (MVD) was significantly correlated with MCT4het+, providing evidence for metabolic heterogeneity and regional hypoxia. In contrast, mechanisms causing pseudohypoxia are indicated for the MCT4hom+ subtype.

Conclusions: Despite their potentially different underlying mechanisms, MCT4hom+ and MCT4het+ were associated with features of aggressive disease (T-, N-, M-stage and tumour relapse). Our 3D cell culture studies, including patient-derived tumoroids, mimic metabolic heterogeneity observed in tumours and highlight MCT4 as a potential therapeutic target.

A 10

Multi-V-Stain: multiplexed virtual staining of histopathology images using deep learning

Ms. Sonali Andani[1]*, Ms. Joanna Ficek-Pascual[2], Mr. Simon Heinke[2], Dr. Ruben Casanova[3], Dr. Marta Nowak[4], Dr. Bettina Sobottka[4], Prof. Bernd Bodenmiller[3], Mx. Tumor Profiler Consortium[5], Prof. Viktor H. Kölzer[4], Prof. Gunnar Rätsch[2]

[1]Department of Pathology and Molecular Pathology, University Hospital Zurich, University of Zurich, Zurich, Switzerland; Department of Computer Science, ETH Zürich, Universitätsstr. 6, 8092 Zürich, Switzerland; [2]Department of Computer Science, ETH Zürich, Universitätsstr. 6, 8092 Zürich, Switzerland; [3]Department of Quantitative Biomedicine, University of Zürich, Winterthurerstrasse 190, 8057 Zürich, Switzerland; [4]Department of Pathology and Molecular Pathology, University Hospital of Zurich; [5]Mx. Tumor Profiler Consortium, Zurich, Switzerland

Background: Hematoxylin and eosin (H&E) images are clinically established for cancer diagnosis; however, they lack explicit information on protein expression, necessary for a comprehensive understanding of the tumor immune microenvironment. Multiplex imaging technologies enable the measurement of multiple markers with spatial context and single-cell resolution but with low throughput and at a high cost.

(a)

Input H&E WSI

Predicted IMC

(b)
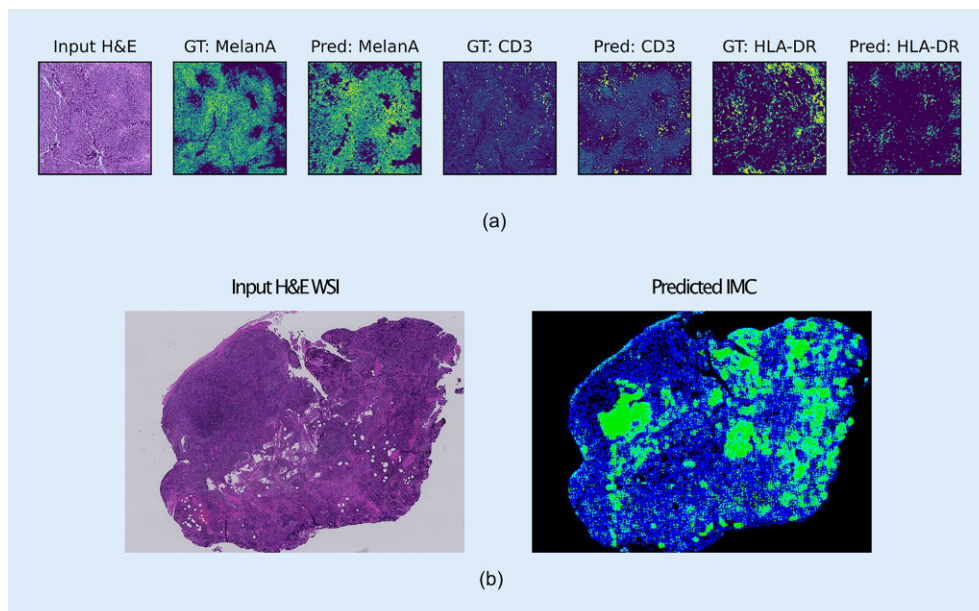
Fig. 1 | A 10 ◄ (a) Example predictions (Pred) on a pixel level from the Multi-V-Stain model, with the input H&E ROI (left) and the GT protein abundance (GT) for three proteins: MelanA, CD3 and HLA-DR. The color scale was determined per protein based on train-set quantiles, with dark blue denoting absence. **(b)** Whole-slide image prediction of multiplexed protein information. Left: Input H&E. Right: Multi-V-Stain output of CD20 and CD3 protein abundance represented by green and blue channels, respectively

	CD16	CD20	CD3	CD31	CD8a	GLUT1	HLA-ABC	HLA-DR	MelanA	S100	gp100
R	0.27	0.18	0.34	0.11	0.26	0.22	0.25	0.21	0.39	0.37	0.36
C	0.34	0.27	0.34	0.27	0.22	0.42	0.44	0.34	0.4	0.39	0.38

Fig. 2 | A 10 ◄ Quantitative evaluation of Multi-V-Stain predictions. Median Pearson's correlation coefficient (R) and median CW-SSIM values (C) on predicted protein multiplex

Methods: We use Deep Learning to predict multiplex protein expression to bridge the present gap, leveraging the rich morphological information encoded in H&E stains. We build a pix2pix-inspired "Multi-V-Stain" conditional GAN framework and apply it to a dataset from the Swiss Tumor Profiler Study, consisting of 336 paired H&E and IMC images from 80 metastatic melanoma patients. Since H&E and ground truth (GT) IMC come from two consecutive slices, we use the Complex Wavelet Structural Similarity Index (CW-SSIM) and a smoothed Pearson's correlation coefficient to robustly measure similarity between GT and predictions. Finally, we compare protein co-expression patterns between GT and predicted IMC by inspecting a joint t-SNE embedding.

Results: Using whole-slide H&E images, our model can predict the spatially-resolved abundance of eleven key protein biomarkers including both functional and lineage markers on region and whole-slide scale (◘ Fig. 1). We observe that the model generates protein expression maps that are well correlated and structurally similar with IMC GT from the consecutive section (Table 1). Further, we show that the co-expression and avoidance patterns of different cell-types observed in GT can also be observed in the predictions.

Conclusions: In this study, we provide a proof of concept that multiplexed protein expression can be predicted on a whole-slide scale from standard H&E images in a cost- and time-efficient manner. This has the potential for assisting clinical diagnosis and predicting response to precision therapy.

A 11
Primary bone diffuse large B-cell lymphoma (PB-DLBCL)–evidence for a distinct lymphoma entity

Dr. Thomas Menter[1]*, Mr. John Davies[2], Prof. Damian Wild[3], Prof. Anne Müller[4], Dr. Fatime Krasniqi[5], Prof. Frank Stenner[5], Dr. Alexandros Papachristofilou[6], Prof. Stefan Dirnhofer[1], Prof. Alexandar Tzankov[1], Ms. Vanesa-Sindi Ivanova[1]

[1]Pathology, Institute of Medical Genetics and Pathology, University Hospital Basel, University of Basel, Basel, Switzerland; [2]Leeds Institute for Data Analytics, University of Leeds, Leeds, UK; [3]Divison of Nuclear Medicine, University Hospital Basel, Basel, Switzerland; [4]Institute of Molecular Cancer Research, Zurich, Switzerland; [5]Division of Medical Oncology, University Hospital Basel, Switzerland; [6]Department of Radiation Oncology, University Hospital Basel, Basel, Switzerland

Background: Primary bone lymphoma (PBL) is rare, accounting for 1–2% of all lymphomas. So far, PBL has not been acknowledged by any current lymphoma classification systems precluding it from being recognised as a separate lymphoma entity/subentity. Herein, in the narrow sense of primary bone DLBCL (PB-DLBCL), we define and highlight its distinctive clinical presentation, morphology, phenotype, gene expression profile (GEP) and molecular genetics.

Methods: We collected 27 cases and investigated the cases by immunohistochemistry (IHC), performed gDNA sequencing with a customised lymphoma panel, covering 172 genes, and carried out FISH to evaluate *MYC, BCL2* and *BCL6* translocations. We also attempted to genetically subclassify cases in terms of DLBCL subtype by using the overt two-step classifier and LymphGen. Finally, we performed GEP for cell-of-origin subtyping and *in-silico* comparison to uncover up- and down-regulated genes as opposed to other DLBCL.

Results: By applying the Hans algorithm, 22 cases (81%) were GCB and only 5–non-GCB. FISH showed 2 *BCL2*, 3 *BCL6* and 1 *MYC* rearranged instances. One case each had *MYC* and *BCL2*, and 1 *BCL2* and *BCL6* rearrangements. DNA sequencing highlighted *TP53* ($n = 7$), *B2M* ($n = 5$), *EZH2* ($n = 5$), *KMT2D* ($n = 5$), *TNFRSF14* ($n = 4$) and *SGK1* ($n = 4$) as the most frequently mutated genes in PB-DLBCL. The two-step classifier subclassified 12 out of

24 cases as EZB ($n = 8$), ST2 ($n = 3$) and MCD ($n = 1$), while LymphGen was not able to subclassify any case. All 19 cases that passed quality control for GEP were classified as GCB, and 1 was molecular high-grade.

Conclusion: We provide molecular evidence that PB-DLBCL is a specific entity. Almost all cases are GCB. PB-DLBCL mutational profile is similar to the one of follicular lymphoma (FL), but its GEP and frequency of *BCL2* rearrangements are unequivocally different from nodal GCB-DLBCL and FL.

A 12
Epigenetic age acceleration is a distinctive trait of epithelioid sarcoma with potential therapeutic implications

Dr. Simon Haefliger[1]*, Dr. Olga Chervova[2], Mr. Christopher Davies[3], Dr. Chet Loh[4], Prof. Roberto Tirabosco[5], Prof. Fernanda Amary[5], Prof. Nischalan Pillay[3], Prof. Steve Horvath[4], Prof. Stephan Beck[2], Prof. Adrienne M Flanagan[3], Prof. Iben Lyskjaer[6]

[1]Institute of Medical Genetics and Pathology, University Hospital Basel, University of Basel, Basel, CH; [2]Medical Genomics Research Group, University College London, UCL Cancer Institute, London, UK; [3]Research Department of Pathology, University College London, UCL Cancer Institute, London, UK; [4]Altos Labs, Cambridge Institute of Science, Cambridge, UK; [5]Department of Histopathology, Royal National Orthopaedic Hospital, Stanmore, UK; [6]Department of Molecular Medicine, Aarhus University Hospital, Aarhus, DK

Background: Recently, DNA methylation-based epigenetic clocks have been proven to be precise age predictors. Their application in cancer tissue has revealed a global age acceleration in a majority of cancer subtypes when compared to normal tissue from the same individual.

Methods: As PRC2 and its regulator SMARCB1 play a crucial role in the aging process, we used three different DNA methylation-based epigenetic clocks (Horvath, Hannum, PhenoAge) to infer epigenetic age (EA) and epigenetic age acceleration (EAA) in SMARCB1-deficient neoplasms ($n = 111$). Then, EA and EAA were determined across 58 different sarcoma subtypes using the reference data set from the Heidelberg sarcoma classifier.

Results: Within the SMARCB1-deficient collection of neoplasms, epithelioid sarcoma showed the highest EA and EAA compared to malignant rhabdoid tumour and atypical teratoid and rhabdoid tumour ($p < 0.01$) across all three DNA methylation-based epigenetic clocks. Within the reference data set from the Heidelberg sarcoma classifier, epithelioid sarcoma showed the highest EA and EAA among all 58 evaluated sarcoma subtypes. However, this was not significantly different when compared to the tumor subtypes with chondroblastoma and giant cell tumor of the bone having the second highest EA and EAA ($p > 0.01$).

Conclusion: By calculating epigenetic age scores from more than 1000 tumor samples, we identified epigenetic age acceleration as a striking feature of epithelioid sarcoma when compared with other SMARCB1-deficient neoplasms, and across all other evaluated sarcoma subtypes (58 subtypes, $n = 952$). As aging pathways have recently been proposed as therapeutic targets for various cancer types, our observations highlight the potential of targeting aging pathways as a potential innovative treatment approach for patients with epithelioid sarcoma.

A 13

Association between image-based consensus molecular subtypes and response to neoadjuvant chemoradiotherapy in rectal cancer biopsies

Dr. Maxime Lafarge[1]*, Dr. Enric Domingo[2], Dr. Korsuk Sirinukunwattana[3], Mrs. Ruby Wood[4], Dr. Leslie Samuel[5], Dr. Graeme Murray[5], Dr. Susan Richman[6], Mr. Andrew Blake[2], Prof. David Sebag-Montefiore[6], Dr. Simon Gollins[7], Dr. Eckhard Klieser[8], Prof. Daniel Neureiter[8], Dr. Florian Huemer[9], Prof. Richard Greil[10], Dr. Philip Dunne[11], Prof. Philip Quirke[6], Prof. Lukas Weiss[10], Prof. Jens Rittscher[12], Prof. Tim Maughan[2], Prof. Viktor H. Kölzer[1]

[1]Department of Pathology and Molecular Pathology, University Hospital Zurich, University of Zurich, Zurich, Switzerland; [2]Department of Oncology, Medical Sciences Division, University of Oxford, Oxford, UK; [3]Ground Truth Labs, Oxford, UK; [4]Department of Engineering Science, University of Oxford, Oxford, UK; [5]School of Medicine, Medical Sciences and Nutrition, University of Aberdeen, Aberdeen, UK; [6]Leeds Institute of Medical Research, University of Leeds, Leeds, UK; [7]North Wales Cancer Treatment Centre, Besti Cadwaladr University Health Board, Bodelwyddan, UK; [8]Institute of Pathology, Paracelsus Medical University, Salzburg, Austria; [9]Department of Internal Medicine III with Haematology, Medical Oncology, Haemostaseology, Infectiology and Rheumatology, Oncologic Center, SCRI-LIMCR, Paracelsus Medical University Salzburg, Salzburg, Austria; [10]Department of Internal Medicine III with Haematology, Medical Oncology, Haemostaseology, Infectiology and Rheumatology, Oncologic Center, SCRI-LIMCR, Paracelsus Medical University Salzburg, Salzburg, Austria; [11]The Patrick G Johnston Centre for Cancer Research, Queens University Belfast, Belfast, UK; [12]Department of Engineering Science, Institute of Biomedical Engineering (IBME), University of Oxford, Oxford, UK

Background: Predicting consensus molecular subtypes from histopathology images using machine learning (imCMS) is a promising route to overcome the limitations of existing molecular profiling methods. In colorectal cancer (CRC), morpho-molecular data from diagnostic biopsies are a powerful source of information to stratify patients for neoadjuvant treatment. Here, we hypothesize that imCMS classification of rectal cancer (RC) biopsies may predict pathological complete response (pCR) to neoadjuvant long course chemoradiotherapy (LCRT) with capecitabine.

Methods: Deep learning models were trained to classify hematoxylin/eosin whole slide images (WSIs) of CRC tumors into one of the four CMS classes. The training dataset was composed of 1057 WSIs from two CRC resection cohorts (FOCUS, SPINAL) and one RC biopsy cohort (GRAMPIAN). Each WSI was labeled with a CMS class identified via transcriptional analysis of strictly consecutive tissue slices.

The trained models were used to predict the imCMS classes for WSIs in a validation dataset composed of two independent diagnostic biopsy cohorts of RC patients selected to have undergone the same LCRT regimen (ARISTOTLE, SALZBURG, total $n = 160$ patients). pCR was determined by histopathological assessment of resections undertaken 6–12 weeks after LCRT ($n = 30$ pCR). Logistic regression models for each imCMS class assessed association with pCR, adjusting by the confounders "cohort" and "pretreatment T/N stage".

Results: Patients classified as imCMS1 showed a significant association with pCR compared to other cases (OR = 2.69, 95%CI 1.01–7.17, $p = 0.048$). Conversely, imCMS4 was associated with lack of pCR (OR = 0.25, 95%CI 0.07–0.88, $p = 0.031$). No significant association was found in imCMS2 or imCMS3.

Conclusions: imCMS classification of CRC biopsies is a promising, fast and inexpensive solution to stratify patient groups that could benefit from neoadjuvant CRT. The significant associations between imCMS1/imCMS4 with pCR suggest the existence of predictive morphological features that could enhance standard pathological assessment. Validation of the clinical utility in prospective clinical trials is recommended.

A 14

B-cell clonality assessment by next generation sequencing

Dr. Thomas Menter*, Dr. Ivana Bratic-Hench, Dr. Ilaria Alborelli, Prof. Stefan Dirnhofer, Mr. Massimiliano Manzo, Prof. Alexandar Tzankov

Pathology, Institute of Medical Genetics and Pathology, University Hospital Basel, University of Basel, Basel, Switzerland

Background: Assessing B-cell clonality is important in haematopathology and a helpful tool in routine diagnostics. PCR-based fragment-length analysis (e.g. based on BIOMED-2 primers) has been a useful method for several decades. Currently, first assays using high throughput sequencing (HTS, also called NGS) have become available.

Methods: To assess robustness and applicability of these novel assays, we compared the results for B-cell clonality via PCR and NGS (Oncomine™ BCR Pan-Clonality Assay, ThermoFisher) in 25 cases, including a variety of B-cell lymphomas and reactive lesions. Blood samples ($n = 3$) and formalin fixed and paraffin embedded (FFPE) tissue blocks ($n = 22$) were used. Evaluation was performed according to the recommendations of the manufacturer and as previously published (J Mol Diagn. 2019 Mar;21(2):330–342).

Results: In 9/13 cases diagnosed as "clonal" and 9/12 cases diagnosed as "polyclonal" by PCR, NGS analysis was concordant. In four cases, the "clonal" result by PCR could not be confirmed by NGS analyzing IgH only, however, taking into account the light chains, clonality could be demonstrated in two of these specimens. The two specimens in which clonality could not be detected by NGS were a marginal zone lymphoma of the skin and a primary cutaneous follicle center lymphoma.

In three probes signed out as polyclonal by PCR analyzing IgH, clonality could be proven by NGS by assessing the light chains.

Conclusions: We could demonstrate that assessing clonality using NGS is a useful adjunct in lymphoma diagnostics. Analyzing both heavy chains and light chains increases sensitivity, yet it seems that especially in cutaneous B-cells lymphomas, it remains difficult. Further work will address the issue of whether the presence of distinct clones or rather the so called "lineages" detected should be considered as diagnostic parameter.

A 15*

Epigenetically repressed CDX2 expression promotes CRC cell migration

Mrs. Rina Mehmeti[1]*, Mr. Nils Bodmer[1], Dr. Cansaran Saygılı Demir[2], Prof. Alessandro Lugli[1], Mr. Jun Xu[1], Mrs. Deborah Krauer[1], Prof. Nassim Ghaffari[3], Prof. Mario P. Tschan[1], Prof. Inti Zlobec[1]

[1]Institute of Tissue Medicine and Pathology, University of Bern, Bern, Switzerland; [2]Lunaphore Technologies S. A., Tolochenaz, Switzerland; [3]Institute of Pathophysiology and Immunology, Medical University of Graz, Graz, Austria

Background: Reduced expression of CDX2 is a poor prognostic factor in colorectal cancer (CRC). CDX2 expression is often lost in tumor buds (TBs), a histological hallmark of aggressive carcinomas, represented by single cells or clusters up to 4 cells at the tumor invasive front. TBs show signs of epithelial-mesenchymal transition (EMT). We hypothesize that CDX2 expression is repressed by histone deacetylases (HDACs) and plays a role in CRC cell migration, EMT and TB.

Methods: Pharmacological and genetic inhibition of HDACs was applied to CDX2 negative CRC cells (HT29, SW620, HCT116), to increase CDX2 expression. We used CRISPR technology to knockout (KO) CDX2 in CDX2 positive LS174T CRC cells and assessed their migratory phenotype using transwell migration and *in ovo* assays. Using multiplex immunofluorescence (mIF) we investigated CDX2 and E-cadherin expression in primary tumor vs. TBs in CRC patient and patient-derived xenograft (PDX) samples.

Results: Screening HDAC inhibitors, we identified UFO10, an HDAC class I and IIb inhibitor, as a dose-dependent CDX2 activator causing upregulation up to 30-fold. Knocking down a series of different HDAC class I and IIb
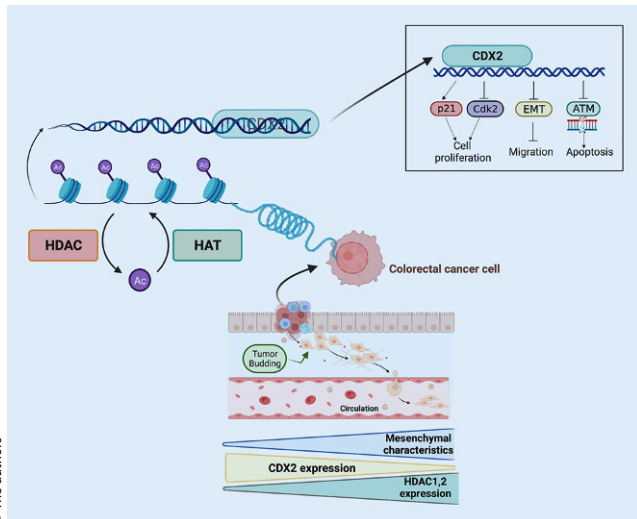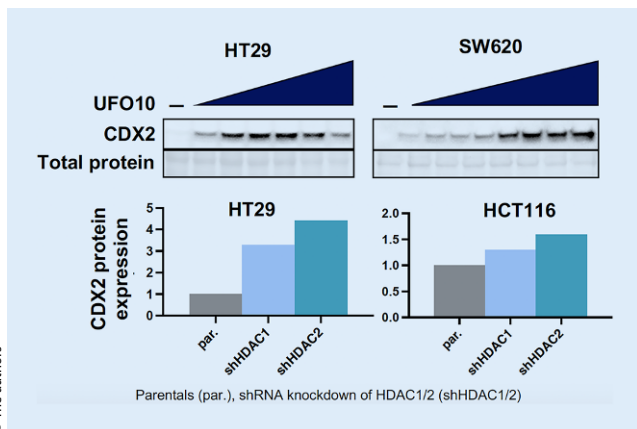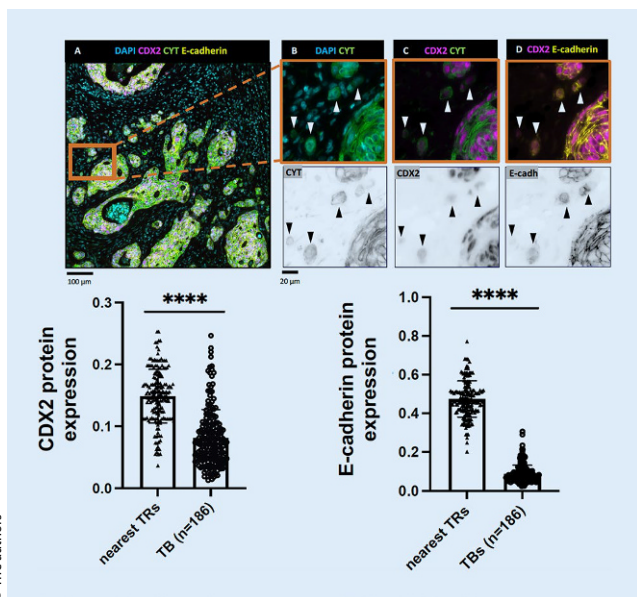
Fig. 1 | A 15 ▲

Fig. 2 | A 15 ▲

Fig. 2 | A 15 ▲

HDAC genes revealed HDAC1 and HDAC2 as the strongest CDX2 repressors. Knocking out CDX2 in LS174T cells resulted in significantly increased cell migration *in vitro*. In line with these findings, LS172T CDX2 KO cells showed markedly increased invasiveness and TB in the chick embryo chorioallantoic membrane (CAM) compared to control cells. Additionally, mIF analysis showed significantly lower CDX2 and E-cadherin in TBs compared to nearest primary tumor regions in primary CRC patient and PDX samples.

Conclusion: We identified HDAC1/2 as critical inhibitors of CDX2 expression. Moreover, depleting CDX2 increased CRC cell migration and its low expression was associated with TB in primary CRC patients and PDX. Our findings suggest that reactivating CDX2 expression using HDAC1/2 inhibitors is a promising CRC treatment strategy.

*Student submission

References

1. ePoster at ECP2023. https://ecp2023-c745.epresenter.com.au/posters?tid=all

A 16
Communicating certainty in pathology reports–a multicentered and multilinguistic study in Switzerland

Dr. Maria Brendle*, Dr. Chiara Saglietti, Prof. Sabina Berezowska

Department of Laboratory Medicine and Pathology, Institute of Pathology, Lausanne University Hospital, University of Lausanne, Rue du Bugnon 25, 1011 Lausanne, Switzerland

Background: The main objective of surgical pathology reports is communication of a diagnosis. Pathologists can adjust the level of certainty of the diagnosis by using modifying phrases (MP), such as "compatible with". However, the degree of certainty associated with MPs is variable. Our aim was to investigate the certainty pathologists in Switzerland assign to different MPs, considering the particularity of three main working languages. Furthermore, we wanted to explore pathologists' opinion on standardizing MPs.

Methods: A questionnaire was used to determine the diagnostic certainty attributed to MPs by means of rating the certainty [%] as well as a ranking of MPs from the highest to the to the lowest certainty. Furthermore, we asked whether expressions of certainty should be standardized, and whether MPs are used because of possible legal implications. The survey also contained questions on demographic data, personal habits in reporting, opinion on standardizing of reports by means of standardized cancer reporting and text modules. The survey was distributed to members of the SGPath via the newsletter in July 2023. Additionally, e-mails were sent to several pathology institutions. Collections period was 06/30/2023–07/15/2023.

Results: Total response rate was 26% (68% for residents and 21% for specialist). There are remarkable differences in the perception of MPs: in all languages, associated certainty levels vary widely. Nearly 80% of participants are in favor of a standardization of expressions of certainty in pathology reports. Nearly 40% of participants use MP because of possible legal consequences.

Conclusions: This first study in Switzerland shows that standardization could promote unambiguity of pathology reports and is endorsed by most participants. Further studies are necessary to a) ask clinicians on how they perceive certainty levels of MPs to explore and define a common basis and b) investigate which MPs are most suitable for a standardized use.
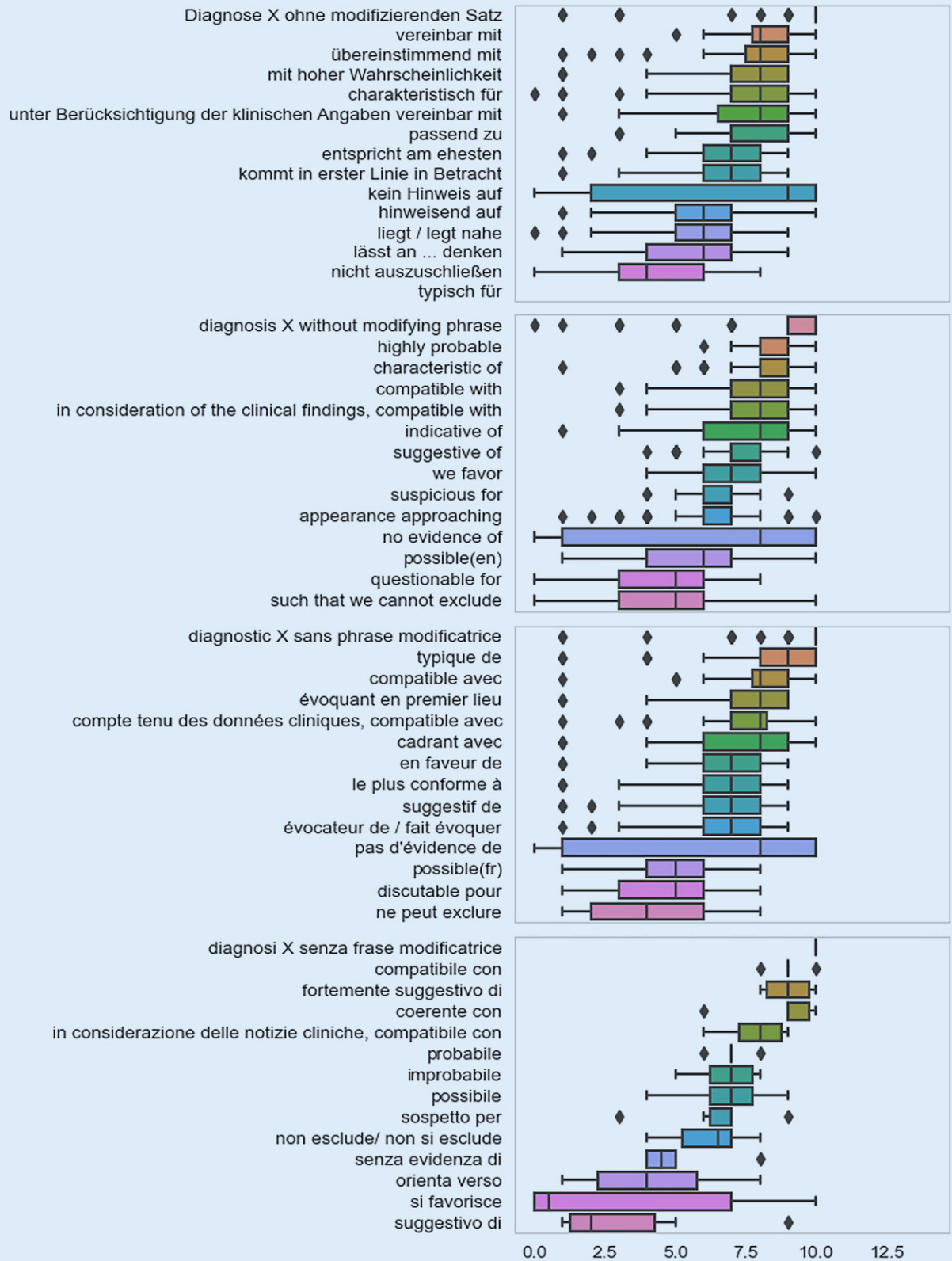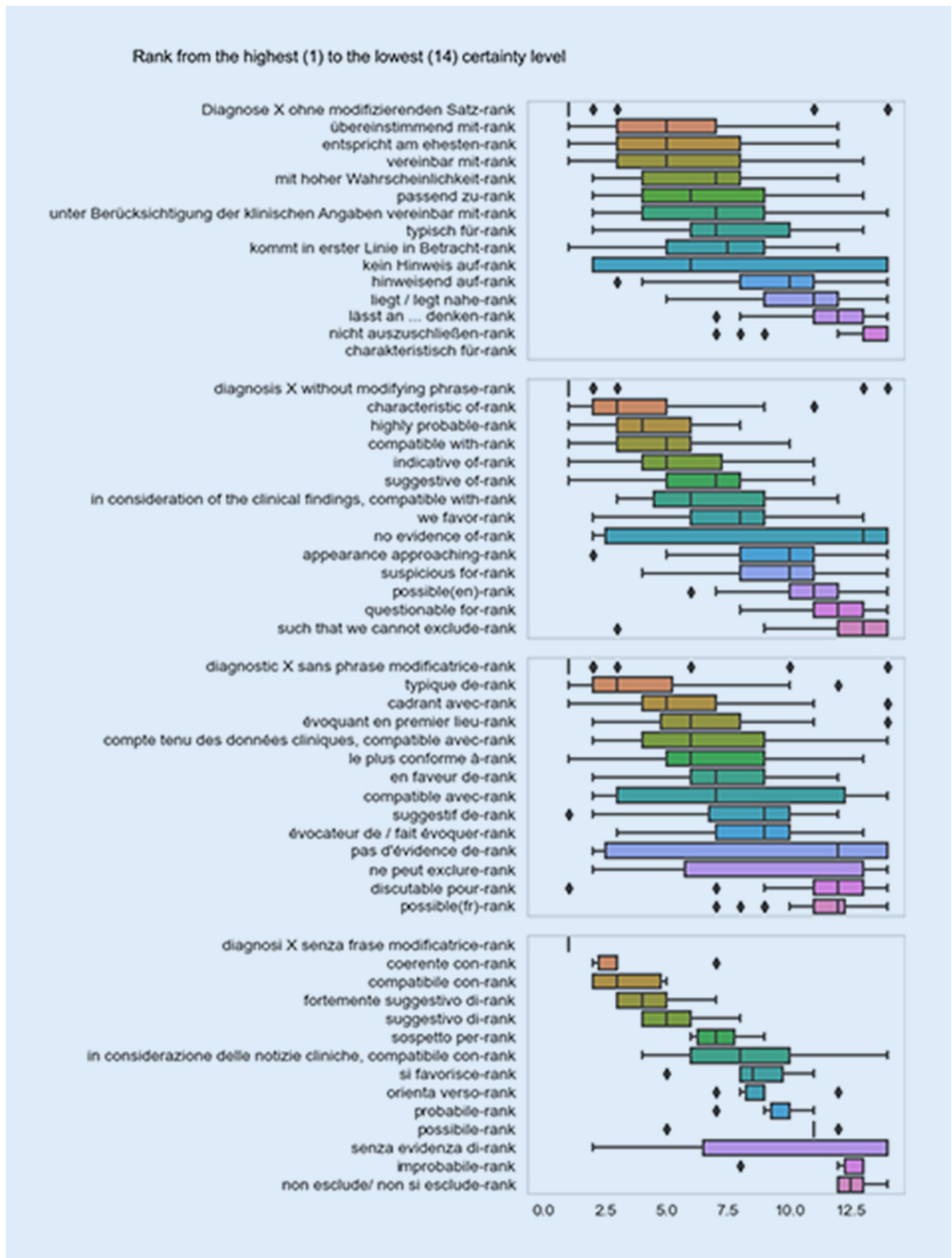
Certainty [10%]

Fig. 1 | A 16 ▲

Fig. 2 | A 16 ▲

A 17

Meningioma-to-malignant peripheral nerve sheath tumor transdifferentiation by a single genetic event

Dr. Arnaud Bakaric[1]*, Dr. Arthur Robert Kurzbuch[2], Dr. Vincent Soubeyran[3], Prof. Doron Merkler[1], Dr. Igor Letovanec[4], Dr. Kristof Egervari[1]

[1]Service of Clinical Pathology, Department of Diagnostics, Geneva University Hospital, Geneva, Switzerland; [2]Service of Neurosurgery, Valais Hospital, Sion, Switzerland; [3]Service of Nuclear Medicine, Valais Hospital, Sion, Switzerland; [4]Histocytopathology, Valais Hospital, Sion, Switzerland

Background: Meningiomas originate from arachnoid cells and malignant peripheral nerve sheath tumors (MPNST) from peripheral nerves. Rare cases of intracranial MPNSTs not associated with cranial nerves have been described, however, their origin remains undefined. Here we describe a case of meningioma with sarcomatous transformation showing morphological, genetic and epigenetic features consistent with an MPNST.

Methods: 72-year-old female presented a fronto-parietal, extra- and intra-cranial, osteolytic lesion with two components and disseminated bone metastases. We performed histopathological characterization and methylation profiling with copy number variation (CNV) predictions of both components.

Results: We found a dense, necrotic and mitotically active (> 20 mitoses/10 high power field) tumor composed of atypical cells, immunopositive for Epithelial Membrane Antigen (EMA), negative for cytokeratine (CK) 5/6 and smooth muscle actin (SMA), morphologically compatible with an anaplastic meningioma. We saw transition to a second component: a spindle cell tumor with mitoses and EMA-negative, CK 5/6- and SMA-positive tumor cells. Methylation profiling and classification (Brain Classifier v12.5, DKFZ, Heidelberg) of the first component gave a match with the family of meningiomas with highest calibrated scores (0.75) for intermediate meningiomas. The sarcomatous part was a match (0.94) with the class of MPNSTs. Near identical CNVs proved the common clonal origin of the two. In addition, the sarcomatous part showed a focal loss of *EED*, a gene frequently altered in MPNSTs. Consistently, we found loss of H3K27me3 in the sarcomatous component.

Conclusion: We describe a neoplastic transdifferentiation of meningioma into MPNST most probably due to a single genetic event of *EED* deletion, leading to H3K27me3 loss and epigenetic reprogramming. Our case raises the hypothesis that intracranial MPNSTs may develop from a meningothelial precursor away from peripheral nerves.

A 18*

Multi-modal deep learning identifies morphological features predictive of distant recurrence from hemoxylin-and-eosin-stained endometrial cancer slides

Mrs.Sarah Fremond[1]*, Dr. Nanda Horeweg[2], Mrs. Sonali Andani[3], Mr. Jurriaan Barkey Wolf[1], Dr. Maxime Lafarge[3], Dr. Gitte Oertoft[4], Dr. Estrid Høgdall[5], Dr. Jouke Dijkstra[6], Dr. Jan Jobsen[7], Dr. Ina Jürgenliemk-Schulz[8], Dr. Ludy Lutgens[9], Dr. Melanie Powell[10], Dr. Naveena Singh[11], Dr. Linda Mileshkin[12], Dr. Helen Mackay[13], Dr. Alexandra Leary[14], Dr. Dionyssios Katsaros[15], Dr. Hans Nijman[16], Dr. Stephanie de Boer[17], Prof. Remi Nout[18], Dr. Marco de Bryun[19], Prof. David N. Church[20], Prof. Vincent Smit[1], Prof. Carien Creutzberg[17], Prof. Viktor H. Kölzer[21], Dr. Tjalling Bosse[1]

[1]Department of Pathology, Leiden University Medical Center, Leiden, The Netherlands; [2]Department of Radiation Oncology, Leiden University Medical Center, Leiden, The Netherlands; [3]Department of Pathology and Molecular Pathology, University Hospital Zurich, University of Zurich, Zurich, Switzerland; [4]Copenhagen University Hospital, Copenhagen, Denmark; [5]Herlev University Hospital, Herlev, Denmark; [6]Department of Vascular and Molecular Imaging, Leiden University Medical Center, Leiden, The Netherlands; [7]Department of Radiation Oncology, Medisch Spectrum Twente, Enschede, The Netherlands; [8]Department of Radiation Oncology, University Medical Center Utrecht, Utrecht, The Netherlands; [9]Department of Radiation Oncology, Maastricht UMC+, The Netherlands; [10]Department of Clinical Oncology, Barts Health NHS Trust, London, UK; [11]Department of Anatomic Pathology, Vancouver General Hospital, Vancouver, BC, Canada; [12]Department of Medical Oncology, Peter MacCallum Cancer Center, Melbourne, Australia; [13]Department of Medical Oncology and Hematology, Odette Cancer Center Sunnybrook Health Sciences Center, Toronto, Canada; [14]Department Medical Oncology, Gustave Roussy Institute, Villejuif, France; [15]Department of Surgical Sciences, Gynecologic Oncology, Città della Salute and S Anna Hospital, University of Turin, Turin, Italy; [16]Department of Obstetrics & Gynecology, University Medical Center Groningen, Groningen, The Netherlands; [17]Department of Radiation Oncology, Leiden University Medical Center, Leiden, The Netherlands; [18]Department of Radiation Oncology, Erasmus University Medical Center, Rotterdam, The Netherlands; [19]Department of Gynaecologic Oncology, University Medical Center Groningen, Groningen, The Netherlands; [20]Cancer Genomics and Immunology Group, The Wellcome Centre for Human Genetics, University of Oxford, UK; [21]Department of Pathology and Molecular Pathology, University Hospital of Zurich, Zurich, Switzerland

Background: Accurate risk prediction of distant recurrence is essential for precision treatment of endometrial cancer (EC) patients. Risk stratification is currently based on histopathological markers and additional molecular assays; the first is challenging due to inter-observer variability, and the second due to costs. Deep Learning (DL) can predict distant recurrence by identifying prognostic features from H&E-whole slide images (WSIs).
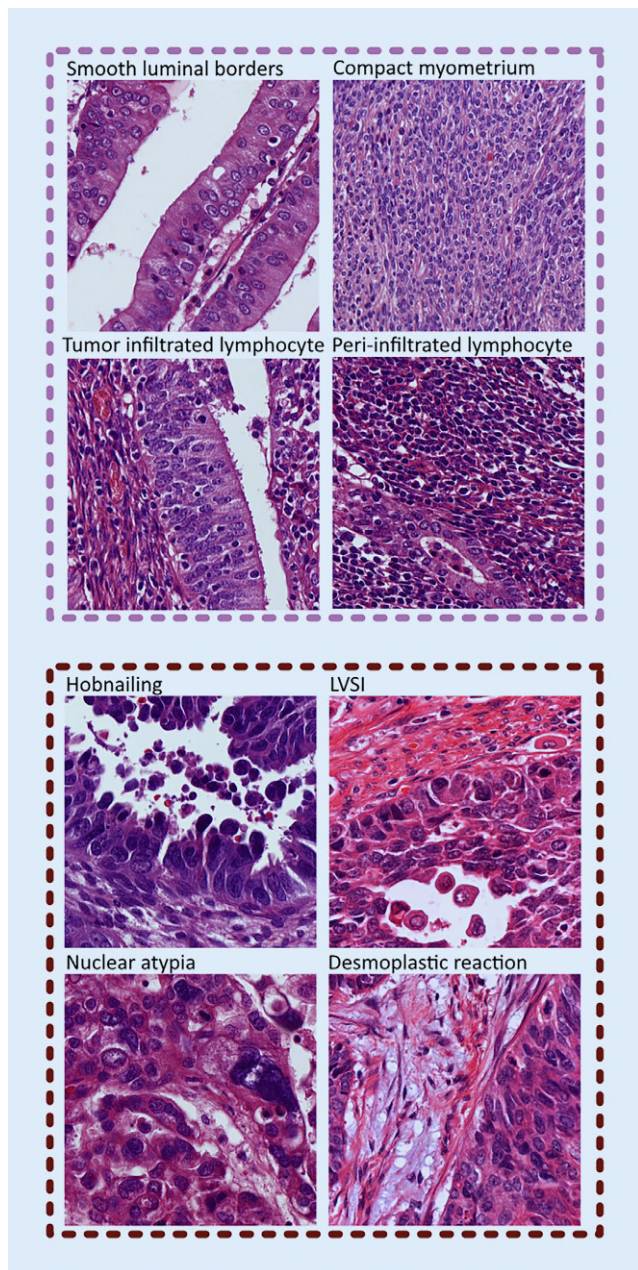
Methods: One representative H&E-WSI, clinicopathological, and outcome data from 2590 patients of the randomized PORTEC-1/-2/-3 trials and 5 clinical cohorts were used. One internal test-set (n = 353) was held-out
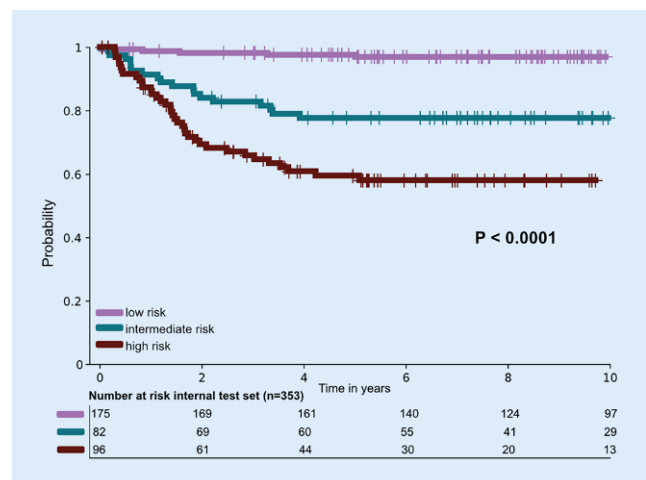
Fig. 1 | A 18 ▲ 10-year distant recurrence-free survival in the test set (n = 353) by predicted risk group

and 5-fold cross-validation ($n = 1408$) performed. A multi-modal attention-based model was trained using the H&E-WSI and FIGO stage. Performance was measured with the Concordance-index, visualized with Kaplan-Meier's analysis, and compared to a Cox' Proportional Hazards (CPH) model using clinicopathological and molecular markers. Highly contributing regions of the WSIs were reviewed and association with clinicopathological data was analyzed in the test-set. Genomic correlations were further analyzed using TCGA EC.

Results: The model achieved a Concordance-index of 0.795 ± 0.031 on cross-validation, and 0.788 on the test-set, as compared to 0.736 ± 0.033 and 0.778 with CPH. 10-year distant recurrence-free survival in the test-set was 97% (low-risk, $n = 175$), 77.7% (intermediate-risk, $n = 82$) and 58.1% (high-risk, $n = 96$), (log-rank-test $p < 0.0001$) (⊡ Fig. 1). Morphological features associated with higher risk scores were (⊡ Fig. 2): hobnailing, lymphovascular space invasion, nuclear atypia, mitotic figures, and desmoplastic stromal reaction; higher FIGO stage; p53abn; and *PPP2R1A* mutation. Associations with lower risk scores were: smooth luminal borders, peritumoral and intraepithelial lymphocytes including CD8+ follicular helper and regulatory T-cells, compact normal myometrium; FIGO stage I; *POLE*-mut and MMRd; mutations in *ARIDIA*, *CTCF*, *CTNNB1*, *PTEN*, *FGFR2*, *KRAS*.

Conclusion: Our model accurately predicts risk of distant recurrence for EC patients with inexpensive input data, outperforming standard approaches. Explainability work provides novel indicators associated with distant recurrence allowing for deeper investigation.

*Student submission

Fig. 2 | A 18 ▲ Morphological features contributing to a lower predicted risk score (above) and higher risk score (below). LVSI = lymphovascular space invasion

A 19
AI-based detection of DNA mismatch repair deficiency in colorectal cancer at the single cell level

Dr. Marta Nowak[1]*, Mr. Faiz Jabbar[2], Dr. Ann-Katrin Rodewald[3], Dr. Luciana Gneo[2], Ms. Tijana Tomasevic[2], Dr. Andrea Harkin[4], Prof. Tim Iveson[5], Dr. Mark Saunders[6], Dr. Rachel Kerr[7], Prof. Karin Oien[8], Dr. Noori Maka[8], Dr. Jennifer Hay[8], Prof. Joanne Edwards[9], Prof. Ian Tomlinson[7], Prof. Owen Sansom[10], Dr. Caroline Kelly[4], Dr. Alistair Easton[7], Dr. Enric Domingo[11], Prof. Viktor H. Kölzer[3], Prof. David N. Church[12]

[1]Department of Pathology and Molecular Pathology, University Hospital Zurich, Zurich, Switzerland; [2]Cancer Genomics and Immunology Group, The Wellcome Centre for Human Genetics, University of Oxford, Oxford, UK; [3]Department of Pathology and Molecular Pathology, University Hospital of Zurich, Zurich, Switzerland; [4]CRUK Clinical Trials Unit, University of Glasgow, Glasgow, UK; [5]Southampton University Hospital NHS Foundation Trust, Southampton, UK; [6]The Christie NHS Foundation Trust, Manchester, UK; [7]Department of Oncology, University of Oxford, Oxford, UK; [8]Glasgow Tissue Research Facility, University of Glasgow, Queen Elizabeth University Hospital, Glasgow, UK; [9]School of Cancer Sciences, University of Glasgow, Glasgow, UK; [10]CRUK Beatson Institute of Cancer Research, Glasgow, UK; [11]Department of Oncology, Medical Sciences Division, University of Oxford, Oxford, UK; [12]Cancer Genomics and Immunology Group, The Wellcome Centre for Human Genetics, University of Oxford, Oxford, UK

Background: Assessment of microsatellite status and mismatch repair (MMR) protein expression is an important part of the standard diagnostic workup for patients with gastrointestinal cancer. Up to 15% of patients with colorectal cancer (CRC) have MMR-deficient (MMRd) tumors indicating favorable prognosis in early stage disease and potential response to immune-checkpoint inhibitors in advanced disease. Since MMR assessment requires substantial pathologist time, several efforts have focused on the development of automated image analysis methods to identify MMRd.

Methods: Using the AI-based image analysis platform HALO AI (Indica Labs), we established the AIMMeR tool to score MMR protein expression at the single-cell level on multi-spot tissue microarrays (TMAs) derived from 2352 stage II-III CRC tumors of the Short Course Oncology Treatment (SCOT) Trial cohort. We combined the nuclear morphological analysis with automated identification of 3-3'Diaminobenzidine (DAB) positivity, to determine MMR protein expression at the single cell level in tumor and non-tumor cell populations in each TMA core (⊡ Fig. 1). We benchmarked the predictions against pathologist consensus review and determined the clinicopathological correlates of MMRd in the SCOT cohort.

Results: AIMMeR classified single cell-types with 0.92 accuracy. Strong positive correlation was observed for tumor MLH1 and PMS2, and for MSH2 and MSH6 expression ($R2 = 0.88$, 0.69 respectively, $P < 1e-04$). Using a cut-off of 10.7% for MMR protein positivity in tumor cells, AIMMeR achieved Youden-index (sensitivity plus specificity) of 1.87 for MMRd detection, and agreement similar to that between pathologists (kappa = 0.79–0.82). Of 1988 cases, the 229 (11.5%) with MMRd showed expected associations with clinicopathological features, such as sidedness, immune infiltration and better recurrence-free interval (RFI) (multivariable-adjusted (mv)HR = 0.62, 95%CI = 0.44–0.88, $P = 0.007$). MMRd did not predict a differential benefit of treatment duration; however, it correlated with variation in clinical outcome by chemotherapy regimen ($P_{int} = 0.04$).

Conclusions: AIMMeR performance is similar to expert pathologist review and holds promise for clinical application.
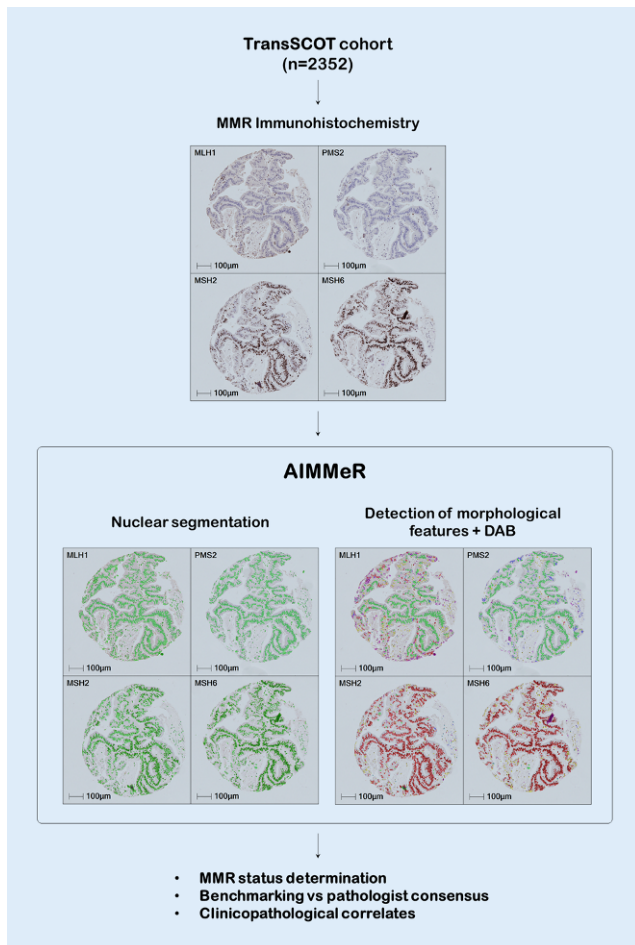
Fig. 1 | A 19 ▲ Development and validation of AI-based tool for detection of MMR protein expression at the single cell level (AIMMER) in the SCOT trial cohort. Using digital image analysis platform HALO (IndicaLabs) nuclei were segmented in each individual TMA spot. Based of morphological features and DAB-positivity, each nucleus was classified into one of the following classes: positive tumor cells (red), negative tumor cells (green), positive stroma cells (yellow), negative stroma cells (blue), lymphocytes (turquoise) and background (purple and pink)

A 20
Mapping the tissue composition with hyperplex immunofluorescence on delicate samples

Dr. Joanna Kowal*, Mr. Jonathan Mignot, Mr. Florent Jeanpetit, Dr. Benjamin Pelz, Dr. Diego Dupouy

Lunaphore, Tolochenaz, Switzerland

Background: Deciphering the tissue architecture is emerging as a crucial step to better understand tissue biology and harness it in a future therapeutic intervention [PMID:32377572]. Newly developed protocols allow detection of dozens of biomarkers simultaneously [PMID:35714588;35132261]. However, fresh frozen sections (FS) analyses remain challenging as harsh procedures used in manual protocols are detrimental to tissue morphology and limit the use of this application [PMID:34811556]. Furthermore, manual protocols are laborious and time-consuming, allowing to process a limited number of samples. Here, we describe the capability to perform automated hyperplex assays for up to 32 biomarkers on FS as a cogent case combining staining quality with tissue preservation.
Methods: COMET™ platform automates sequential immunofluorescence (seqIF™) assays based on an iterative series of fast tissue staining, imaging, and antibody elution cycles. FS tissue of human and murine origins were fixed and permeabilized prior to staining protocols. Up to 32 biomarkers were detected on a single tissue slide. To assess the tissue morphology preservation, standard hematoxylin and eosin (H&E) staining was performed on FS freshly processed or post-seqIF™.
Results: Murine tissues were stained with panels of up to 6 proteins showing an accurate detection of both immune and organ-specific biomarkers. For a deep characterization of human lung cancer, 32 biomarkers were simultaneously detected on a single FS with optimal staining and a total procedure time of 23 h. An H&E staining performed on the slide retrieved from the platform after the seqIF™ showed excellent preservation of the tissue architecture in comparison with an unprocessed FS slide.
Conclusion: This work demonstrates the feasibility of performing automated hyper-plex assays on a variety of delicate frozen samples with high-quality results. With this new toolbox, we aim to support and hasten discovery studies across multiple research fields by overcoming current limitations in spatial biology.

A 21
Rapid toluidine blue staining for on-site evaluation of cytological specimens: the Lausanne experience

Ms. Claire Royer[1]*, Ms. Marie Maillard[1], Ms. Estelle Dubruc[1], Prof. Ekkehard Hewer[2]

[1]Institute of Pathology, Centre Hospitalier Universitaire Vaudois (CHUV), Université de Lausanne, Lausanne, Switzerland; [2]Institute of Pathology, Lausanne University Hospital, Lausanne University, Lausanne, Switzerland

Background: Rapid toluidine blue staining for on-site evaluation (ROSE) of cytological specimens takes less than a minute, offering excellent morphology. In this study, we assess the performance of ROSE using toluidine blue (TB) staining in our institution, regarding its adequacy and its diagnostic output, and illustrate its morphological characteristics.
Methods: Over 4.5 years, we evaluated 499 thyroid, lung, and head and neck fine-needle aspiration (FNA) specimens with ROSE performed for adequacy and, if possible, to provide a preliminary diagnostic. Additionally, we illustrate the features identified in TB stained slides compared to the definitive Papanicolaou staining.
Results: Adequate material was obtained in 475 of 499 (95.2%) samples. In only one case (0.2%), ROSE had erroneously suggested an adequate specimen. 10 samples (2%) were inadequate according to ROSE, but adequate according to definite evaluation. 5 samples were doubtful for adequacy on ROSE, including 2 finally adequate samples and 3 inadequate. 463 specimens were adequate on both ROSE and definite evaluation, including 201 samples both positive for tumoral cells (43.4%) and 149 samples both negative (32.2%). For 3 samples (0.6%), tumor cells were identified during ROSE, but absent in the definite sample; and for 7 samples (1.4%) tumor cells were not identified during ROSE, but present in the definite samples, corresponding to 98.0% specificity and 96.6% sensitivity of the ROSE. Evaluation for the presence of neoplastic cells was deferred for 102 samples (22%). 83 of the 85 (97.6%) specific diagnoses rendered during ROSE were concordant with the final diagnoses.
Conclusions: Our rapid TB staining protocol allows reliable ROSE of FNA specimens with high concordance between rapid and definite evaluation, with excellent diagnostic specificity (98%) and sensitivity (96.6%). Nuclear morphology is very similar to the Papanicolaou technique. As the staining is non-permanent, it is fully compatible with subsequent Papanicolaou staining of the same slides.

A 22
Decoding metastasis with functional microvasculature models for predictive pathological assessment

Dr. Soheila Zeinali[1]*, Mrs. Karin Schmid[1], Mrs. Christelle Dubey[2], Dr. Thomas Marti[3], Dr. Patrick Dorn[4], Prof. Olivier Guenat[1]

[1]Organs-on-chip Technologies Laboratory, ARTORG Center, University of Bern, Bern, Switzerland; [2]Division of General Thoracic Surgery, Inselspital, University Hospital of Bern, Bern, Switzerland–Department of BioMedical Research, University of Bern, Bern, Switzerland; [3]Division of General Thoracic Surgery, Inselspital, University Hospital of Bern, Bern, Switzerland–3Department of BioMedical Research, University of Bern, Bern, Switzerland; [4]Division of General Thoracic Surgery, University Hospital of Bern, Bern, Switzerland

Background: Advances in understanding metastasis have provided valuable insights, yet critical questions persist. Patient-specific evaluation of metastasis is pivotal for informed clinical decisions. Genomic markers within primary tumors offer glimpses of metastatic risk, although challenges endure in early prediction and deriving functional insights. Addressing these issues, in vitro models emulating metastasis hold promise as predictive tools.

Methods: To address these challenges, we developed a functional microvasculature system aimed at replicating the cancer cell metastasis journey in vitro. This system incorporates a functional microvasculature formed through de novo vasculogenesis involving endothelial and mural cells. To assess cancer cell extravasation potency, cells were introduced into microvessels and observed for 24 h. As a proof of concept, stem cell-like and mesenchymal cell-like adenocarcinoma cell lines underwent this process, where their metastatic potentials were gauged by their ability to exit the microvasculature network and infiltrate the surrounding matrix.

Results: Our study reveals that stem cell-like and mesenchymal cell-like adenocarcinoma lines diverge not only in tumor initiation ability and sensitivity but also in their metastatic potential. Specifically, stem cell-like lung cancer cells exhibited confinement within the microvasculature, while mesenchymal cell-like counterparts extravasated into the surrounding matrix within a 24-hour timeframe.

Conclusions: Our findings underscore the potential of functional microvasculature models, such as the one developed in this study, as predictive tools for assessing cancer metastasis. Through the utilization of patient-specific tumor cells obtained from resections or surgeries, this approach enables the prediction of patient-specific metastasis potential, thus offering novel insights for clinical decision-making aimed at effective cancer treatment strategies. By combining biological fidelity and patient specificity, this innovative model holds promise for advancing our understanding of cancer metastasis and improving patient outcomes.

A 23
Genetic profiles of oligometastatic non-small cell lung cancer and corresponding brain metastases

Dr. Raphael Werner[1]*, Dr. Markus Rechsteiner[2], Prof. Holger Moch[3], Prof. Alessandra Curioni-Fontecedro[4], Prof. Michael Weller[5], Dr. Tobias Weiss[5], Prof. Luca Regli[6], Dr. Emilie Le Rhun[6], Prof. Isabelle Opitz[1], Prof. Alex Soltermann[7]

[1]Department of Thoracic Surgery, University Hospital Zurich, Zurich, Switzerland; [2]Department of Pathology and Molecular Pathology, University Hospital Zurich, Zurich, Switzerland; [3]Department of Pathology and Molecular Pathology, University Hospital Zurich, University of Zurich, Zurich, Switzerland; [4]Department of Oncology, University Hospital Zurich, Zurich, Switzerland; [5]Department of Neurology, University Hospital Zurich, Zurich, Switzerland; [6]Department of Neurosurgery, University Hospital Zurich, Zurich, Switzerland; [7]Pathologie Länggasse, Ittigen, Switzerland

Background: In patients with oligometastatic non-small cell lung cancer (NSCLC), systemic therapy in combination with local ablative treatment of the primary tumor and all metastatic sites is associated with improved prognosis. For patient selection and treatment allocation, further knowledge about the molecular characteristics of the oligometastatic state is necessary. Here, we performed a genetic characterization of primary NSCLC and corresponding brain metastases (BM).

Methods: We identified 49 oligometastatic NSCLC patients with synchronous (< 3 months) or metachronous (> 3 months) BM who underwent surgical resection of the primary tumor and BM. Genetic characterization of the primary tumor and corresponding metastases was performed by targeted next-generation sequencing.

Results: Sequencing was successful in 46 paired samples. An oncogenic alteration was present in 31 primary tumors (67.4%) and 40 BM (86.9%). The alteration of the primary tumor was most commonly preserved in the corresponding BMs (29 out of 31 cases, 93.5%). The most prevalent oncogenic driver of the primary tumor were KRAS-mutations ($n = 21$). In 16 patients (34.8%), the BMs harbored private oncogenic alterations. The presence of a MYC amplification in the BM was an independent predictor of shorter OS.

Conclusions: In oligometastatic NSCLC, oncogenic drivers of the primary tumor were maintained in the majority of corresponding BMs. There is a high prevalence of KRAS mutations and targeted inhibition may play a significant role in this disease entity. MYC amplifications of the BMs are predictive for shorter OS and MYC-pathways may be a promising target.

A 24
Morphological deconvolution of tumor heterogeneity in triple negative breast cancers using an image processing software

Dr. Frederic Lifrange[1]*, Dr. Xiaoxiao Wang[2], Mr. David Venet[2], Dr. Denis Larsimont[3], Dr. Mattia Rediti[2], Ms. Linnea Stenbeck[4], Ms. Floriane Dupont[2], Ms. Ghizlane Rouas[2], Mr. Joakim Lundeberg[4], Ms. Francoise Rothe[2], Dr. Christos Sotiriou[2]

[1](1) Department of Pathology, University Hospital Center of Liège, Liège, Belgium; [2]Breast Cancer Translational Research Laboratory J-C Heuson, Institut Jules Bordet, Université Libre de Bruxelles, Brussels, Belgium; [3]Department of Pathology, Institut Jules Bordet, Université libre de Bruxelles, Brussels, Belgium; [4]Science for Life Laboratory, Department of Gene Technology, KTH Royal Institute of Technology, Stockholm, Sweden

Background and objectives: Triple negative breast cancer (TNBC) is poor prognosis disease with few dedicated treatments. Intra-tumoral heterogeneity has been reported according to the Bareche classification. Each subtype is associated with different altered molecular pathways and clinical outcomes. The classification reported by our group defined five subtypes, namely basal like (BL), immunomodulatory (IM), luminal AR (LAR), mesenchymal (M) and mesenchymal stem like (MSL).

Here we aim to morphologically characterize the five molecular subtypes by annotating different histomorphological structures and by studying the distribution of each element using an image processing software.

Materials and methods: 94 frozen breast cancer samples were manually annotated by breast cancer dedicated pathologists using artificial intelligence tools (Qupath). This allowed the slides to be annotated at single cell resolution for tumour, lymphocytic and stromal cells, and at region level for high TIL (Tumour-Infiltrating Lymphocytes) stroma, low TIL stroma, adipose tissue, carcinoma in situ, lactiferous ducts, lymphoid nodules, necrosis and vessels. All these annotations were then quantified in percentage pixels. All molecular subtypes of Bareche were obtained by bulk RNA sequencing.

Results: We found that BL and IM had the most tumour cells, while LAR and MSL had the least, the reverse being true for the stroma. IM had a higher amount of lymphocytes and lymphoid nodules, while LAR had the least. Carcinoma in situ was typical of LAR and MSL tumours. Fatty tissue and vessels were uncommon in BL and IM tumours. Lactiferous ducts were typical of MSL tumours. ($p < 0.05$)

Conclusion: Morphological analysis of tumours mapped down to the cellular level by a supervised artificial intelligence software allowed the characterisation of genetic subtypes of TNBC. This suggests the possibility of assessing the molecular subtype from imaging data alone.

A 25*
Hematon units: an access point to elucidate human bone marrow stromal niche heterogeneity

Dr. Rita Sarkis[1]*, Mr. Yang Zhang[2], Dr. Linus Angenendt[2], Mr. Charles Bataclan[1], Dr. Nathalie Piazzon[3], Mr. Damien Maison[3], Dr. Mariangela Costanza[4], Dr. Nathacha Dewarrat[4], Dr. Sabine Blum[4], Dr. Olivier Spertini[4], Dr. Stephane Cherix[5], Prof. Bart Deplancke[6], Prof. Timm Schroeder[2], Prof. Laurence de Leval[3], Prof. Olaia Naveiras[7]

[1]Laboratory of Regenerative Hematopoiesis, Institute of Bioengineering & ISREC, Ecole Polytechnique Fédérale de Lausanne (EPFL) & Department of Biomedical Sciences, University of Lausanne (UNIL), Lausanne, Switzerland; [2]Department of Biosystems Science and Engineering, ETH Zurich, Zurich, Switzerland; [3]Institute of Pathology, Lausanne University Hospital, Lausanne University, Lausanne, Switzerland; [4]Hematology Service, Departments of Oncology and Laboratory Medicine, Lausanne University Hospital (CHUV) and University of Lausanne (UNIL), Lausanne, Switzerland; [5]Department of Orthopedics and Traumatology, Lausanne University Hospital and University of Lausanne, Lausanne, Switzerland; [6]Laboratory of Systems Biology and Genetics, Institute of Bioengineering, School of Life Sciences, Ecole Polytechnique Fédérale de Lausanne (EPFL), Lausanne, Switzerland; [7]Department of Biomedical Sciences, University of Lausanne (UNIL/CHUV), Lausanne, Switzerland

Background: The heterogeneity of the human bone marrow (BM) stromal niche is critical for understanding its role in physiology and disease, as well as applying novel concepts of BM niche regulation in regenerative medicine. Here, we used hematon units (HUs) to analyze in-situ the relative stromal cell composition and the spatial organization of the human BM niche.
Methods: We obtained HUs through gentle dissociation of BM tissue debris from either orthopedic patient samples or BM aspirates and developed a panel of fifteen human stromal markers in full BM tissue specimens using immunohistochemistry. Expression patterns in HUs were compared to the bone-containing tissue specimens employing multiplex immunofluorescence and advanced multicolor whole-mount 3D imaging to assess HUs stromal heterogeneity.
Results: We cultured the HUs after gentle mechanical dissociation, and we were able to recover the stromal components and validate their presence using flow cytometry. We established and validated an immunohistochemistry panel of fifteen human BM stromal markers covering the different BM non-hematopoietic sub-niches (endosteal, perivascular, adipocytic, and BM stromal cells). We then compared their expression to nonneoplastic complete BM tissue specimens and applied multicolor 3D imaging to determine HU stromal heterogeneity. We describe, for the first time, the co-expression of human BM stromal cell surface markers in situ, as well as their highly multiplexed spatial distribution and micro-anatomic localization.
Conclusions: Our findings confirm the existence of stromal heterogeneity within the human hematopoietic BM niche, both in composition and spatial distribution and suggest the potential for HUs as an ex vivo model to study the heterogeneity of the human BM stroma in physiological and malignant hematopoiesis.
*Student submission

A 26
Potenzial and feasibility of federated learning in digital pathology

Ms. Lydia Schönpflug[1]*, Mr. Ruben Bagan Benavides[2], Dr. Marta Nowak[3], Dr. Fahime Sheikhzadeh[2], Dr. Yao Nie[2], Mr. Norbert Wey[3], Mr. Michael Zhou[2], Mr. Jacob Reimers[4], Mr. Lukas Loeffel[4], Mr. Mark Rominski[4], Mr. Kamil Wasąg[2], Ms. Yasmin Koeller[4], Mr. Raghavan Venugopal[2], Mr. Michael Rivers[2], Prof. Holger Moch[1], Prof. Viktor H. Kölzer[3], Mx. Tumor Profiler Consortium[5]

[1]Department of Pathology and Molecular Pathology, University Hospital Zurich, University of Zurich, Zurich, Switzerland; [2]Roche Diagnostics Solution, Computational Science and Informatics, Santa Clara, CA, USA; [3]Department of Pathology and Molecular Pathology, University Hospital of Zurich, Zurich, Switzerland; [4]Roche Diagnostics International AG, Rotkreuz, Switzerland; [5]Various institutions, Zurich, Switzerland

Background: In digital pathology (DP), deep learning (DL) enables automated analysis of whole slide images, but requires many heterogeneous training examples. Due to data privacy, interoperability and security restrictions, building centralized data repositories is increasingly seen as an obsolete strategy, limiting the progress of technology development in digital healthcare. Federated Learning (FL) addresses these challenges. Instead of transferring data out of the institute of origin, its key technological principle is to bring the model to the data in a federated training process. Here we demonstrate the feasibility of implementing FL in DP across several institutions and provide a proof of principle for DP algorithm development.
Methods: We train DL algorithms in a federated manner for two key tasks in DP, tumor compartment segmentation and cell detection, utilizing a cohort from the Swiss Tumor Profiler study. The cohort consists of $n=126$ high-quality digital scans of CD8 immunohistochemistry stained slides, originating from 116 melanoma patients. It was split into a training ($n=34$) and test dataset ($n=80$). Our FL setup includes three clients located in Switzerland and the U.S. and a cloud-based server (**Fig. 1**). The performance of FL models is evaluated against centralized models on the test set.
Results: As a proof-of-principle, we successfully established connection between all FL participants and jointly trained models for DP biomarker development. The tumor compartment segmentation and cell detection algorithms achieved mean F1-Score of 0.801 and mean average precision of 0.713, respectively, when trained in a federated manner, compared to 0.816 and 0.675 when trained in a centralized manner (Tables 1 and 2).

	Centralized Training	Federated Learning
Mean average precision (mAP)	0.675	**0.713**
Precision	0.7217	**0.7557**
Recall	0.8040	**0.8167**
CCC	0.9860	**0.9911**
F1-Score	0.7681	**0.7850**

Fig. 1 | A 26 ▲ Comparison of cell detection performance on the test dataset between Centralized Training and FL. The cell detection model output is a heatmap, with pixel values ranging from 0 to 1, indicating their probability of being a cell. For this reason, a threshold is required to detect possible cell candidates from the heatmap. Mean average precision is a composite metric that measures model performance across all possible thresholds. We additionally give the detailed performance for a specific threshold that was selected based on maximizing the F1-Score on a separate validation dataset. All metrics range from 0 to 1, higher value indicates better performance
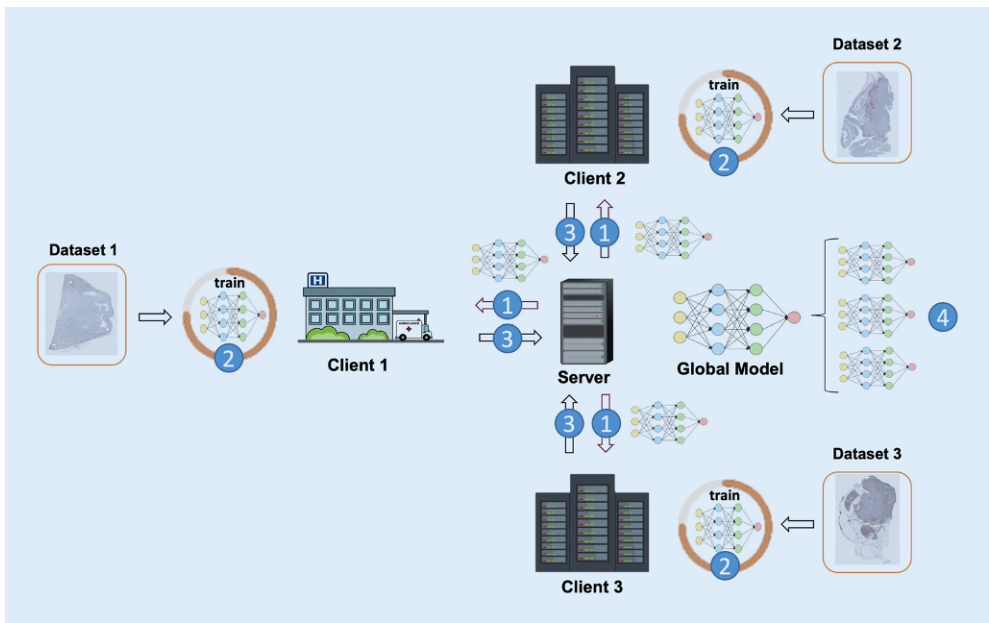
Fig. 2 | A 26 ◄ Federated Learning setup. Each iteration consists of the following steps: (1) Distribution of the global model to each client, (2) local training of the model on each client's data, (3) returning the trained client models to the server and (4) model aggregation into an updated global model

| Centralized Training				Federated Learning			
	IoU	F1-Score	CCC		IoU	F1-Score	CCC
Tumor	**0.938**	**0.968**	0.974	Tumor	0.931	0.965	0.974
Desmoplastic stroma	**0.575**	**0.730**	**0.971**	Desmoplastic stroma	0.517	0.683	0.958
Inflamed stroma	0.633	0.775	0.945	Inflamed stroma	**0.637**	**0.778**	**0.965**
Artifact	**0.656**	**0.792**		Artifact	0.640	0.781	
- Pigment			0.989	- Pigment			**0.997**
- Necrosis			**0.96**	- Necrosis			0.900
- Glass			0.939	- Glass			**0.943**
Mean	**0.700**	**0.816**	**0.963**	Mean	0.681	0.801	0.956

Fig. 3 | A 26 ◄ Comparison of tumor compartment segmentation performance on the test dataset between Centralized Training (left) and FL (right). IoU: Intersection over Union, CCC: Concordance Correlation Coefficient. All metrics range from 0 to 1, higher value indicates better performance

Conclusions: We demonstrated the feasibility of training a DL model across multiple institutions while maintaining data privacy and achieving equivalent algorithm performance. In future experiments, we plan to investigate the impact of data heterogeneity, different aggregation methods and potential threats.

A 27
Immunoprofiling of the SCOT and QUASAR2 clinical trials of stage II and stage III colorectal cancer by image analysis and multiplex immunofluorescence

Ms. Anja L. Frei[1]*, Mr. Anthony McGuigan[2], Mr. Ritik Sinha[2], Dr. Mark Glaire[2], Mr. Faiz Jabbar[2], Dr. Luciana Gneo, Ms. Tijana Tomasevic[2], Dr. Andrea Harkin[3], Prof. Tim Iveson[4], Dr. Mark Saunders[5], Prof. Karin Oien[6], Dr. Noori Maka[6], Prof. Francesco Pezzella[7], Ms. Leticia Campo[8], Dr. Jennifer Hay[6], Prof. Joanne Edwards[9], Prof. Owen Sansom[10], Dr. Caroline Kelly[3], Prof. Ian Tomlinson[8], Dr. Wanja Kildal[11], Dr. Rachel Kerr[8], Prof. David Kerr[7], Prof. Håvard Danielsen[11], Dr. Enric Domingo[12], Prof. David N. Church[2], Prof. Viktor H. Kölzer[1]

[1]Department of Pathology and Molecular Pathology, University Hospital of Zurich, Zurich, Switzerland; [2]Nuffield Department of Medicine, University of Oxford, Oxford, UK; [3]CRUK Clinical Trials Unit, University of Glasgow, Glasgow, UK; [4]Southampton University Hospital NHS Foundation Trust, Southampton, UK; [5]The Christie NHS Foundation Trust, Manchester, UK; [6]Glasgow Tissue Research Facility, University of Glasgow, Queen Elizabeth University Hospital, Glasgow, UK; [7]Nuffield Division of Clinical Laboratory
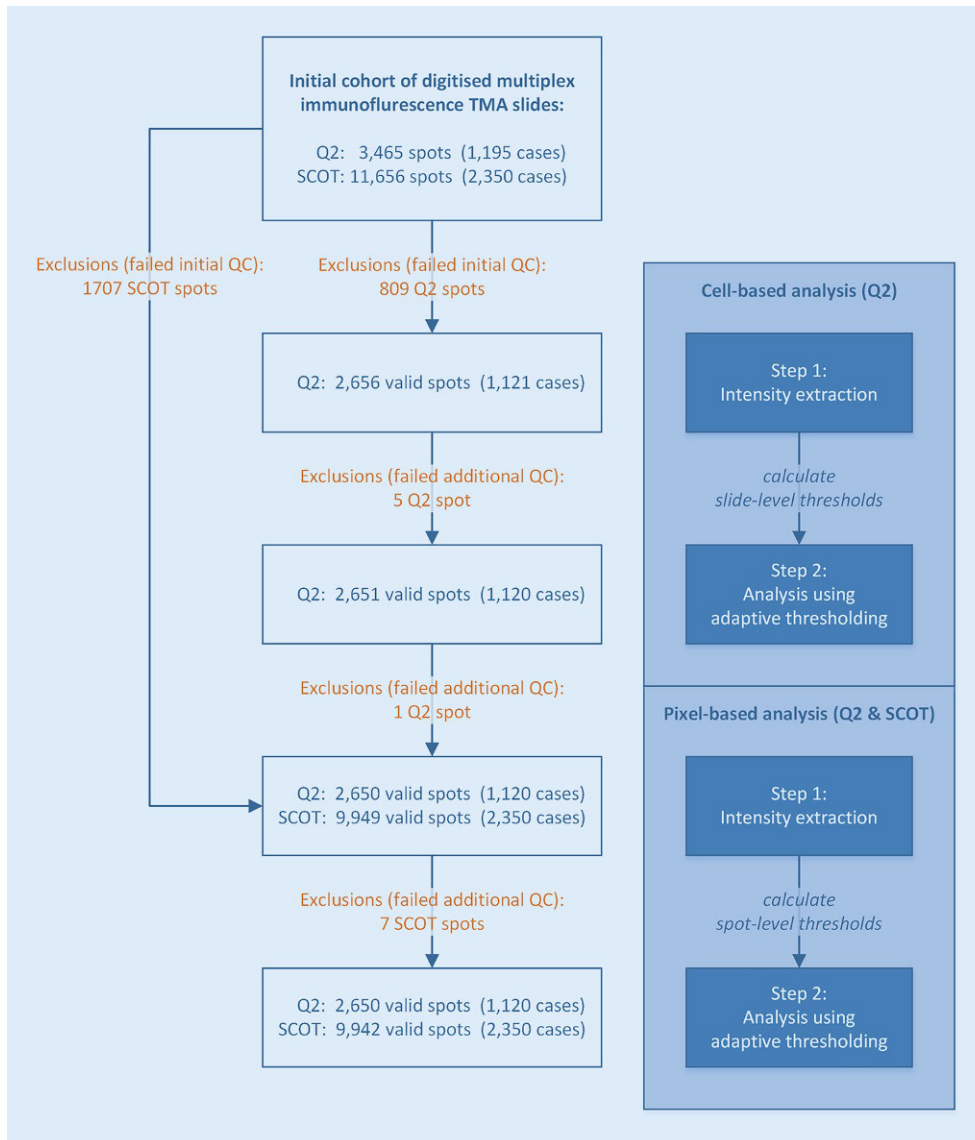
Fig. 1 | A 27 ◀ Schematic analysis workflow. Schematic visualisation of the analysis workflow and corresponding numbers of included/excluded spots and cases based on manual quality control (QC) [1]. (published under CC BY 4.0 international license https://creativecommons.org/licenses/by/4.0)

Initial cohort of digitised multiplex immunoflurescence TMA slides:

Q2: 3,465 spots (1,195 cases)
SCOT: 11,656 spots (2,350 cases)

Exclusions (failed initial QC): 1707 SCOT spots

Exclusions (failed initial QC): 809 Q2 spots

Q2: 2,656 valid spots (1,121 cases)

Exclusions (failed additional QC): 5 Q2 spot

Q2: 2,651 valid spots (1,120 cases)

Exclusions (failed additional QC): 1 Q2 spot

Q2: 2,650 valid spots (1,120 cases)
SCOT: 9,949 valid spots (2,350 cases)

Exclusions (failed additional QC): 7 SCOT spots

Q2: 2,650 valid spots (1,120 cases)
SCOT: 9,942 valid spots (2,350 cases)

Cell-based analysis (Q2)
Step 1: Intensity extraction
calculate slide-level thresholds
Step 2: Analysis using adaptive thresholding

Pixel-based analysis (Q2 & SCOT)
Step 1: Intensity extraction
calculate spot-level thresholds
Step 2: Analysis using adaptive thresholding

Sciences, University of Oxford, Oxford, UK; [8]Department of Oncology, University of Oxford, Oxford, UK; [9]School of Cancer Sciences, University of Glasgow, Glasgow, UK; [10]CRUK Beatson Institute of Cancer Research, Glasgow, UK; [11]Institute for Cancer Genetics and Informatics, Oslo University Hospital, Olso, Norway; [12]Department of Oncology, Medical Sciences Division, University of Oxford, Oxford, UK

Background: Tumour immunoprofiling is important to understand the dynamic relationship of cancer cells and the local microenvironment. Multiplex immunofluorescence (mIF) imaging and digital image analysis are a powerful tool to provide comprehensive quantitative and spatial information on multiple immune markers. However, digital image analysis of large multi-centric clinical trial cohorts can be challenging due to pre-analytical heterogeneity and technical variation in staining results.

Methods: We analysed tissue microarrays (TMAs) containing samples from 3545 colorectal cancers (CRC) sourced in two clinical trials (QUASAR 2 and SCOT) and stained for CD4, CD8, CD20, CD68, FoxP3, pan-cytokeratin and DAPI by mIF. We performed tissue segmentation for spatial marker localization in epithelial and stromal area and applied cell-based and pixel-based marker analysis. Additionally, we developed an adaptive thresholding method for handling inter- and intra-slide staining variation in digital image analysis of TMA cohorts and performed an integrative analysis of image-derived data with clinical outcomes.

**Results:** Applying our image analysis approach substantially improved results of digital analysis as determined expert pathologist. Pixel-based and cell-based analysis results were highly correlated (Spearman's rank correlation coefficient $\rho > 0.8$, $p \ll 0.01$, except for CD20 in epithelium region). Correlation of mIF-derived CD8 data with orthogonal immunohistochemistry-derived CD8 data emphasized validity of our analysis approach ($\rho = 0.63$–0.66, p-value $\ll 0.01$). Analysis of markers with clinical outcome data showed prognostic value of intraepithelial CD8 as well as for intrastromal FoxP3. A composite marker showed even higher prognostic value as either marker alone (hazard ratio for 75th vs 25th percentile $HR^{75vs25} = 0.70$, 95% CI $= 0.63$–0.78, $p \ll 0.01$), refining risk groups with respect to recurrence-free survival.

Conclusions: Our proposed method for handling staining variation in multiplexed TMA cohorts could enable immunoprofiling on large-scale clinical trial datasets showing substantial pre-analytical heterogeneity. Our results suggest that combined evaluation of intraepithelial CD8 and intrastromal FoxP3 could improve risk stratification in CRC.

References

1. Frei AL, McGuigan A, Sinha Ritik RAK. Accounting for intensity variation in image analysis of large-scale multiplexed clinical trial datasets. https://doi.org/10.1002/cjp2.342
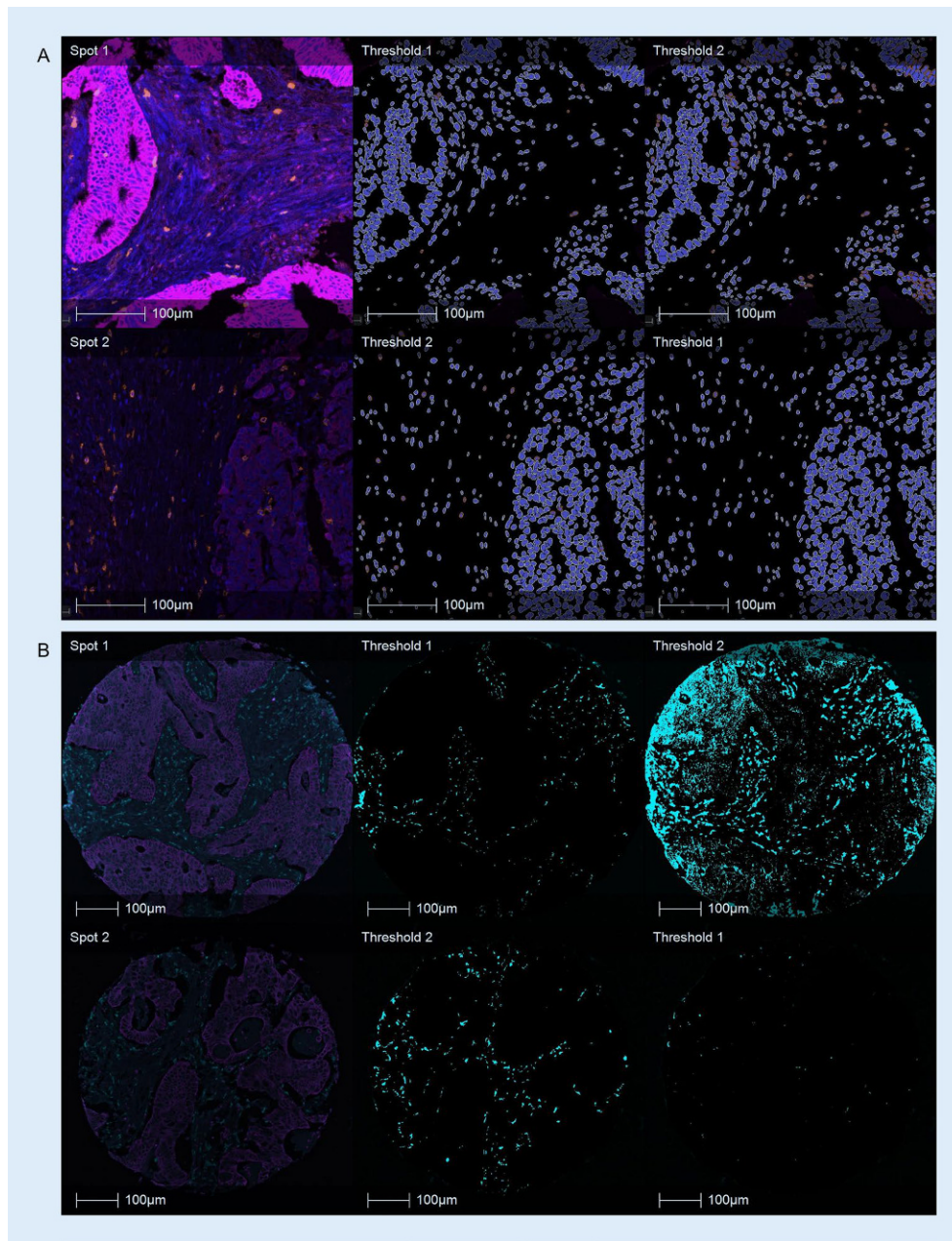
Fig. 2 | A 27 ◄ Visual comparison of image analysis with and without adaptive thresholding. a Example from the Q2 cohort for cell-based marker analysis (CD8) with and without slide-specific thresholding. The two spots are sourced from different slides. Left: original image (blue, DAPI channel; orange, CD8 channel; magenta, pan-cytokeratin channel); middle: cell-level markup using suggested slide-specific threshold; right: cell-level analysis markup using slide-specific threshold suggested for the other spot, simulating global thresholding. Cells marked as marker positive are indicated by orange cytoplasm in the analysis markup. b Example from the SCOT cohort for pixel-based marker analysis (CD68) with and without spot-specific thresholding. Both spots are from the same slide. Left: original image (turquoise, CD68 channel; magenta, pan-cytokeratin channel); middle: pixel-level markup using suggested spot-specific threshold; right: pixel-level analysis markup using spot-specific threshold suggested for the other spot, simulating global thresholding. Pixels marked as CD68 positive are indicated by turquoise colour in the analysis markup [1]. (published under CC BY 4.0 international license https://creativecommons.org/licenses/by/4.0)
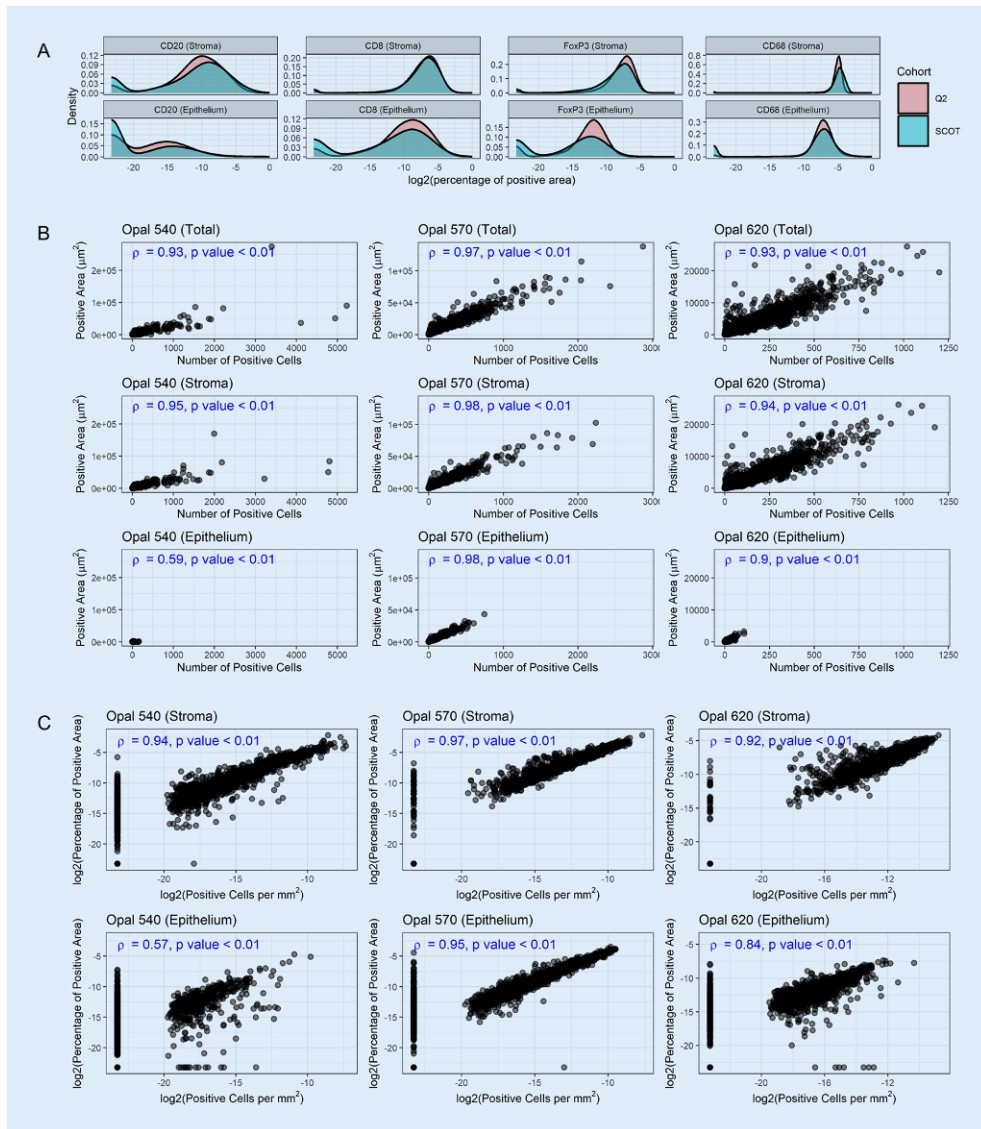
Fig. 3 | A 27 ◄ Pixel-based analysis: density distribution and comparison with cell-based analysis. **a** Comparison of the density distribution across the Q2 and the SCOT cohort. **b** Comparison of absolute measurements: number of positive cells versus the amount of positive area, separated per marker and stromal/epithelial compartment, in the Q2 cohort. **c** Comparison of density measurements: number of positive cells per area versus the amount of positive area in relation to the total area, separated per marker and stromal/epithelial compartment, in the Q2 cohort [1]. (published under CC BY 4.0 international license https://creativecommons.org/licenses/by/4.0)

A 28
Swiss digital pathology recommendations: results from a Delphi process conducted by the Swiss Digital Pathology Consortium of the Swiss Society of Pathology

Prof. Andrew Janowczyk[1]*, Prof. Inti Zlobec[2], Mr. Cedric Walker[3], Prof. Sabina Berezowska[4], Dr. Viola Huschauer[5], Prof. Marianne Tinguely[6], Mr. Joel Kupferschmid[7], Mr. Thomas Mallet[8], Prof. Doron Merkler[9], Dr. Mario Kreutzfeldt[10], Mr. Radivoje Gasic[11], Dr. Tilman Rau[12], Prof. Luca Mazzucchelli[13], Dr. Isgard Eyberg[14], Prof. Gieri Cathomas[15], Prof. Kirsten Mertz[16], Prof. Viktor H. Kölzer[17], Dr. Davide Soldini[18], Prof. Wolfram Jochum[19], Dr. Matthias Rössle[20], Dr. Maurice Henkel[21], Prof. Rainer Grobholz[22]

[1]Department of Diagnostics, Division of Clinical Pathology, Geneva University Hospitals, Geneva, Switzerland; [2]Institute of Tissue Medicine and Pathology, University of Bern, Bern, Switzerland; [3]Institute of Animal Pathology, University of Bern, Bern, Switzerland; [4]Department of Laboratory Medicine and Pathology, Institute of Pathology, Lausanne University Hospital, University of Lausanne, Rue du Bugnon 25, 1011 Lausanne, Switzerland; [5]Institute of Pathology Enge, Zurich, Switzerland; [6]Pathologie Institut Enge, Enge, Switzerland; [7]Basys Data GmbH; [8]Division of Clinical Pathology, Geneva University Hospital, Geneva, Switzerland; [9]Service of Clinical Pathology, Department of Diagnostics, Geneva University Hospital, Geneva, Switzerland; [10]Department of Diagnostics & Department of Pathology and Immunology, Division of Clinical Pathology, Geneva University and Geneva University Hospitals, Geneva, Switzerland; [11]Cantonal Hospital Aarau, Aarau, Switzerland; [12]Institute of Pathology, University Hospital and Heinrich-Heine University Düsseldorf, Germany; [13]Institute of Pathology, Ente Ospedaliero Cantonale (EOC), Locarno, Switzerland; [14]Institute of Pathology, Cantonal Hospital Aarau; [15]Institute of Tissue Medicine and Pathology, University of Bern, Bern, Switzerland; [16]Institute of Pathologie, Cantonal Hospital Baselland, Liestal, Switzerland; [17]Department of Pathology and Molecular Pathology, University Hospital of Zurich, Zurich, Switzerland; [18]Pathologie Zentrum Zürich medica, Zurich, Switzerland; [19]KSSG, Institut für Pathologie, St-Gallen, Switzerland; [20]Pathologie Luzerner Kantonsspital, Lucerne, Switzerland; [21]Research & Analytic Services University Hospital Basel, Basel, Switzerland; [22]Institute of Pathlogy Kantonspital Aarau, Aarau, Switzerland

Background: Integration of digital pathology (DP) into clinical diagnostic workflows is increasingly receiving attention as new hardware and software become available. To facilitate adoption of DP, the Swiss Digital Pathology Consortium (SDiPath) organized a Delphi process to produce a series of recommendations for DP integration within Swiss clinical environments.

Methods: This process saw creation of 4 working groups, focusing on various components of DP systems: (1) Scanners, Quality Assurance and Validation of Scans, (2) Integration of WSI-scanners and DP systems into the Pathology Laboratory Information System, (3) Digital Workflow–compliance with general quality guidelines, and (4) Image analysis (IA)/artificial intelligence (AI), with topic experts for each recruited for discussion and statement generation:

Results: The work product of the Delphi process is 83 consensus statements, forming "SDiPath Recommendations for Digital Pathology". We are happy to report significant concordance between existing national recommendations and our own, likely due to the converging nature of what appears to be emerging best practices for DP. These recommendations integrate and update upon previous guidelines, providing a dedicated section on the implementation of AI and IA. This fills a niche absent from other recommendations, likely due to the nascent nature of AI/IA field during their creation.

Conclusions: Using a Delphi process, members of SDiPath reached consensus on practical recommendations for the implementation and validation of DP in clinical workflows. These recommendations focused on its safe usage, with attempts at maximizing patient safety and benefit while minimizing overhead. As a result, we put forward these statements as best-practices when adopting DP within Switzerland. Of particular note was that working groups appreciated how rapidly the field is maturing, and realized that, unlike other more established technologies, these DP recommendations will likely need to undergo revisions as technology and the associated implications of this paradigm-shifting technology become more clear.

A 29*

Lymph node immune landscaping in COVID-19 infection: germinal center Bcl6 reactivity is associated with a distinct immune cell composition and spatial transcriptomic profile.

Mrs. Cloé BRENNA[1]*, Mr. MICHAIL ORFANAKIS[1], Mrs. Kalliopi IOANNIDOU[1], Prof. Giuseppe Pantaleo[2], Dr. Petrovas Konstantinos[1]

[1]Institute of Pathology, Department of Laboratory Medicine and Pathology, Lausanne, Switzerland; [2]Service of Immunology and Allergy, Department of Medicine, CHUV, Lausanne, Switzerland

Background: The human follicular immune dynamics during an acute viral infection are largely unknown. COVID-19 infection is associated with higher viral loads and general inflammation in elderly people. We took advantage of available autopsic LN from COVID 19 infected individuals to investigate the *in situ* follicular dynamics at cellular and molecular level and with respect to aging.

Methods: Hilar (draining site for infected lungs) (>60y, $n = 22$ and <60y, $n = 10$, hospitalization time; 3–45d) and sub-diaphragmatic (distal, control site) LNs (>60y, $n = 8$) subjects were analyzed by i) multiplex immunofluorescence (mIF) assays allowing for the in situ detection of CD4, CD8, B cell, innate immunity cell types, and metabolic profile of cell type and ii) the GeoMx digital spatial profiling platform and the Human Atlas gene set. Quantitative analysis of imaging data was carried out by HistoCytom-

etry. Transcriptomic data were analyzed using the GeoMx DSP program and Python scripts.

Results: Despite the presumed inflammation, several tissues were characterized by follicles without or low expression of Bcl6, in line with previously reported data (Kaneko N et al., Cell 2020 Oct1,183(1)). An association between the measured Bcl6+CD20+ and proliferating Ki67+ B cells, PD1+Ki67+ and PD1+CD57+ TFH cells was found, indicating more mature GCs in tissues with high Bcl6 positivity. The numbers of CD20+Ki67+/+Bcl6+ and PD1+Bcl6+ cells were reduced in sub-diaphragmatic LNs compared to hilar LNs indicating less active follicles in this control site. Increased CD68 and myeloperoxidase numbers were found in high Bcl6 positivity tissues. Distinct molecular profiles between tissues with different GC Bcl6 positivity were found, while increased interferon alpha/gamma and TNF-mediated pathways were found in GCs from donors without Bcl6 activity.

Conclusion: a compromised germinal center maturation in draining LNs from several COVID 19 infected donors. Our data point to possible in situ operating pathways mediating the development of Bcl6 GC reactivity in COVID-19 infection.

*Student submission

A 30*

Cell instance segmentation and detection in fresh frozen h&e-stained histopathology slides using deep learning techniques

Mr. Meisam Asgari Jirhandeh[1]*, Ms. Ana Leni Frei[2], Prof. Andreas Fischer[3], Prof. Inti Zlobec[2]

[1]Institute of Computer Science, University of Bern, Bern, Switzerland; [2]Institute of Tissue Medicine and Pathology, University of Bern, Bern, Switzerland; [3]Institute of Artificial Intelligence and Complex Systems (iCoSys), University of Applied Sciences and Arts Western Switzerland (HES-SO), Fribourg, Switzerland

Background: Biomedical research increasingly employs Fresh Frozen (FF) tissue, due to its molecular components preservation and faster sample preparation benefits. This trend has led to a rising interest in automating cell segmentation/detection for FF cell-based analysis. However, pursuit of this automation comes with numerous challenges arising from the rapid preparation process, resulting in highly variable cell shapes and staining patterns. Our objective is to adapt established deep learning cell segmentation solutions from Formalin-Fixed Paraffin-Embedded (FFPE) samples, fine-tuning them for Hematoxylin and Eosin (H&E) sections of frozen tissue samples.

Methods: Two widely-used FFPE cell segmentation deep learning models, Cellpose and StarDist, alongside a baseline Unet model enhanced by Watershed algorithm, were investigated for FF samples. Training involved FF H&E-stained tiles from CryoNuSeg, MoNuSeg, and a colorectal cancer dataset from the Tissue Biobank Bern (TBB), while testing employed a dis-

Model	AP@0.5		F1-Score	
	Mean	95% CI	Mean	95% CI
Cellpose	**0.587** ± 0.194	[0.525, 0.648]	**0.801** ± 0.134	[0.759, 0.844]
StarDist	0.553 ± 0.189	[0.494, 0.613]	0.771 ± 0.147	[0.724, 0.817]
Unet with Watershed	0.393 ± 0.189	[0.333, 0.453]	0.684 ± 0.161	[0.633, 0.735]

Fig. 1 | A 30 ◄ Optimized models' performance on the test set

Model_Pair	p-value (Paired t-test)				p-value (Wilcoxon Signed-Rank test)			
	AP@0.5	<5%	F1-Score	<5%	AP@0.5	<5%	F1-Score	<5%
Cellpose-StarDist	0.0204	✓	0.0050	✓	0.0137	✓	0.0017	✓
Cellpose-Unet	1.94e-10	✓	1.18e-06	✓	3.45e-09	✓	6.30e-06	✓
StarDist-Unet	1.18e-07	✓	0.0005	✓	2.95e-07	✓	0.0008	✓

Fig. 2 | A 30 ◄ Comparative statistical analysis of the optimized models' performance on the test set
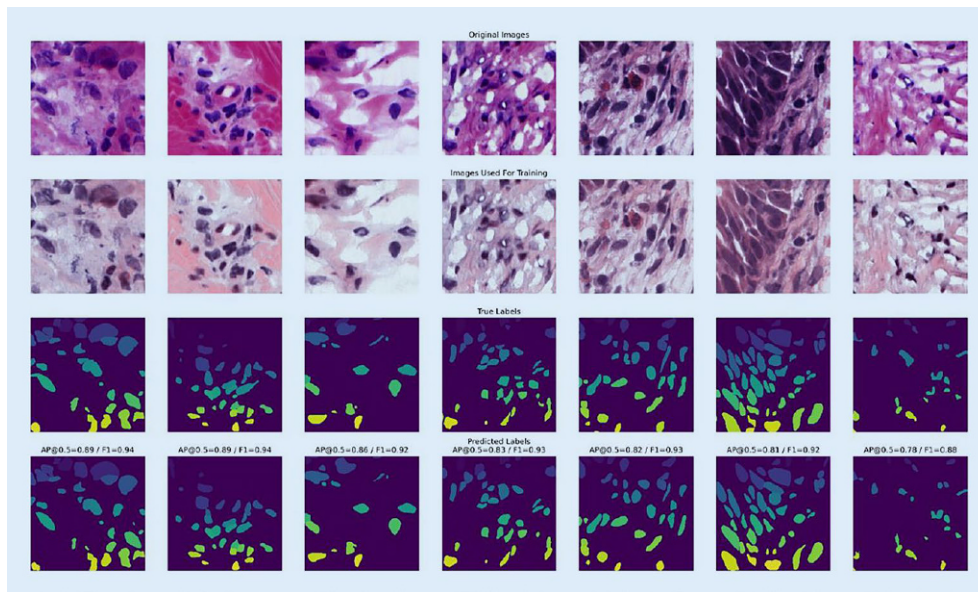
Fig. 3 | A 30 ▲ Illustration of the segmentation results obtained with the fine-tuned Cellpose model on a subset of the test dataset. *Top Row*: Original images, *Second Row*: Stain normalized images used by the model (pre-processed images), *Third Row*: Ground truth instance labels, *Bottom Row*: Segmentation predictions by the optimized Cellpose model

tinct subset of colorectal cancer samples from TCGA and TBB datasets. Meticulous cell annotations were performed for TCGA and TBB tiles. All tiles were stain normalized using the Macenko method. Leveraging transfer learning, existing pre-trained Cellpose and StarDist models were fine-tuned for FF H&E-stained tiles.

Results: The fine-tuned "cyto2" Cellpose model significantly outperformed the other two models in cell segmentation and detection on the test set (p-value < 0.05). It achieved 80.1% average F1-score and 58.7% mean Average Precision at 50% overlap threshold (mAP@0.5) for cell detection and instance segmentation, respectively. Compared to StarDist, Cellpose demonstrated 3% higher average F1-Score and 3.4% higher mAP@0.5, while outperforming Unet with Watershed by a significant 11.7% in average F1-Score and 19.4% in mAP@0.5.

Conclusion: The fine-tuned Cellpose model exhibited remarkable proficiency in tackling the automating cell segmentation challenges in FF H&E-stained slides, particularly in accurately delineating and detecting cells with irregular or non-round shapes. This advancement facilitates quantitative analysis of FF slides and mitigates inter/intra-observer variability and subjectivity.

*Student submission

A 31

Overcoming inter-observer-variability for assigning slide-level tumor content estimates by deep-learning tissue segmentation

Ms. Lydia Schönpflug[1]*, Dr. Enric Domingo[2], Dr. Maxime Lafarge[1], Ms. Anja L. Frei[3], Dr. Aikaterini Chatzipli[4], Dr. Susan Richman[5], Mr. Andrew Blake[2], Ms. Claire Hardy[4], Ms. Celina Whalley[6], Dr. Keara Redmond[7], Prof. Ian Tomlinson[8], Dr. Philip Dunne[7], Dr. Steven Walker[9], Prof. Andrew Beggs[6], Dr. Ultan McDermott[4], Dr. Graeme Murray[10], Dr. Leslie Samuel[10], Prof. Matthew Seymour[5], Prof. Philip Quirke[5], Prof. Tim Maughan[2], Prof. Viktor H. Kölzer[3]

[1]Department of Pathology and Molecular Pathology, University Hospital Zurich, University of Zurich, Zurich, Switzerland; [2]Department of Oncology, Medical Sciences Division, University of Oxford, Oxford, UK; [3]Department of Pathology and Molecular Pathology, University Hospital Zurich, Zurich, Switzerland; [4]Wellcome Trust Sanger Institute, Hinxton, UK; [5]Leeds Institute of Cancer and Pathology, University of Leeds, Leeds, UK; [6]Institute of Cancer and Genomic Science, University of Birmingham, UK; [7]The Patrick G Johnston Centre for Cancer Research, Queens University Belfast, Belfast, UK; [8]Department of Oncology, University of Oxford, Oxford, UK; [9]Almac Diagnostics, Craigavon, UK; [10]School of Medicine, Medical Sciences and Nutrition, University of Aberdeen, Aberdeen, UK

Background: Reliably estimating tumor content (TC) in H&E slides is crucial for molecular pathology diagnostics including the selection of samples for molecular testing and correcting CNV calls. However, assigning a slide-level score by visual pathological review (VPR) can be difficult, as it requires combining all slide characteristics into a single score. This is prone to subjectivity and inter-observer variability. Deep learning (DL) methods provide more objective and reproducible results, but tend to lack explainability.

Methods: We train a U-Net model for tissue segmentation on the semi-supervised-learning for colorectal cancer detection (SemiCOL) dataset and derive a robust tumor detection score (◘ **Fig. 1**a). We validate our methodology by systematically comparing DL results with two slide-based technologies (VPR, pathologist-supervised tissue segmentation using HALO A[ITM]) and two molecular pathology approaches (bioinformatic deconvolution of TC from RNA sequencing data and DNA methylation arrays) on 470 cases with complete datasets and 573 cases with ≥2 technologies from the CRUK-MRC Stratification in Colorectal Cancer (S:CORT) Consortium.

Results: We achieve an AUROC score of 0.837 for tumor detection on the SemiCOL test set. On the S:CORT dataset, correlation of our method is strong with HALO A[ITM] TC estimates ($r = 0.88$), moderate with RNA- ($r = 0.65$) and weak ($r = 0.39$) with DNA-based TC estimates (◘ **Fig. 2**). Correlation of VPR with RNA- and DNA-based estimates is overall weaker ($r = 0.41$, $r = 0.30$, ◘ **Fig. 3**) and VPR tends to systematically underestimate TC, with only 21.8% of TC being > 50, in contrast to 67.7% for our method, highlighting the ability of DL tissue segmentation to support diagnostic practice.

Conclusions: DL enables objective and explainable slide-level TC estimation. The high performance on the SemiCOL dataset and better correlation with biological data as compared to VPR underlines the potential of DL in overcoming inter-observer variability. Moreover, mark-up of the segmentation results adds explainability, and can thus support expert pathologists in their assessment.
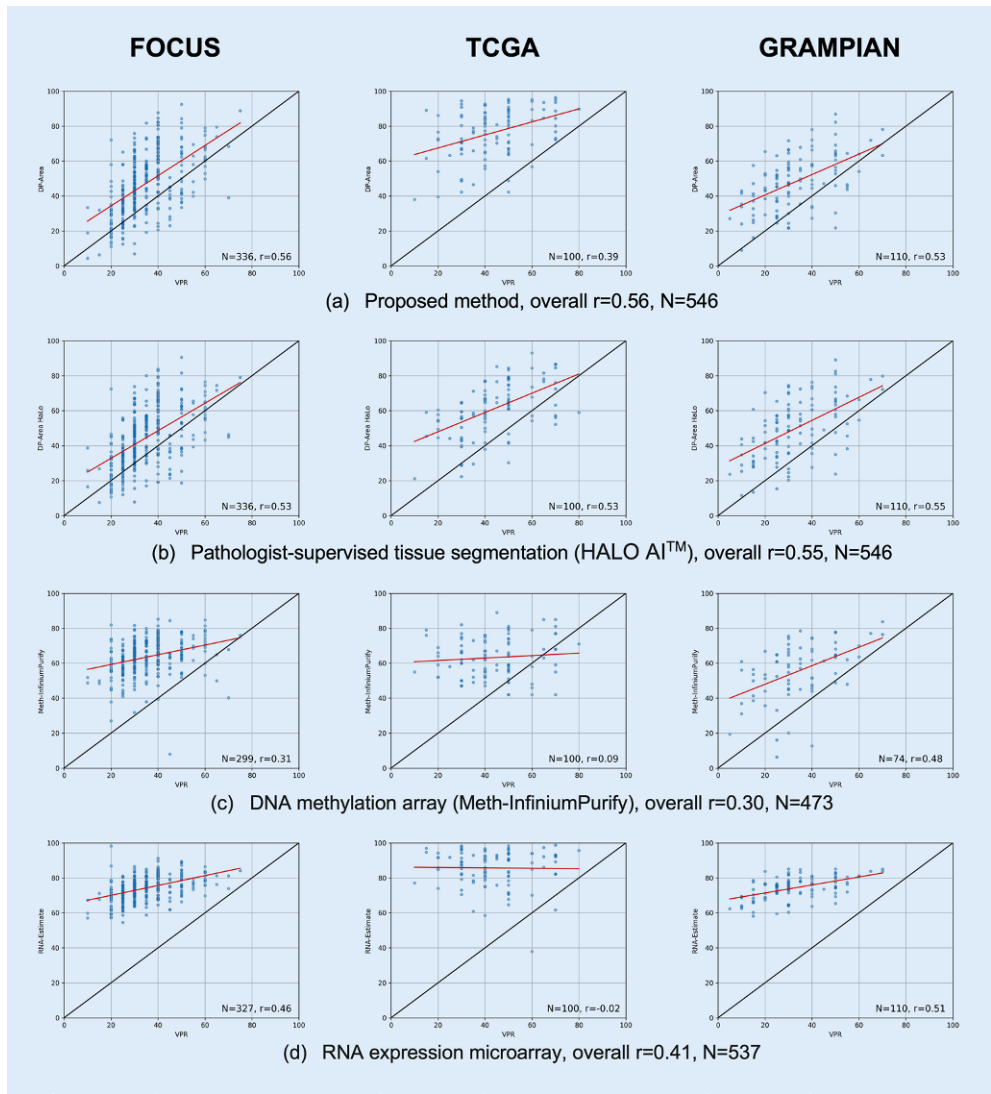
References

1. Schoenpflug LA, Laaefgr MW, Frei AL, Koelzer VH. Multi-task learning for tissue segmentation and tumor detection in colorectal cancer histology slides. https://arxiv.org/abs/2304.03101
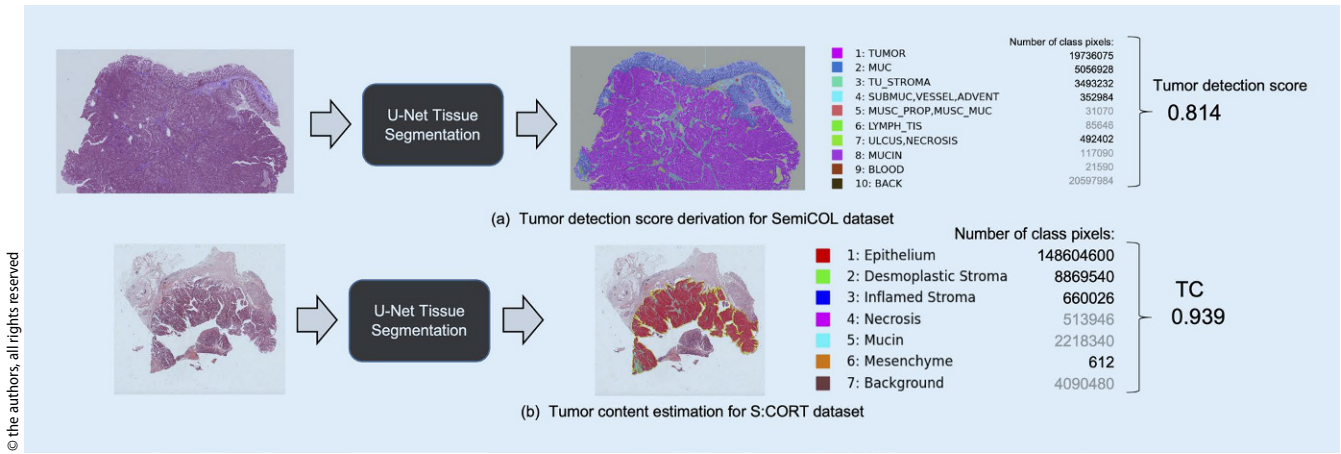
Fig. 1 | A 31 ▲ Workflow for deriving slide-level scores based on U-Net tissue segmentation: We compute the tissue segmentation prediction for the region of interest and combine the number of predicted class pixels into (a) Tumor detection score: TDS = (Tumor + Tumor stroma + ulcus and necrosis)/(Tumor + Tumor stroma + ulcus and necrosis + benign mucosu + submucosa) and (b) Tumor Content Estimation: TC = (Epithelium)/(Epithelium + Desmoplastic Stroma + Inflamed Stroma Mesenchyme). Overlay of the segmentation mask with the whole slide image allows for direct interpretation of the results and could potentially support pathologist slide assessment
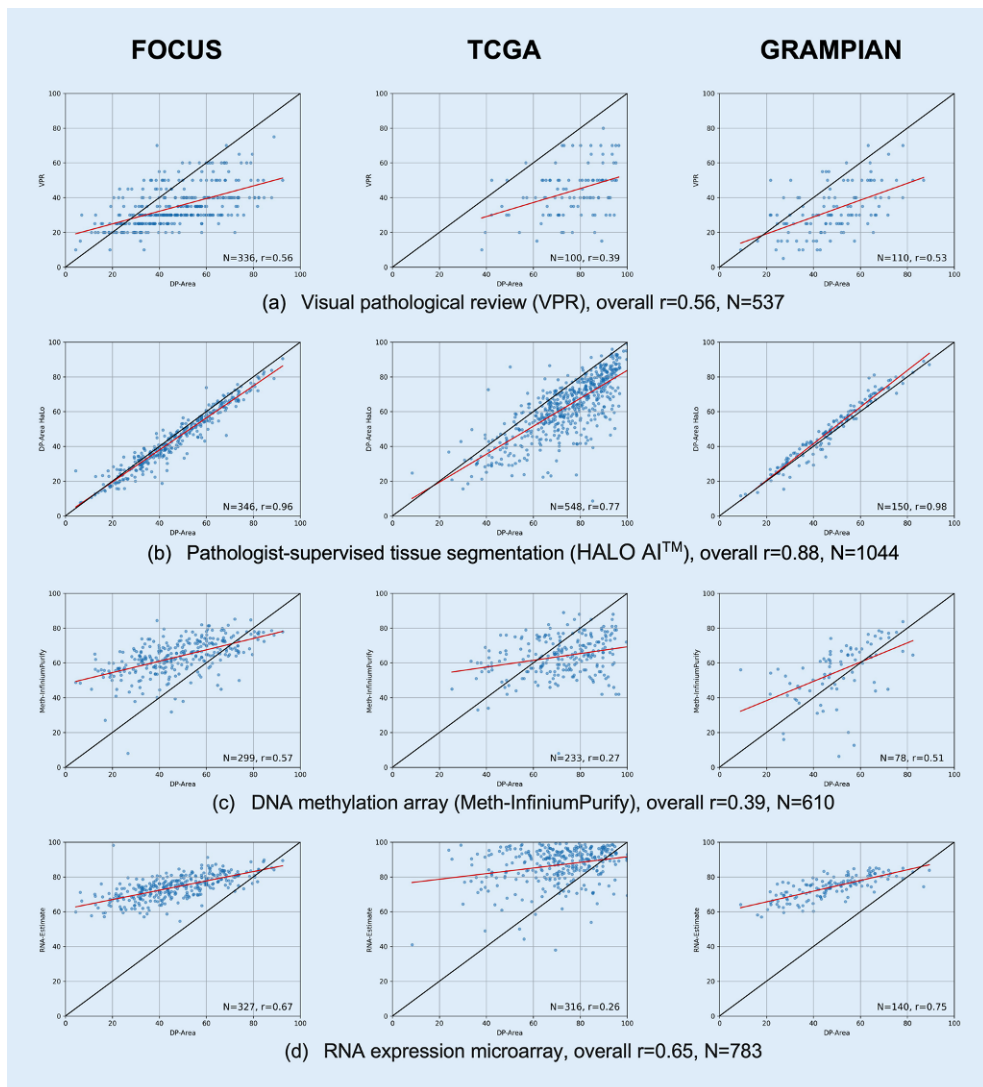
Fig. 2 | A 31 ◄ Correlation of tissue segmentation based TC estimation (DP-Area) with other methods. For $N = 470$ cases results are available across all 5 methods, for all other cases (additional $N = 574$) results are available for a subset of methods. For this reason, the sample size varies depending on the compared methods in the correlation analysis

FOCUS **TCGA** **GRAMPIAN**

(a) Proposed method, overall r=0.56, N=546

(b) Pathologist-supervised tissue segmentation (HALO AI™), overall r=0.55, N=546

(c) DNA methylation array (Meth-InfiniumPurify), overall r=0.30, N=473

(d) RNA expression microarray, overall r=0.41, N=537

Fig. 3 | A 31 ◀ Correlation of visual pathological review (VPR) based TC estimation with other methods. For $N = 470$ cases results are available across all 5 methods, for all other cases (additional $N = 574$) results are available for a subset of methods. For this reason, the sample size varies depending on the compared methods in the correlation analysis

A 32
Artificial intelligence solution for diagnosis and grading of prostate cancer biopsies in clinical practice

Prof. Rainer Grobholz[1]*, Ms. Mona Spoerri[2], Dr. Felice Burn[3], Mr. Philip Nahm[3], Prof. Maciej Kwiatkowski[4], Mrs. Leigh-Anne McDuffus[5], Mrs. Dana Mevorach[5], Mrs. Manuela Vecsler[5]

[1]Institute of Pathology Kantonspital Aarau, Aarau, Switzerland; [2]Institute of Pathology, Kantonsspital Aarau, Aarau, Switzerland; [3]Department of Informatics, Kantonsspital Aarau, Aarau, Switzerland; [4]Department of Urology, Kantonsspital Aarau, Aarau, Switzerland; [5]Ibex Medical Analytics, Tel Aviv, Israel

Background & objective: We aimed to test the accuracy of an artificial intelligence (AI)-tool for primary diagnosis of prostate carcinoma using real-world data. Emphasis was given on the accuracy of detection of Gleason patterns and assigning to the Gleason grade groups (GG).
Methods: The project included validation of the AI solution in clinical practice on 89 prostate biopsy cases that were retrieved from the archive (2017–2022). 19 cases with GG1, 15 with GG2, 16 with GG3, 22 with GG4 and 19 with GG5 were selected, reporting on 674 H&E slides. Accuracy for adenocarcinoma detection and Gleason grading of the original diagnosis were compared to the results of the AI. Cases with discrepancies were revised.
Results: The AI solution agreed with the ground truth (GT) in 100% of cases for carcinoma and generated identical or +1/−1 GG to the GT for 91%

of cases ($n = 81$). In 8 cases (9%) no GG was assigned by the AI. The highest levels of agreement were for GG 1 and 5 (100% and 89%, respectively). For GG 2–4, the AI findings were identical or +1/−1 GG to the GT for 100% of cases but had higher disagreement rates with respect to the amount of pattern 4. For GG2 and GG3 concordance rate was 57.1% and 26.6%, respectively. Part-level analysis demonstrated high accuracy, with an AUC of 0.992 (95% CI: 0.9857–0.999), NPV of 98.5% and PPV of 98.7% for carcinoma detection.
Conclusions: This study demonstrates the successful validation of a multi feature AI solution that aids to accurately detect all cancer areas and assign an accurate Gleason score. However, detection and quantifying of Gleason pattern 4 remains challenging, and some cases showed discrepancies and unresolved issues. AI can aid to detect and quantify the amount of this pattern in order to accurately assign the respective GG.

A 33
How many pathologists are working in Switzerland?

Dr. Philip Went[1]*, Prof. Zsuzsanna Varga[2], Dr. Sylvia Höller[3]

[1]Institute of Pathology, Kantonsspital Graubünden, Chur, Switzerland; [2]Department of Pathology and Molecular Pathology, University Hospital of Zurich, Zurich, Switzerland; [3]Institute of Pathology, Stadtspital Triemli, Zürich, Switzerland

Background: After a transitional period of several years, the cantons have now begun to restrict the number of physicians. This is the result of a federal law and the respective enforcement ordinance to determine maximum numbers of physicians. It concerns freely practicing and employed pathologists at hospitals. Exact figures on how many pathologists are active in Switzerland and how many are needed do not exist.

Methods: The specifications of the pathologists registered in MedReg were extracted in February 2023. The total of pathologists was retrieved from the register of FMH by the end of August 2023. Both registers are open to public inspection.

Results: In the MedReg, 576 pathologists were found (f: 289, m:287), including 49 molecular pathologists and 81 cytopathologists. The average number of years of professional experience after specialisation was 18.5 years, the average working time as a specialist in Switzerland, if specialisation has been done abroad, is 9.5 years. 330 pathologists (57%; 275 < 65a) have a residence licence to practice under own professional responsibility in 1 or more cantons. The pathologists working in Switzerland have obtained their medical diploma in 29 different countries and their specialisation in 18 countries. 78% of the registered specialists are < 65a, the average age of pathologists < 65a is 49a (m: 51a, f: 48a).
In doctorfmh.ch, the registry of the FMH, 507 pathologists are included (57 molecular pathologists, 112 cytopathologists).

Conclusions: There are various registers of pathologists (MedReg, SGPath, FMH), which differ from each other and are therefore all inaccurate. The calculation proposed by the federal government (Obsan Report 5/2022) to determine cantonal maximum numbers of physicians is not applicable to pathologists. There is therefore a great risk that authorities will make disadvantageous decisions on the basis of false premises resulting in deteriorated pathology services for the Swiss population.

A 34*
Colorectal cancer screening in the canton graubünden: first preliminary results

Ms. Mia Cecilia Joost[1]*, Dr. Tatjana Vlajnic[1], Dr. Gianfranco Zala[2], Dr. Tanja Gradistanac[1], Dr. Philip Went[3]*

[1]Institute of Pathology, Kantonsspital Graubünden, Chur, Switzerland; [2]Krebsliga Graubünden, Chur; [3]Institute of Pathology, Kantonsspital Graubünden, Chur, Switzerland

Background: Colorectal cancer is one of the three most common cancers in Europe. To decrease the incidence, a colon cancer screening program was introduced in the canton Graubünden in 2020. Participation is voluntary following either personal invitation or self-registration. As screening method, a fecal immunochemical test (FIT) or a colonoscopy was available for selection. Here, we examined the results of the screening to date in terms of participation and pathologic findings.

Methods: A total of 20,018 individuals were invited to participate in the period from 01.10.2020 to 21.12.2022. Data regarding place of residence, screening method, age and gender were retrieved from databases of the Pathology Institute KSGR and the Cancer League GR. Biopsies were analyzed in terms of number of submissions, samples per person and diagnoses.

Results: In total, 5672/20'018 (28.3%) individuals were screened, with equal distribution of the sexes (f:2862, m:2810). The preferred screening method was colonoscopy (colonoscopies:4332, FIT:1340, *p* value < 0.00001). Regarding participation frequency, there was a difference between the different regions of the canton. Of the 4332 colonoscopies, 2465 submissions and 4285 samples were collected. Pathologic examina-

tion revealed 3711 benign epithelial proliferations (2086 adenomas, 717 serrated lesions, 908 others), 12 benign mesenchymal tumors, 2 neuroendocrine neoplasms and 18 adenocarcinomas.

Conclusions: The screening program in the canton Graubünden is a success in terms of quality. The participation rate was initially lower than in other countries, but an increasing participation over time was recorded. A possible reason is the remote geographical distribution of the population. Concurrent opportunistic screening (outside the programm) of the target population may contribute to the calculated participation rate. Furthermore, it can also be stated that these examinations represent a significant additional workload for the involved specialists.
*Student submission

A 35
dentification of miRNAs-mRNA circuits discriminating between monomorphic epitheliotropic intestinal T-cell lymphoma and enteropathy associated T-cell lymphoma

Dr. David Vallois[1]*, Mr. Vimel Rattina[1], Dr. Luis Veloza[1], Dr. Bettina Bisig[1], Prof. Philippe Gaulard[2], Dr. Edoardo Missiaglia[1], Prof. Laurence de Leval[1]

[1]Institute of Pathology, Lausanne University Hospital, Lausanne University, Lausanne, Switzerland; [2]Département de Pathologie, Hôpitaux Universitaires Henri Mondor, Assistance Publique des Hôpitaux de Paris, Créteil, France

Background: Primary intestinal T-cell lymphomas (ITCLs) encompass two main entities, enteropathy-associated T-cell lymphoma (EATL) and monomorphic epitheliotropic intestinal T-cell lymphoma (MEITL). These are rare and highly aggressive diseases. A previous study identified members of the miR-17/92 cluster as upregulated in 6 MEITL compared to 12 EATL. We aimed to characterize the miRNAs-mRNA circuits discriminating MEITL and EATL in a larger cohort.

Methods: We examined 75 Formalin Fixed Paraffin Embedded ITCLs samples (27 EATL and 48 MEITL) by total RNA sequencing and 54 samples (19 EATL and 35 MEITL) by the HTG EdgeSeq miRNA Whole Transcription Assay (2083 miRNAs). We searched for most impactful miRNA on gene expression by integrating RNA and miRNA sequencing data. After pairing miRNA-mRNA within differentially expressed mRNA and miRNA using the multimiR tool, we identified the most dominant miRNAs in this miRNA-mRNA network using miRmapper software. Finally, mRNAs targets of those miRNAs were functionally annotated using EnrichR and Cytoscape softwares.

Results: The supervised comparison identified 281 and 312 overexpressed miRNAs in EATL and MEITL, respectively. Members of the miR-106a-363 cluster were the most upregulated (Fold Change FC [12-94]) miRNAs in MEITL, together with some members of two other paralogous clusters (miR-17-92 and miR-106b-25). Upregulated miRNAs in EATL showed lower FC (29 miRNAs with a FC>2 [2–3.13]). Furthermore, several members of the miR-105/107 family (upregulated in MEITL) were identified among the most impactful miRNAs on mRNA expression. The functional annotation of their target mRNAs identified genes leading to inhibition of PI3K-AKT-mTor, cytokine and toll-like receptors signaling pathways and upregulation of cell cycle and EMT (Epithelial to mesenchymal Transition) pathways in MEITL samples.

Conclusions: miRNAs members of miR-105/107 family seemed to affect the most the gene expression profile comparison between MEITL and EATL, with PI3K-AKT-mTOR inhibition and cell cycle upregulation among the pathways most impacted by these miRNAs.

A 36
Robust identification of conventional and leukemic non-nodal mantle cell lymphomas using epigenetic biomarkers

Mr. Marco Bühler[1]*, Dr. Marta Kulis[2], Dr. Martí Duran-Ferrer[2], Dr. Cristina Lopez[2], Dr. Guillem Clot[2], Dr. Ferran Nadeu[2], Ms. Monica Romo[2], Dr. Eva Giné[3], Dr. Armando Lopez-Guillermo[3], Dr. Silvia Bea[2], Dr. Elias Campo[2], Dr. Jose Ignacio Martin-Subero[2]

[1]Department of Pathology and Molecular Pathology, University Hospital of Zurich, Zurich, Switzerland; [2]Institut d'Investigacions Biomèdiques August Pi i Sunyer (IDIBAPS), Barcelona, Spain; [3]Hematology Department, Hospital Clínic, Barcelona, Spain

Background: Mantle cell lymphoma (MCL) is a B cell lymphoma with heterogeneous clinical presentation and outcome. Recent tumor classifications (WHO5/ICC) recognize two subtypes of MCL: conventional MCL (cMCL) and leukemic non-nodal MCL (nnMCL). Current methods to identify the two subtypes include SOX11 expression, IGHV mutational status and gene expression profiling. Previous studies on the DNA methylation landscape of MCL identified two subtypes (C1 and C2) which broadly correspond to cMCL and nnMCL respectively.

Methods: Using available DNA methylation microarray data, 3 CpGs were determined to be sufficient to differentiate C1 MCL (cMCL) from C2 MCL (nnMCL). Locus specific DNA methylation pyrosequencing assays (BisPyroSeq) were developed with PCR products of 110 to 180 base pairs to ensure assay compatibility with all types of clinical material, including samples with low quality DNA.

Results: 17 MCL cases with multiple sample types were analyzed to validate the universal applicability of the assay, showing a concordant classification across sample types. Samples of 115 MCL patients were analyzed with the developed assays, identifying 98 C1 and 14 C2 cases, whereas 3 cases could not be unambigously classified. We found a very high correlation of classification with other available methods (SOX11, L-MCL16 gene expression assay, IGHV mutational status), although few cases had discordant results.

Conclusions: We developed a robust assay for the determination of MCL methylation subtypes by only analysing the DNA methylation level of 3 CpG, which can be applied to all types of clinical samples with sufficient tumor cell content (>60%). While there is a high correlation between different methods (DNA methylation, SOX11, IGHV, L-MCL16), few cases with discordant results were identified.

A 37
Fetal thyroid dysfunction, an uncommon cause of fetal demise

Dr. Valérie Kesseler[1]*, Dr. Joanna Sichitiu[2], Dr. Carole Gengler[1]

[1]Departement of Laboratory medicine and Pathology, Institute of Pathology, Lausanne University Hospital and University of Lausanne, rue du bugnon 25, 1011 Lausanne, Switzerland; [2]Service of gynecology and Obstetrics–Department of Woman–Mother–Child, Lausanne University Hospital and University of Lausanne, avenue Pierre-Decker 2, 1011 Lausanne, Switzerland

Background: Fetal hyperthyroidism is a rare, life-threatening condition that complicates 0.2% of pregnancies and is caused by transplacental transfer of thyroid-stimulating antibodies (TSA) in the setting of maternal Grave's disease (GD), even in clinically euthyroid mothers. The risk of fetal thyroid dysfunction is directly linked to maternal TSA titer.

We report a case of a fetal demise at 33 weeks gestational age (GA), in which the mother was previously treated by thyroidectomy for GD. No monitoring of the fetal thyroid was undertaken until referral to our center at 28 weeks. By that point, the fetus was already exhibiting advanced manifestations of hyperthyroidism (goiter, advanced bone maturation, fetal tachycardia, right heart hypertrophy). Concurrently, the mother's TSH receptor antibodies were markedly elevated (194.2 UI/L, reference range
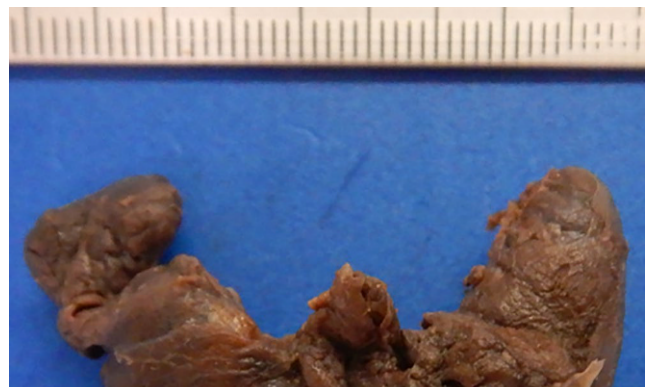

Fig. 1 | A 37 ▲

Fig. 1 | A 37 ▲

<1.75 UI/L). Despite administration of antithyroid drugs (propylthiouracil) and regular check-ups, fetal death occurred at 33 weeks GA.

Methods: The fetal autopsy procedure followed the Royal College of Pathologists standard protocol, including external and in situ internal examination with iconographic documentation and whole-body X-ray. The placenta was evaluated macroscopically according to the consensus statement of the Amsterdam Placental Workshop Group. Internal fetal organs and placenta were routinely processed for histology.

Results: The autopsy of a hypothrophic female fetus (body weight: 10th–30th percentiles) revealed a goiter (thyroid weight: 6.28 g), a bilateral ventricular hypertrophy and non-specific signs of acute fetal distress. X-rays confirmed advanced bone maturation (>41 weeks GA) and showed long tubular bones (70th–90th percentiles). Histology revealed a hyperplastic, non-inflammatory and congestive thyroid parenchyma and confirmed cardiac myocyte hypertrophy. Placental histology showed signs of fetal malperfusion, possibly related to cardiac arrhythmia.

Fig. 3 | A 37 ▲

Conclusion: Fetal thyroid dysfunction is a rare complication of maternal GD, with early intrauterine multidisciplinary management (regular check-ups, antithyroid medication) being crucial in preventing adverse perinatal outcome.

A 38
Placental fetal erythroblastosis, not always a sign of parvovirus B19 infection: a case presentation

Dr. Simona Stoykova[1]*, Dr. Raffaele Renella[2], Dr. Lydie Beauport[3], Dr. Jean-Marc Good[4], Dr. Carole Gengler[1]

[1]Department of Laboratory Medicine and Pathology, Institute of Pathology, Lausanne University Hospital and University of Lausanne, Lausanne, Switzerland; [2]Department of Pediatric Hematology-Oncology, Lausanne University Hospital and University of Lausanne, Lausanne, Switzerland; [3]Department of Neonatology, Lausanne University Hospital and University of Lausanne, Lausanne, Switzerland; [4]Department of Medical Genetics, Lausanne University Hospital and University of Lausanne, Lausanne, Switzerland

Background: Fetal placental erythroblastosis reflects a response to fetal anemia, with a wide differential diagnosis, including congenital infections (i. e. parvovirus B19), immune-mediated hemolysis, maternal fetal transfusion, and less commonly hemoglobinopathies or metabolic diseases. Congenital dyserythropoietic anemia (CDA) is a heterogeneous group of rare inherited disorders, characterized by ineffective erythropoiesis, without any other lineage defects. Currently several sub-types have been phenotypically delineated, and putative genetic lesions identified in *CDAN1, CDN1/C15ORF41, SEC23B, KIF23, KLF1* and *GATA-1* genes. We report the histological findings in a placenta in the clinical setting of a neonatal presentation of CDA type I.

Methods: The placenta was evaluated macroscopically according to the consensus statement of the Amsterdam Placental Workshop Group and was routinely processed for histology. Giemsa special staining and immu-
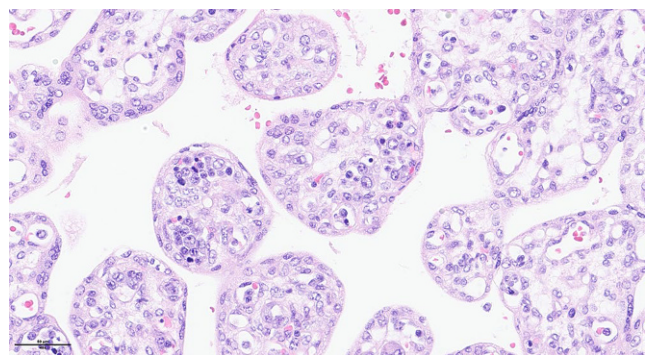

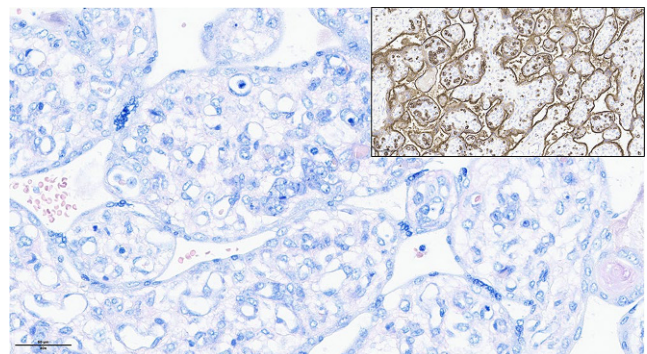**Fig. 1 | A 38 ▲**

Fig. 2 | A 38 ▲

Fig. 3 | A 38 ▲

nohistochemistry (IHC) for parvovirus B19, CD34, CD45 and CD71 were performed on selected blocks.

Results: The placenta was collected during an emergency caesarean section for fetal distress at 37 weeks gestation. The neonate presented with intrauterine growth restriction (3rd percentile), severe anemia (40 g/l), signs of extramedullary hematopoiesis, persistent pulmonary hypertension, cholestasis and severe hyperferritinemia. Macroscopic examination of the placenta showed extreme placentomegaly (1103 g, > P95). Histology demonstrated severe fetal erythroblastosis, without evidence of parvovirus B19 viral inclusions on routine stains or IHC. Giemsa staining revealed macro- and megaloblastic maturation of the numerous CD71-positive proerythroblasts with irregular nuclear contours. No nuclear chromatin bridges or bi- or multinucleations were identified. There were no CD34-positive blasts. Analysis of whole exome sequencing data demonstrated the pathogenic variants c.2140C>T (p.Arg714Trp) and c.2173C>T

(p.Arg725Trp) in compound heterozygosity in the *CDAN1* gene, confirming the diagnosis of CDA type I.

Conclusions: Megaloblastic erythroblastosis in the placenta is an uncommon finding. Rare inherited disorders affecting erythropoiesis, such as CDA among others, should be considered in the differential diagnosis, especially when macro-/megaloblastic features are most prominent.

A 39*
Human secondary lymphoid organ immune landscaping revealed by multiplex imaging analysis

Mr. MICHAIL ORFANAKIS[1]*, Dr. Spiros Georgakis[1], Mrs. Cloé BRENNA[1], Dr. Craig Fenwick[2], Prof. Giuseppe Pantaleo[2], Dr. Oliver Y. Chén[3], Dr. Petrovas Konstantinos[1]

[1]Institute of Pathology, Department of Laboratory Medicine and Pathology, Lausanne, Switzerland; [2]Service of Immunology and Allergy, Department of Medicine, CHUV, Lausanne, Switzerland; [3]Department of Medicine and Department of Laboratory Medicine and Pathology, CHUV, Lausanne, Switzerland

Background: The comprehensive analysis of follicular/germinal center (GC) immune reactivity will greatly improve our understanding of the development of B cell responses as well as the role of specific GC immune cell subsets in diseases like HIV and lymphomas. Multiplex tissue imaging represents a fundamental experimental tool in this regard.

Methods: We have developed cycling (2-rounds) multiplex imaging assays for the deep *in situ* phenotypic characterization of i) adaptive immune cells (CD20/CD3/CD4/CD8/PD1/TIGIT/GITR/ICOS/CXCR3/CD57/ Ki67/Bcl6/GATA3/Tcf1/Blimp1/GrzB/SYTO), ii) stromal and innate immunity cells (CD20/CD11c/CD163/CD68/FDC/CD123/MPO/CD31/CXCL13/ IL21/IL10/SYTO) and iii) suppressor CD4 T cells (CD20/CD4/FOXP3/CD25/ MCT1/MCT4/Helios/Neuropilin/IL10/SYTO). FFPE tissue sections from tonsils ($n = 4$) and reactive lymph nodes ($n = 3$) were analyzed. Tonsillar cells in suspension were used for CyTOF analysis. Following dye separation and alignment (SimpleITK), images were processed (Imaris) and the generated data were analysed by HistoCytometry/FLowJo plugins, KL divergence script (similarity analysis) and distance analysis (Python).

Results: CyTOF and Histocytometry revealed a high phenotypic heterogeneity of the follicular helper CD4 T cell (Tfh) compartment. Hand gating and FlowSOM clustering showed specific Tfh cell phenotypes with distinct localization across the follicular areas. Similarity analysis unveiled Tfh biomarkers with similar density distributions within respective tonsil and LN tissue populations (*e.g.*, Bcl6) and those with less distinct profile (*e.g.*, ICOS). The majority of FOXP3hiCD25hi/lo CD4 T cells (Tregs) were extrafollicular. Extrafollicular Tregs were characterized by increased expression of Glut1 and MCT4, while MCT1hi Tregs were localized mostly in the follicular areas. A considerable co-expression of CXCL13, IL21 and FDC was observed, particularly in tonsils. A lower frequency of monocytic subsets was found in LNs compared to tonsils in follicular and extrafollicular areas.

Conclusion: Our experimental approach reveals the high heterogeneity and compartmentalization of immune landscaping in human secondary lymphoid organs. Furthermore, our analysis could support the identification of disease specific cellular signatures as part of a multiomics approach.

*Student submission

A 40
Multiple lung tumour nodules with a shared KRAS G12C mutation: unrelated primary lung adenocarcinomas or intrapulmonary metastasis? Report of two cases with different answers

Dr. Mark Keyter[1]*, Dr. Edoardo Missiaglia[2], Dr. Karine Lefort[2], Dr. Bettina Bisig[2], Prof. Sabina Berezowska[3]

[1]Department of Laboratory Medicine and Pathology, Institute of Pathology, Lausanne University Hospital and University of Lausanne, Lausanne, Switzerland; [2]1. Institute of Pathology, Lausanne University Hospital, Lausanne University, Lausanne, Switzerland; [3]Department of Laboratory Medicine and Pathology, Institute of Pathology, Lausanne University Hospital, University of Lausanne, Rue du Bugnon 25, 1011 Lausanne, Switzerland

Background: Distinguishing between multiple primary lung carcinomas and intrapulmonary metastasis is challenging but important, as it affects staging, prognosis and clinical management. Molecular approaches assist with this distinction through the comparison of "trunk" (initiating) and "branching" (subclonal) mutations. We describe two patients with multiple lung tumours sharing a *KRAS* G12C mutation, the most frequent alteration in lung adenocarcinomas, highlighting the difficulties to determine clonal relationship when facing common oncogenic drivers.

Methods: Targeted NGS (52 gene hotspot panel) was performed on each lung tumour of patient A (3 tumours) and patient B (2 tumours), on lobectomy specimens. Histological pattern, mutations and copy number variations (CNVs) were compared.

Results: Case A: Tumours 1 and 2 were adenocarcinomas of the left upper lobe, with overlapping growth patterns, an identical *KRAS* G12C mutation (trunk) and similar CNVs (1q23 gain and 19p13 deletion), which led us to interpret them as clonally related despite different mutations in *STK11* +/− *CTNNB1* (branching). Tumour 3 was a left lower lobe adenocarcinoma with a distinct growth pattern (papillary) and a different trunk mutation (*KRAS* G12A), interpreted as an unrelated primary lung carcinoma.

Case B: Tumours 1 and 2 were adenocarcinomas of the same lobe, with different growth patterns (solid *versus* lepidic and acinar), an identical *KRAS* G12C mutation, and different *TP53* +/− *ATM* mutations (branching). CNV analysis was non-contributory. Despite a shared *KRAS* G12C, due to different histology and branching mutations, the hypothesis of two distinct primary lung carcinomas was favoured, although this could not be confirmed with certainty.

Conclusion: Due to the high frequency of *KRAS* G12C in lung adenocarcinoma, its detection in multiple lung tumour nodules cannot be used alone to establish their clonal relatedness. Histological pattern, additional mutations and CNVs provide complementary information, though equivocal findings still occur, highlighting the need for more comprehensive molecular approaches.

A 41
Morphologic and molecular analysis of liver injury after SARS-CoV-2 vaccination reveals distinct characteristics

Dr. Sarp Uzun[1]*, Dr. Carl Zinner[1], Ms. Amke C. Beenen[1], Dr. Ilaria Alborelli[2], Dr. Ewelina M. Bartoszek[3], Dr. Jason Yeung[4], Dr. Byron Calgua[1], Mr. Matthias Reinscheid[5], Dr. Peter Bronsert[6], Dr. Anna K. Stalder[1], Dr. Jasmine Haslbauer[1], Dr. Juerg Vosbeck[1], Dr. Luca Mazzucchelli[7], Dr. Hoffmann Tobias[8], Prof. Luigi M. Terracciano[9], Prof. Gregor Hutter[10], Dr. Michael Manz[11], Dr. Isabelle Panne[11], Prof. Tobias Boettler[5], Dr. Maike Hofmann[5], Prof. Bertram Bengsch[5], Prof. Markus H. Heim[11], Prof. Christine Bernsmeier[11], Dr. Sizun Jiang[4], Prof. Alexandar Tzankov[2], Prof. Benedetta Terziroli Beretta-Piccoli[12], Dr. Matthias S. Matter[1]

[1]Institute of Pathology, University Hospital Basel, Basel, Switzerland; [2]Pathology, Institute of Medical Genetics and Pathology, University Hospital Basel, University of Basel, Switzerland; [3]Microscopy Core Facility, Department of Biomedicine, University of Basel, Basel, Switzerland; [4]Center for Virology and Vaccine Research, Beth Israel Deaconess Medical Center, Boston, MA, USA; [5]Department of Medicine II (Gastroenterology, Hepatology, Endocrinology and Infectious Diseases), Freiburg University Medical Center, Faculty of Medicine, University of Freiburg, Freiburg, Germany; [6]Institute for Surgical Pathology, Freiburg University Medical Center, University of Freiburg, Freiburg, Germany; [7]Istituto Cantonale di Patologia, Locarno, Switzerland; [8]Innere Medizin, Spital Dornach, Dornach, Switzerland; [9]Department of Biomedical Sciences, Humanitas University, Pieve Emanuele, Milan, Italy; [10]Brain Tumor Immunotherapy Lab, Department of Biomedicine, University of Basel, Basel, Switzerland; [11]Gastroenterology and Hepatology, University Centre for Gastrointestinal and Liver Diseases Basel, Switzerland; [12]Faculty of Biomedical Sciences, Università Della Svizzera Italiana, Lugano, Switzerland

Background: Liver injury after COVID-19 vaccination is very rare and shows clinical and histomorphological similarities with autoimmune hepatitis (AIH). Little is known about the pathophysiology of COVID-19 vaccine-induced liver injury (VILI) and its relationship to AIH. Therefore, we aim to characterize VILI by comparing with AIH.

Methods: Formalin-fixed and paraffin-embedded (FFPE) liver biopsy samples from patients with VILI ($n = 6$) and from patients with an initial diagnosis of AIH ($n = 9$) were included. Total RNA was extracted from all FFPE biopsy samples. Both cohorts were compared by histomorphological evaluation, whole-transcriptome and spatial transcriptome sequencing, multiplex immunofluorescence staining, and immune repertoire sequencing.

Results: Histomorphology was similar in both cohorts but showed more pronounced centrilobular necrosis in VILI. Gene expression profiling showed that mitochondrial metabolism and oxidative stress-related pathways were more and interferon response pathways were less enriched in VILI. Multiplex immunofluorescence staining revealed that inflammation in VILI was dominated by CD8+ effector T cells, similar to drug-induced autoimmune-like hepatitis. In contrast, AIH showed a dominance of CD4+ effector T cells and CD79a+ B and plasma cells. T-cell receptor and B-cell receptor sequencing revealed that VILI had a more oligoclonal T- and B-cell immune repertoire compared to AIH. Analysis of TCR beta chain and Ig heavy chain variable-joining gene usage further showed that TRBV6-1, TRBV5-1, TRBV7-6, and IgHV1-24 genes were used differently in VILI than in AIH.

Conclusions: Our analyses support that VILI is related to AIH but also show distinct differences from AIH in histomorphology, pathway activation, cellular immune infiltrates, and immune repertoire architecture. Therefore, VILI may be a separate entity, which is distinct from AIH and more closely related to drug-induced autoimmune-like hepatitis.
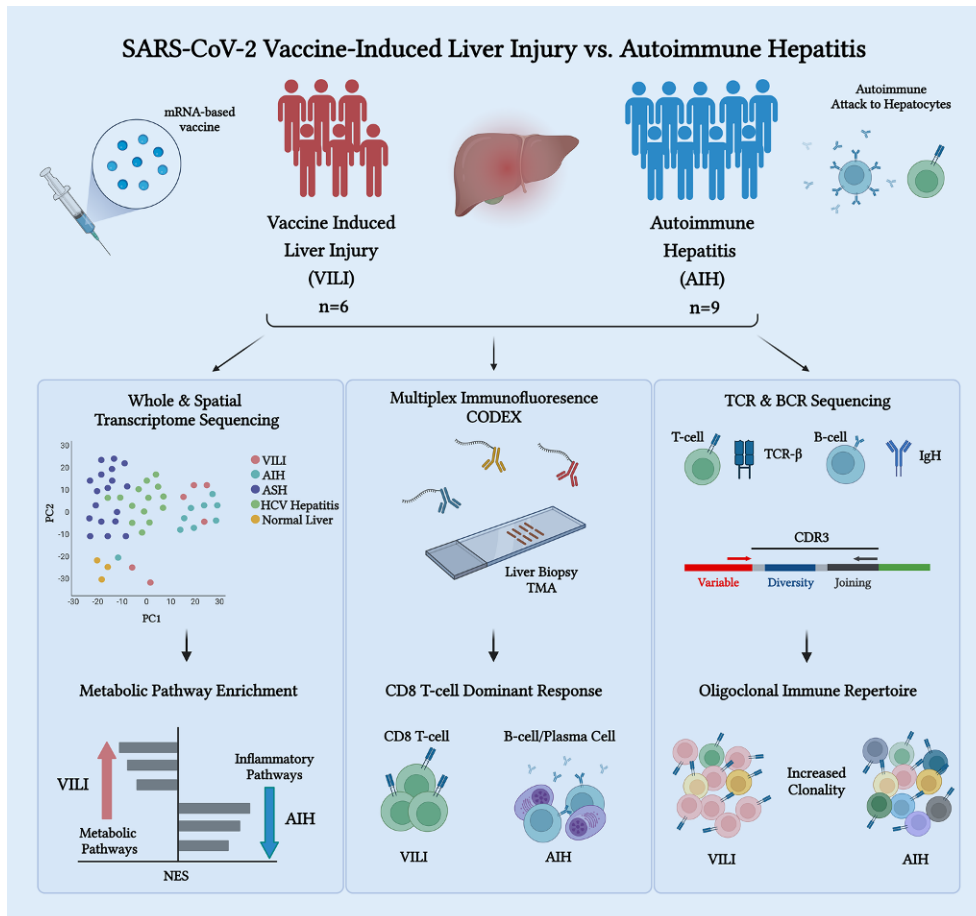
Fig. 1 | A 41 ◄ [1] (published under CC BY 4.0 international license https://creativecommons.org/licenses/by/4.0)

References

1. Uzun S, Zinner CP, Beenen AC et al (2023) Morphologic and molecular analysis of liver injury after -SARS-CoV-2 vaccination reveals distinct characteristics. Journal of Hepatology. https://doi.org/10.1016/j.jhep.2023.05.020

A 42*
Metastatic postpubertal-type teratoma of the testis with pure stromal component: a diagnostic challenge

Dr. Marie Barbesier[1], Dr. Nathalie Sala[1]*, Mrs. Cloé Bregnard[1]*, Dr. Paul Martel[2]*, Dr. François Crettenand[2]*, Dr. Sofiya Latifyan[3], Dr. Dominik Berthold[3], Prof. Beat Roth[2], Dr. Igor Letovanec[1], Dr. Bettina Bisig[1], Dr. Julien Dagher[1]

[1]Department of Laboratory Medicine and Pathology, Institute of Pathology, Lausanne University Hospital, University of Lausanne, Rue du Bugnon 25, 1011 Lausanne, Switzerland; [2]Department of Urology, Lausanne University Hospital (CHUV) and University of Lausanne, Lausanne, Switzerland.; [3]Department of Oncology, Lausanne University Hospital (CHUV) and University of Lausanne, Lausanne, Switzerland

Background: Postpubertal-type teratomas comprise a spectrum of epithelial and stromal components arising from one or multiple germ layers (endoderm, mesoderm, ectoderm). They are germ cell neoplasia in situ-derived tumors with metastatic potential. Gains of 12p are present in the majority of these tumors. We report a challenging case manifesting at progression as a purely mesenchymal proliferation.
Methods: We performed 12p/CEP 12 FISH and targeted NGS for hotspot mutations and fusions (52 and 145 gene panel respectively), and comparative FISH in 3 previous metastases.
Results: A 41-year-old male received neoadjuvant chemotherapy for a "non seminomatous germ cell tumor" of the left testis. Post-treatment orchiectomy showed no viable tumor. The patient subsequently underwent 3 retroperitoneal and mediastinal lymphadenectomies, showing metastatic teratoma, with epithelial and stromal components. During follow-up, a 2 cm iliac adenopathy was resected. Serum tumor markers (BetaHCG, AFP and LDH) were within normal range. Histologically, it consisted of a variably cellular proliferation, exclusively composed of monomorphic spindle cells, without mitotic figures, in a myxoid matrix devoid of necro-

sis. Extensive sampling did not show any epithelial or germ cell component. The differential diagnosis included nonspecific fibrous proliferations. No mutations nor fusions were detected. FISH analysis revealed a 12p gain in 78% of the cells (12p/centromere ratio = 1.73), which was identical to that observed in the mesenchymal components of the metastatic teratoma samples previously resected.
Conclusions: These results are in favor of a pure mesenchymal teratoma, with no epithelial component. In lymph node resections of testicular germ cell tumors subsequent to chemotherapy, teratoma is the most prevalent sub-type. While somatic-type transformation into a spindle cell sarcoma was considered, the lack of atypia, absence of mutations or fusion transcripts, resemblance to the stromal component and identical 12p FISH profile to previous samples, underpin an overgrowth involving the mesenchymal spindle cell component.
*Student submission

A 43
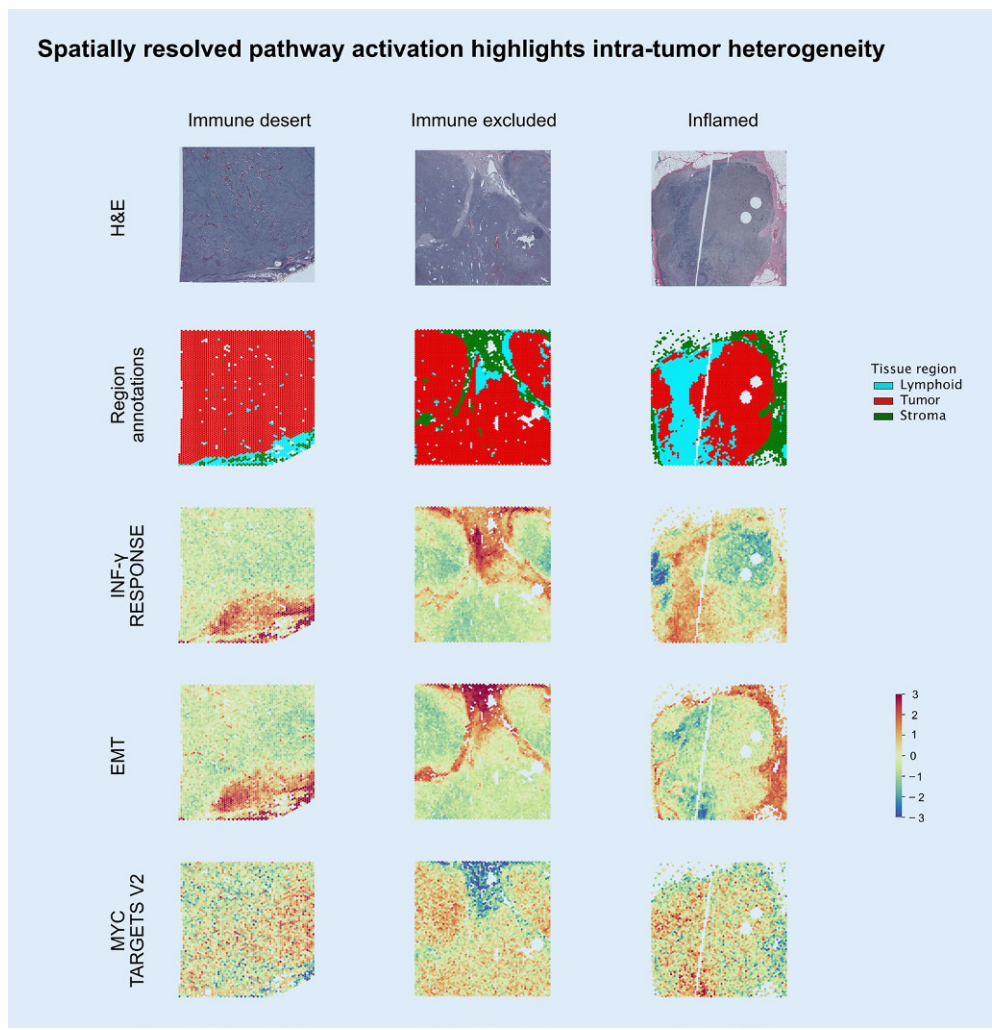## Spatial landscape of hallmark pathway activation in metastatic melanoma

Ms. Joanna Ficek-Pascual[1], Ms. Sonali Andani[2]*, Dr. Marta Nowak[3], Mx. Tumor Profiler Consortium[4], Prof. Gunnar Rätsch[1], Prof. Viktor H. Kölzer[3]

[1]Department of Computer Science, ETH Zürich, Universitätsstr. 6, 8092 Zürich, Switzerland; [2]Department of Pathology and Molecular Pathology, University Hospital Zurich, University of Zurich, Zurich, Switzerland Department of Computer Science, ETH Zürich, Universitätsstr. 6, 8092 Zürich, Switzerland; [3]Department of Pathology and Molecular Pathology, University Hospital of Zurich, Zurich, Switzerland; [4]Mx. Tumor Profiler Consortium, Zurich, Switzerland

Background: Recent developments in spatial transcriptomic technologies enable the spatially resolved analysis of pathway activation in clinical tissue samples. Obtaining spatial maps of key pro-tumorigenic gene signaling pathways representing the "hallmarks of cancer" could advance our understanding of tumor-host interaction and provide further insights into tumor progression and biological heterogeneity. We use 10x Visium Spatial Transcriptomics in the Swiss Tumor Profiler Cohort to analyze hallmark pathway activation of metastatic melanoma and the anti-tumoral immune response.
Methods: We produce whole slide images, generate digital immune phenotypes, and profile 8 lymph-node melanoma metastases with additional
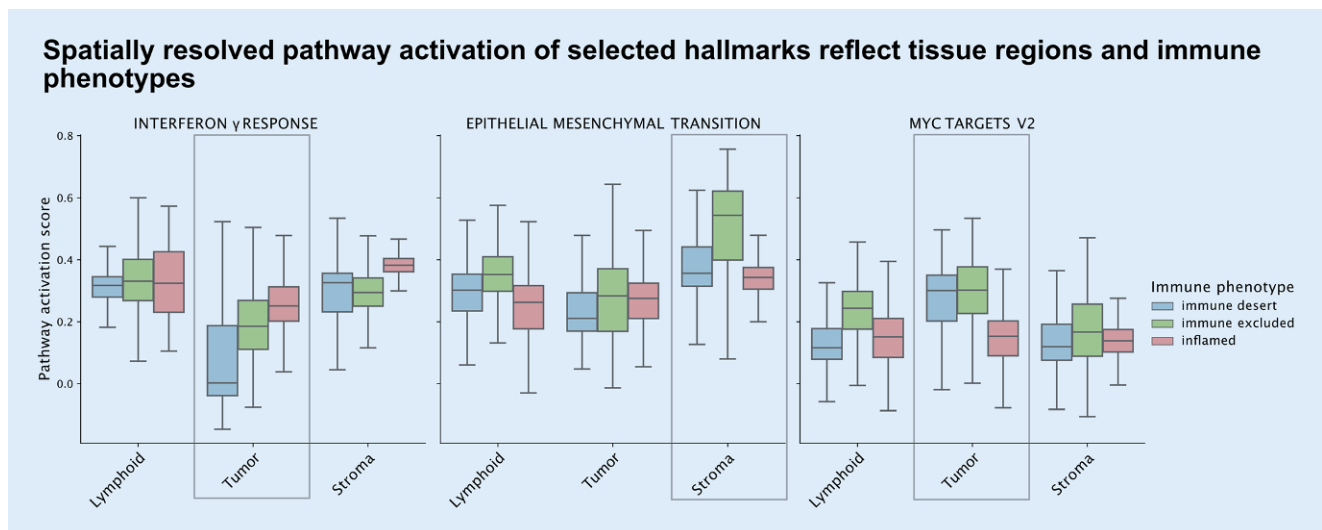
Fig. 1 | A 43 ▲ Pathway activation scores of immune-activation-related Interferon y (left), stroma-related EMT (middle), and tumor-specific MYC targets v2 (right). The scores are stratified by the tissue region (x-axis) and the sample's immune phenotype reflecting the anti-tumoral immune response (color-coded). We observe some expected patterns (gray rectangles), for instance lower activation among immune desert in comparison to inflamed of interferon y in the tumor region as well as overall higher EMT activation at the Tumor-Stroma interface in comparison to Tumor and Lymphoid regions (middle plot) and higher tumor-specific MYC targets V2 in the Tumor region, especially among the immune desert and excluded samples where the region borders are clearly defined

Spatially resolved pathway activation highlights intra-tumor heterogeneity

Fig. 2 | A 43 ◄ Spatially resolved activation of selected hallmark pathways in three samples: immune desert, immune excluded and inflamed. The pathway activation scores (row 3 to 5) are z-scored per pathway per sample, with activation in comparison to other spots depicted in orange-red and downregulation in green-blue, as indicated by the color legend. The pathway activation maps for immune-related Interferon y (IFN y RESPONSE, 3rd row), EMT (4th row) and tumor-specific MYC Targets V2 (5th row) are plotted along with the underlying H&E image (1st row) and the tissue region annotations (2nd row). The plots highlight intra-tumor heterogeneity with Interferon y and ENT activated at the tumor-immune interface and the MYC targets activated in the tumor center, with variability across the tumor region. Note: The pathway activation highlights the heterogeneity within the tumor region, but does not reflect the overall high/low activation

replicates from the Tumor Profiler Cohort, with a total of 74,000 spots of 55 μm diameter spatially mapping the whole transcriptome for each tumor slide. We measure the pathway activation score(PAS) of cancer hallmark pathways in each spot from MSigDBv7.2 database, with PAS calculated using ssGSEA. We compare PAS in each tumor compartment and between anti-tumoral immune phenotypes: desert, excluded, and inflamed.

Results: Spatially resolved hallmark pathway activation reflects the anti-tumoral immune response within the tumor region with highest IFNγ response in inflamed samples (median: 0.25, IQR: [0.2–0.31]) and lowest in the desert samples (median: 0, IQR: [−0.04–0.19]). The activation maps recapitulate the tissue regions(◘ **Fig. 1**), with the highest activation of EMT and IFNγ at the TME-tumor intersection and of MYC targets in the tumor region. Moreover, we observed heterogeneity in hallmarks across the tumor region(◘ **Fig. 2**), with activation of IFNγ and EMT mainly observed at the tumor front and intratumoral variability in MYC target activation.

Conclusions: The spatial distribution of hallmark pathway activation reflects tissue regions and anti-tumoral immune response within the samples. Analysis of spatial patterns of activation within the tumor regions reveals pathways activated at the intersection with the TME and those activated in the tumor center, highlighting intra-tumor heterogeneity.

A 44
Homologous-recombination deficiency detection in ovarian carcinomas by shallow whole genome sequencing

Dr. Julien Dagher[1]*, Dr. Karine Lefort[2], Mr. Vimel Rattina[2], Mrs. Veronique Vocat Mottier[2], Prof. Laurence de Leval[2], Dr. Edoardo Missiaglia[2], Dr. Bettina Bisig[2]

[1]Department of Laboratory Medicine and Pathology, Institute of Pathology, Lausanne University Hospital, University of Lausanne, Rue du Bugnon 25, 1011 Lausanne, Switzerland; [2]1. Institute of Pathology, Lausanne University Hospital, Lausanne University, Lausanne, Switzerland

Background: Homologous recombination (HR) is a DNA repair mechanism impaired in around half of high-grade serous ovarian carcinomas (HGSOC), predicting increased sensitivity to PARP inhibitors. MyChoiceCDx (Myriad) is currently the reference test for detection of HR deficiency (HRD) in HGSOC, combining the evaluation of *BRCA1/2* mutations and genomic instability score (GIS). The aim of this study is to validate shallow whole genome sequencing (sWGS) to assess HRD, based on a Large-scale Genomic Alteration score (LGA), and define a threshold for diagnostic implementation in HGSOC.

Methods: sWGS was performed on 44 HGSOC with known *BRCA1/2* status (12 with pathogenic mutations, 32 wild-type) +/− Myriad GIS ($N = 38$). Libraries were sequenced on a NextSeq instrument (Illumina) and aligned to the hg19 human genome assembly. LGA score was computed using shallowHRD software, and correlated with GIS.

Results: On average 24 million (M) reads (range 11–42M) per sample were generated, with a median coverage of 0.8X (range 0.3–1.6X). LGA showed a significant correlation with GIS (Spearman rank rho 0.94; $P < 0.0001$). A LGA cut-off of 19 (95% confidence interval (CI) 17–21) was predicted starting from GIS cut-off (≥ 42) using a regression model, splitting our dataset into three HRD groups: 15 negative (< 17), 3 borderline (≥ 17 and ≤ 21) and 20 positive (> 21) cases. When compared to Myriad GIS status, LGA achieved 95% sensitivity, 87% specificity and 91% (CI 77–98%) accuracy with a Kappa coefficient of 0.83 (CI 0.5–1). Moreover, LGA score was positive in 92% of *BRCA* mutated cases (11/12), with values significantly higher than in wild-type patients (median 31.5 (range 20–43) vs 16 (range 0–50), Wilcoxon rank test $P = 0.002$).

Conclusions: Analysis of 44 HGSOC by sWGS showed significant concordance of LGA score with Myriad GIS score and *BRCA* status, supporting the use of this approach as a decentralized method to assess HRD status in HGSOC.

A 45
Post-integration insights into "MetAssist": a colorectal cancer lymph node metastasis detection model

Dr. Amjad Khan*, Mr. Stefan Reinhard, Prof. Aurel Perren, Dr. Bastian Dislich, Prof. Inti Zlobec

Institute of Tissue Medicine and Pathology, University of Bern, Bern, Switzerland

Background: Microscopic evaluation of lymph node tissues for potential metastases can be a time-intensive task in diagnostic routine. To assist pathologists, we recently developed and integrated a deep learning-based colorectal cancer (CRC) lymph node metastasis detection model named MetAssist for quality control. In this study, we highlight an insight into post-integration utilization by expert pathologists on routine CRC cases at the institute.

Methods: The integration utilizes a remote High-Performance Cluster (HPC) at the University with an automatic workflow between the institute and HPC, alongside a simplified web interface for pathologists' interaction and outcome visualization. Since June 2023, a total of 30 CRC resection specimens (339 slides with locoregional lymph nodes) have been diagnosed by 12 pathologists, who then compared their diagnosis with the predictions of MetAssist and reviewed cases with discrepancies.

Results: The sensitivity and specificity of MetAssist compared with that of pathologists were around 0.982 and 0.793 respectively. The disparity in negative slides could be attributed to various tissue artifacts, mainly tissue folds and fragments of primary cancer that were erroneously detected. For each false detection or diagnosis, the pathologists provided comments. There were three slides where the initial decision by pathologists was changed (both from positive to negative and vice versa). MetAssist's indications prompted a review of the slides, leading to improved diagnosis, with newly improved values of sensitivity and specificity of 0.798 and 1.0 respectively.

Conclusions: Overall, pathologists found the MetAssist integration to be supportive. They also provided valuable comments that could be helpful in improving both the model and the integration process in the future.

A 46
Cross-domain applicability of a deep learning model: from colorectal cancer to upper gastrointestinal adenocarcinoma lymph node metastases detection

Dr. Amjad Khan*, Prof. Inti Zlobec, Dr. Bastian Dislich

Institute of Tissue Medicine and Pathology, University of Bern, Bern, Switzerland

Background: Screening lymph nodes for potential metastases is a labor-intensive task in the pathology routine. To help pathologists assess lymph node status, "MetAssist" a deep learning-based colorectal cancer (CRC) lymph node metastasis detection model, was recently developed and integrated into the clinic for quality control. We explore the adaptability of MetAssist to Upper Gastrointestinal Adenocarcinoma (UGA) lymph nodes without any additional fine-tuning or UGA-specific training. We compared the predicted slide-level scores by the model with a pathologist's diagnosis.

Methods: 114 lymph node-positive slides from patients with UGA were scanned and then run through MetAssist, which automatically segments the lymph node tissue, detects metastases in each segmented tissue, creates overlays of predicted regions, and calculates the slide-level score (e.g., positive, or negative). A slide having more than two contiguous positive tiles (tumor probability threshold > 85%) was classified as positive. All false-negative cases were re-evaluated by the pathologist using the predicted overlays to thoroughly assess the performance of the model.

Results: MetAssist achieved a sensitivity of 0.84 without any additional fine-tuning or UGA-specific training. Around 18 cases were detected as false negatives by the model. In these cases, poor quality stains, signet ring cell phenotypes, micropapillary growth patterns, and very few cells of adenocarcinoma were challenging for the model. The model was still able to indicate adenocarcinoma regions in falsely predicted cases, however, the optimal threshold still needs to be explored.

Conclusions: Our results show that MetAssist was able to detect the metastases in most UGA-positive cases. However, the model should be evaluated on a larger cohort, which includes negative slides and tumors with morphological subtypes that are more common in UGA than CRC, e.g., poorly cohesive, and signet-ring cell phenotypes. Therefore, we will extend our study to further evaluate the adaptability of the CRC-trained model for UGA cases.

A 47*
Niches and how to find them: tumor budding microenvironment assessment in immunofluorescence images based on point-density maps

Mr. Mauro Gwerder[1]*, Dr. Cansaran Saygılı Demir[2], Dr. Cristina Graham Martinez[1], Dr. Hannah L. Williams[3], Dr. Amjad Khan[3], Dr. Philipp Kirchner[1], Dr. Martin Weigert[4], Prof. Inti Zlobec[1]

[1]Institute of Tissue Medicine and Pathology, University of Bern, Bern, Switzerland; [2]Lunaphore Technologies S. A., Tolochenaz, Switzerland; [3]Institute of Tissue Medicine and Pathology, University of Bern, Bern, Switzerland; [4]Institute of Bioengineering, School of Life Sciences, Ecole Polytechnique Fédérale de Lausanne (EPFL), Lausanne, Switzerland
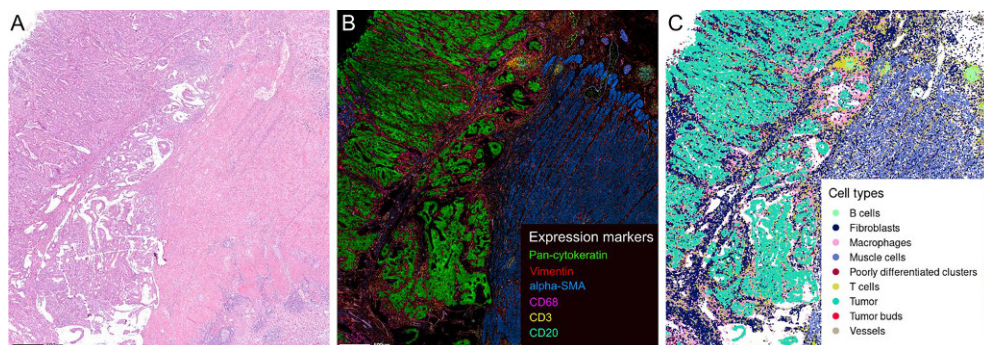
Fig. 1 | A 47 ◄ An example tissue section, visualized in three different ways. (A) H&E-restain after immunofluorescence, (B) Immunofluorescence with selected expression markers exhibiting the main cell types, (C) the assigned cell types represented as a point pattern
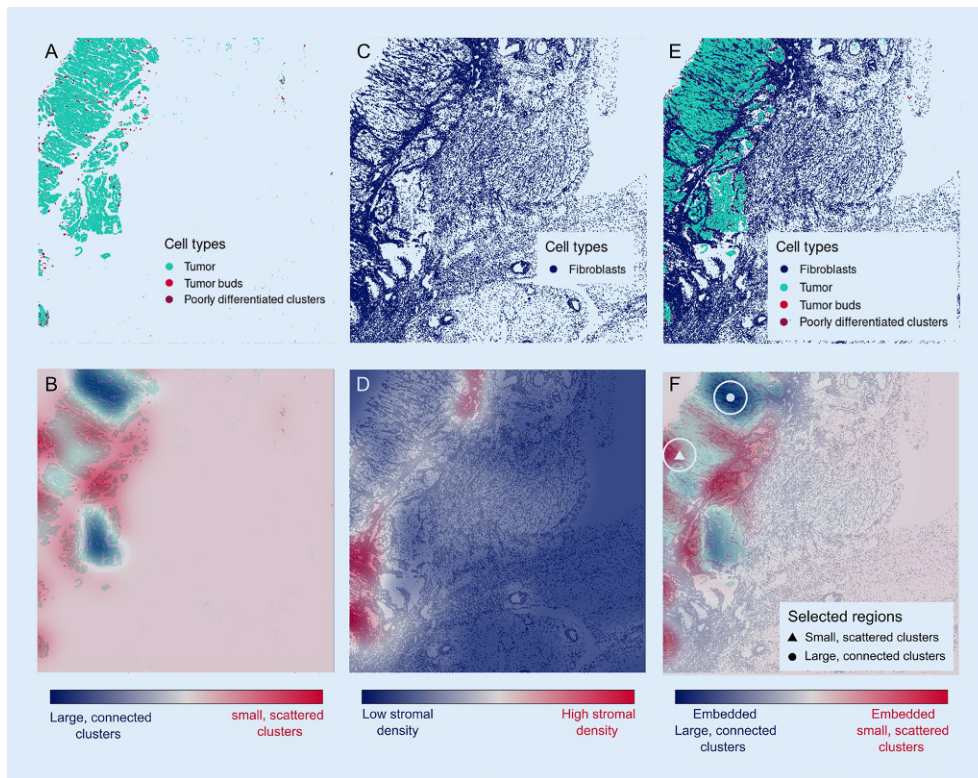
Fig. 2 | A 47 ◄ Visualizations of the utilized point patterns and the resulting density maps. (A) Point pattern visualization of all tumor cells, including tumor buds and poorly differentiated clusters, (B) The resulting tumor density map, with large connected cluster regions as local minima and small scattered cluster regions as local maxima, (C) Point pattern visualization of all stromal cells, (D) The resulting stromal density map, (E) Point pattern visualization of Tumor cells and stromal cells, (F) The adjusted tumor density map with a higher focus on high stromal density areas, as well as the final selected regions for niche analysis
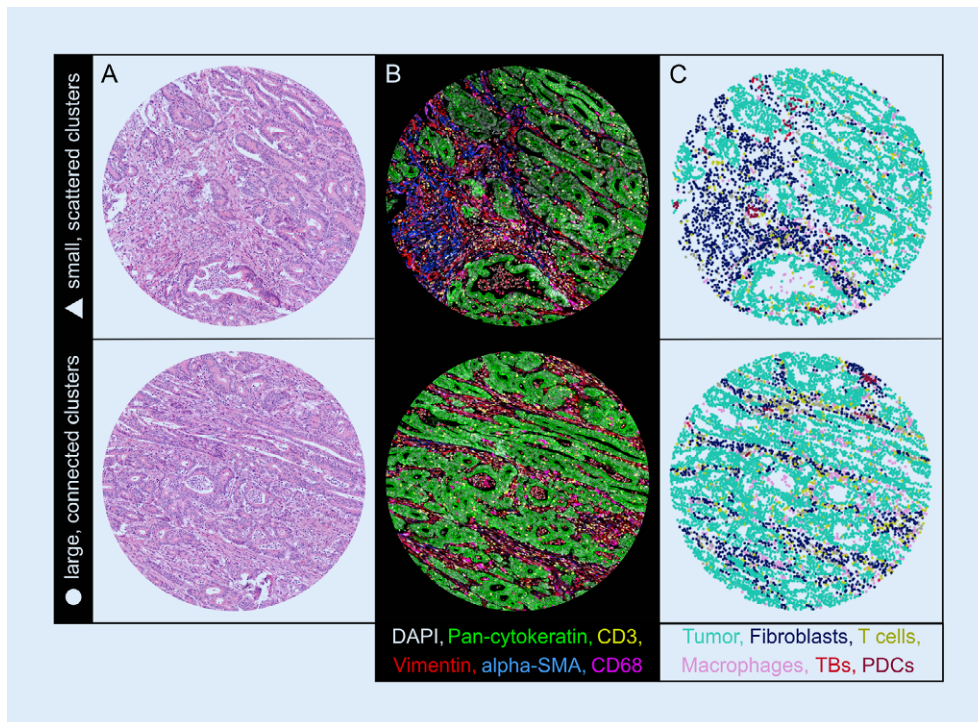
Fig. 3 | A 47 ◄ The selected regions representing the two niches of interest, "large, connected clusters" and "small, scattered clusters". (A) H&E-restaining after immunofluorescence, (B) Immunofluorescence with selected expression markers exhibiting the main cell types (C) the assigned cell types represented as a point pattern

Introduction: In colorectal cancer (CRC), tumor budding is a powerful independent prognostic factor. Tumor buds (TB) are defined as clusters of < 5 tumor cells detached from the primary tumor. Assessment of their micro-environment is difficult, as there currently exists no phenotypic marker for TBs and they are rare within the tissue. Therefore, there is a need to automatically find tumor niches, where TBs as well as poorly differentiated clusters are enriched.

Materials and methods: Seven CRC sections underwent sequential Immunofluorescence (seqIF™) protocol on COMET™ (Lunaphore Technologies). We first phenotyped each cell using an automated gating strategy (◘ Fig. 1). We then segmented the epithelial tissue based on Pan-cytokeratin expression and counted the number of tumor cells within each epithelial segment. To find niches representing different tumor growth patterns ("*large, connected clusters*" or "*scattered, small clusters*", ◘ Fig. 3), we use cell counts within each epithelial segment as a "cluster size" feature.

We created density maps based on point patterns and weighted them according to the inverse of the cluster size, prioritizing areas with smaller clusters. We further used density maps of fibroblasts to guarantee that our selected areas are embedded in the stroma. Finally, we selected regions of 1 mm in diameter according to local minima and maxima of the resulting density map, finding both niches, respectively (**◻ Fig. 2**).

Results: We found a lower immune cell infiltration ($p = 0.0098$, pairwise Wilcoxon test) in *scattered, small cluster* niches. This finding was previously reported in literature. We also found a higher fraction of M2 macrophages ($p = 0.002$) in *large, connected cluster* regions.

Conclusions: Using concrete extracted features and point-pattern based density maps, we found niches within tissue sections in an unbiased and targeted way. These findings confirm our pipeline can extract relevant biological features automatically.

*Student submission

A 48
HPyloriDet: a clinically deployable tool for computer-aided helicobacter pylori detection in immunohistochemically stained slides

Dr. Nicolas Brandt[1]*, Dr. Aurélie Bornand[1], Dr. Antonin Bouroumeau[1], Dr. Giacomo Puppa[1], Dr. Mario Kreutzfeldt[2], Prof. Doron Merkler[2], Prof. Andrew Janowczyk[3]

[1]Department of Diagnostics, Division of Clinical Pathology, Geneva University Hospitals, Geneva, Switzerland; [2]Department of Diagnostics & Department of Pathology and Immunology, Division of Clinical Pathology, Geneva University and Geneva University Hospitals, Geneva, Switzerland; [3]Department of Diagnostics & Department of Oncology, Division of Clinical Pathology & Precision Oncology, Geneva University Hospitals, Geneva, Switzerland

Background: Helicobacter Pylori (HP) is a common stomach bacteria linked to conditions including stomach cancer. Although immunohistochemical (IHC) staining of HP facilitates diagnosis, reviewing whole slide images (WSI) remains time-consuming. We investigated our computer-aided screening tool, HPyloriDet, for improving diagnostic speed.

Methods: HPyloriDet was developed using $n = 20$ pathologist-annotated HP IHC WSIs and clinically validated using $n = 66$ WSIs. Regions of interest were identified via IHC stain deconvolution, driving the extraction of 300×300 pixel patches split into 80/20 train/test split. A DenseNet was trained to detect the presence of HP on these patches, and its performance metrics evaluated. For workflow integration, slides are scanned as
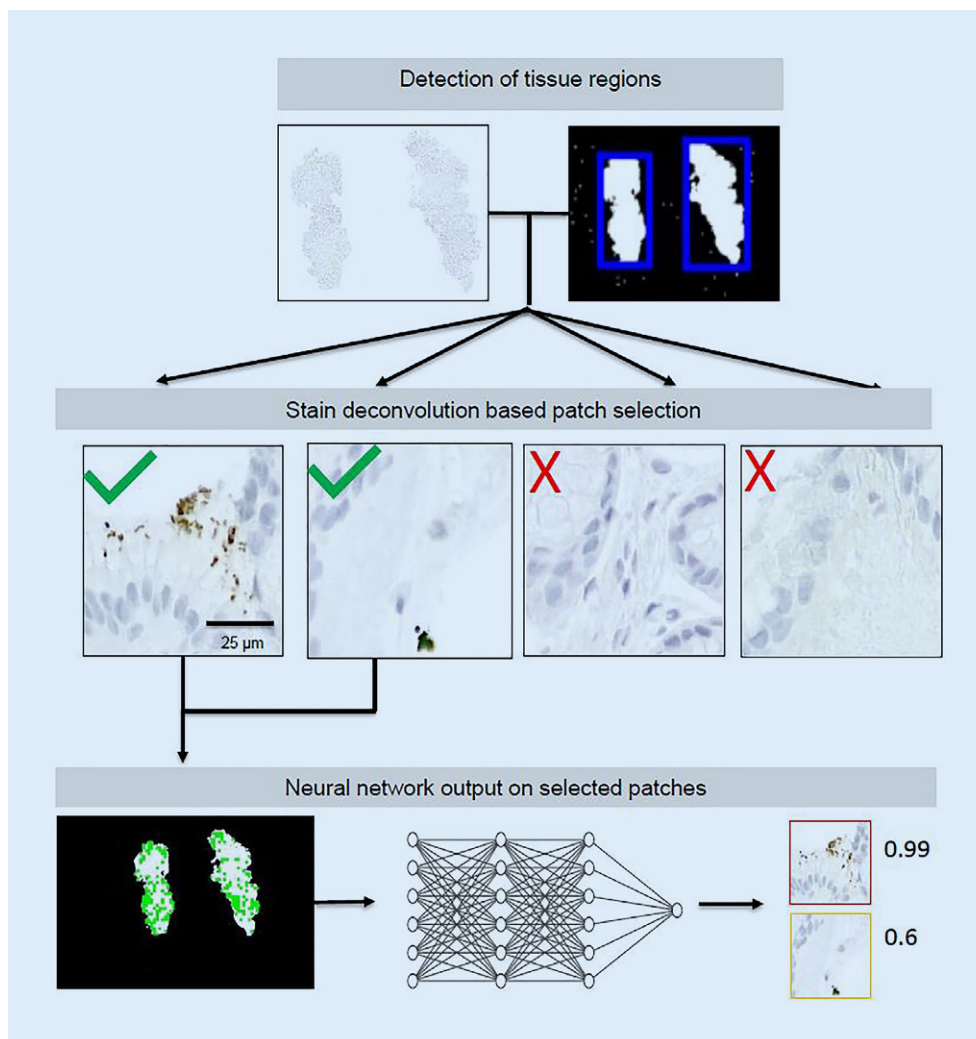
Fig. 1 | A 48 ◄ Slide processing pipeline. From detected tissue regions, patches are accepted if enough DAB stain content is found. The kept patches are ranked by the neural network
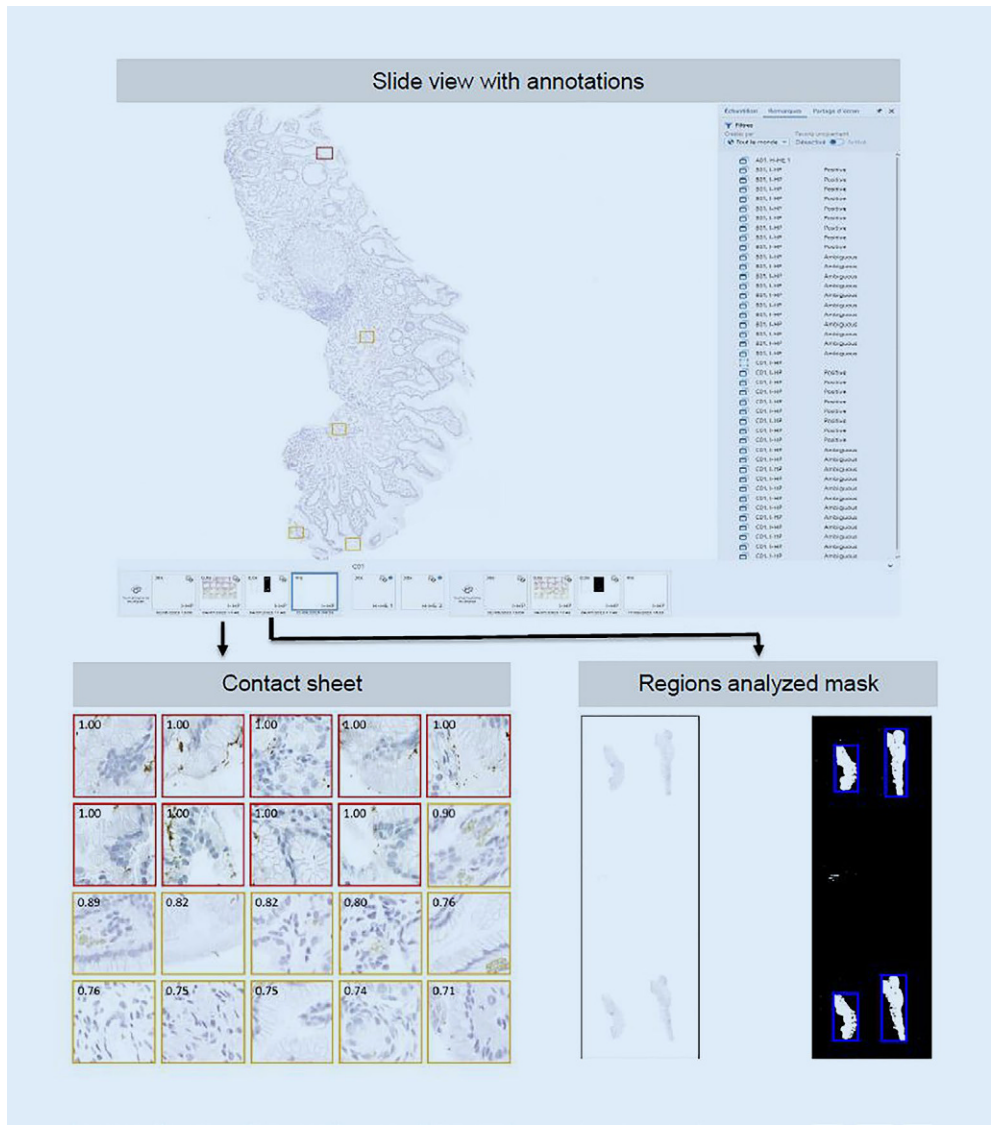
Fig. 2 | A 48 ◄ Sectra integration for display to pathologists. Top ranked regions are shown on the contact sheet and are displayed as annotation on the slide viewer. For ease of interpretation, the model's scores are shown on the contact sheet and corresponding patches are color-coded, red showing higher confidence positive and orange lower confidence positive
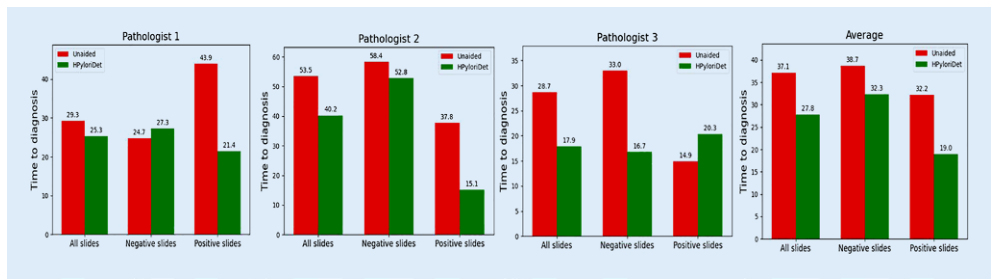
Fig. 3 | A 48 ◄ Time to diagnosis for unaided vs HPylori Det-aided slide for 3 pathologists and pathologist average

WSIs and processed automatically by HPyloriDet. Pathologists have access to the ranked top 20 model predictions via a contact sheet for fast vizualization, annotations on the WSI and a mask showing which regions of the slides have been analyzed (☐ Fig. 2). Clinical benefit was estimated via comparison of conventional and HPyloriDet-aided diagnostic times for 3 pathologists, using sequential slides from a week of clinical workflow.

Results: On extracted patches, HPyloriDet achieved an accuracy of 95%, alongside 92% sensitivity and 95% specificity. The positive predictive value was 65% while the negative predictive value reached 99%. The average time for pathologists to diagnosis was 25% faster with HPyloriDet (27.8 vs 37.1 s, $P = 0.017$) and distinct advantages were observed for individual pa-

thologists (☐ Fig. 3). HPyloriDet did not result in any false negatives, as all positive slides were identified using the top 20 predictions.

Conclusions: Standard HP detection on large IHC slides is time-consuming and our computer-aided tool HPyloriDet demonstrates preliminary evidence that this burden can be ameliorated. Preliminary findings indicate potential time-saving benefits in clinical settings, without loss of diagnostic accuracy. Future work will involve external validation and collecting additional data during deployment for retraining to further improve HPyloriDet's accuracy.

A 49*

Identification of phenotypic switching of colorectal tumour buds in response to tumour-microenvironment using spatially resolved transcriptomics

Mr. Mohamed Mansour Faye[1]*, Ms. Yoana A. Doncheva[2], Ms. Claire Dietrich[2], Prof. Nigel Jamieson[2], Prof. Inti Zlobec[3], Dr. Yannick Palmowski[4], Prof. Christian Schürch[4], Prof. Alessandro Lugli[3], Dr. Hannah L. Williams[1]

[1]Institute of Tissue Medicine and Pathology, University of Bern, Bern, Switzerland; [2]Wolfson Wohl Cancer Research Center, University of Glasgow, Glasgow, UK; [3]Institute of Tissue Medicine and Pathology, University of Bern, Bern, Switzerland; [4]Department of Pathology and Neuropathology, University Hospital and Comprehensive Cancer Center, Tübingen, Germany

Introduction: High grade tumour budding (TB) is an established biomarker of tumour progression and worse survival in colorectal cancer (CRC). The development of anti-budding therapy would support the therapeutic management of CRC patients. The profiling of CRC TBs is extremely important but challenging. Recent technological developments enable spatially resolved transcriptomic analysis on tissues facilitating the assessment of gene expression with unprecedented accuracy and depth.

Methods: We applied spatially resolved transcriptomic sequencing (Nanostring GeoMx Digital Spatial Profiler) using the whole transcriptome atlas panel (18,000 genes) on 2 tissue-microarrays comprising TB cores to examine whether TB phenotypes change in response to tumour-microenvironment (■ Fig. 1). TB cores were classified by location: tunica submucosa (TSM), tunica muscularis propria (TMP), tunica subserosa (TSS). Data pre-processing comprised removal of segments with < 60% aligned reads and of targets with < 10% of segments above limits-of-quantitation.

Results: We obtained results for 26 cores (6TSM, 9TMP, 11TSS) and 6920 genes. Differential gene expression and gene set enrichment analysis revealed TB phenotypes specific to invasion depth. In the TSM, we observed enrichment of antigen presenting and processing gene-sets. Assessment of H&Es by expert pathologist confirms absence of intra-epithelial immune contamination (■ Fig. 2a&b) in TB. In the TMP, TBs showed increased expression of genes linked to cellular motility and ECM modulation. These changes were also visible at the histological level in the form of high-grade tumour budding and tumour-microenvironment (■ Fig. 2c&d). TSS was characterized by an increase in O-glycosylation of transmembrane glycoproteins, in particular mucins, a process which has been associated with invasion and metastasis (■ Fig. 2e&f).

Conclusion: These preliminary results suggest that TBs exhibit epithelial plasticity in response to the tumour-microenvironment (■ Fig. 3). The difference in tumour intrinsic phenotype indicates that future TB therapies may need to be tailored to each specific environmental compartment.

*Student submission
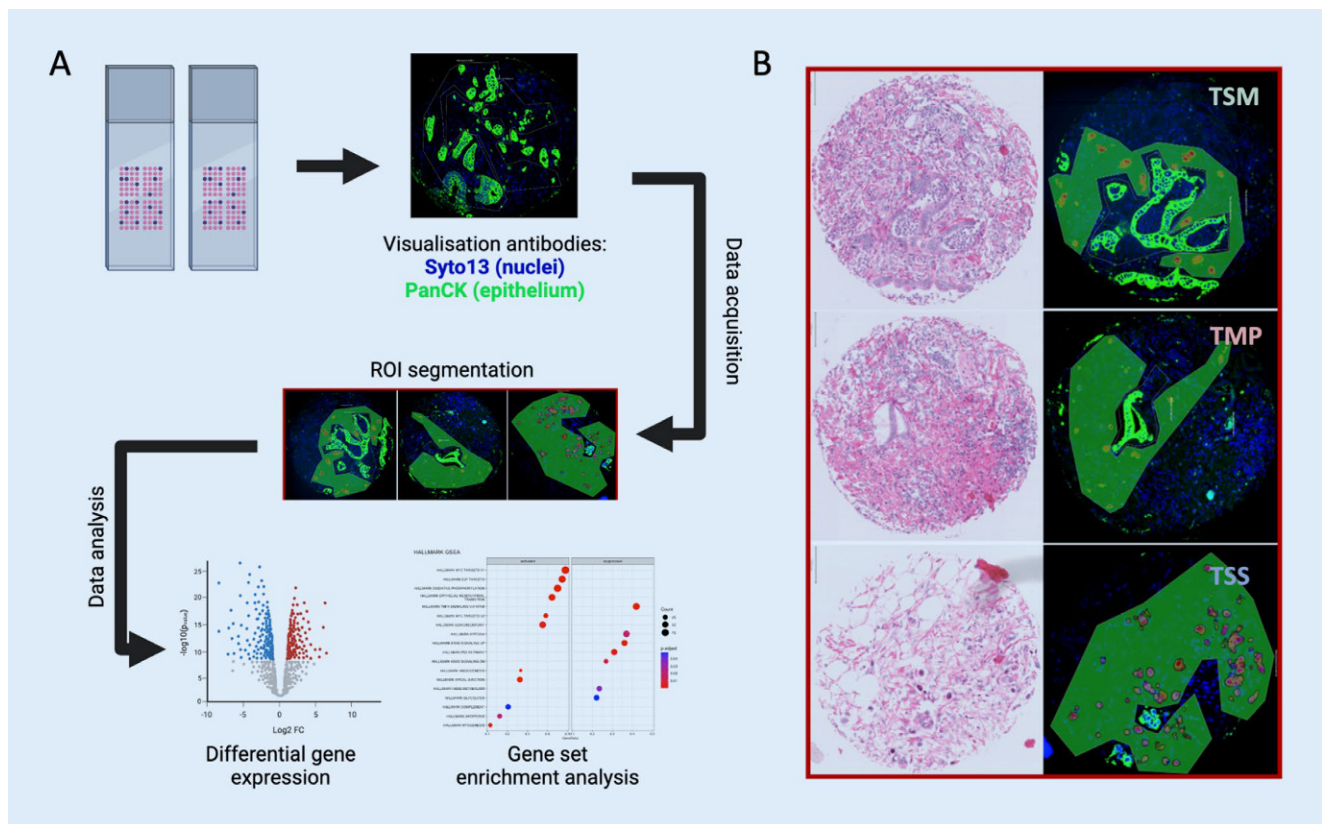
Fig. 1 | A 49 ▲ Summary of data acquisition workflow. A. Two tissue microarrays comprising cores from colorectal cancer primary resections with tumour budding were profiled using the spatial transcriptomic platform, Nanostring GeoMx Digital Spatial Profiler. Visualisation antibodies Pan-cytokeratin (epithelium) and SYT013 (DNA) were used to guide region of interest selection and probe aspiration. Pan-cytokeratin positive tumour buds were selected as epithelial regions of interest. Spatially tagged libraries from aspirated probes for each ROI were prepared and sequenced. Data pre-processing steps involved the removal of segments with <50% aligned reads and removal of genes above limits of quantitation in <10% of segments. This resulted in 26 cores and 6,920 genes for downstream analysis. B. Tumour buds from the 26 cores were categorized based upon location (depth of invasion): tunica submucosa (TSM), tunica muscularis propria (TMP) or tunica subserosa (TSS)
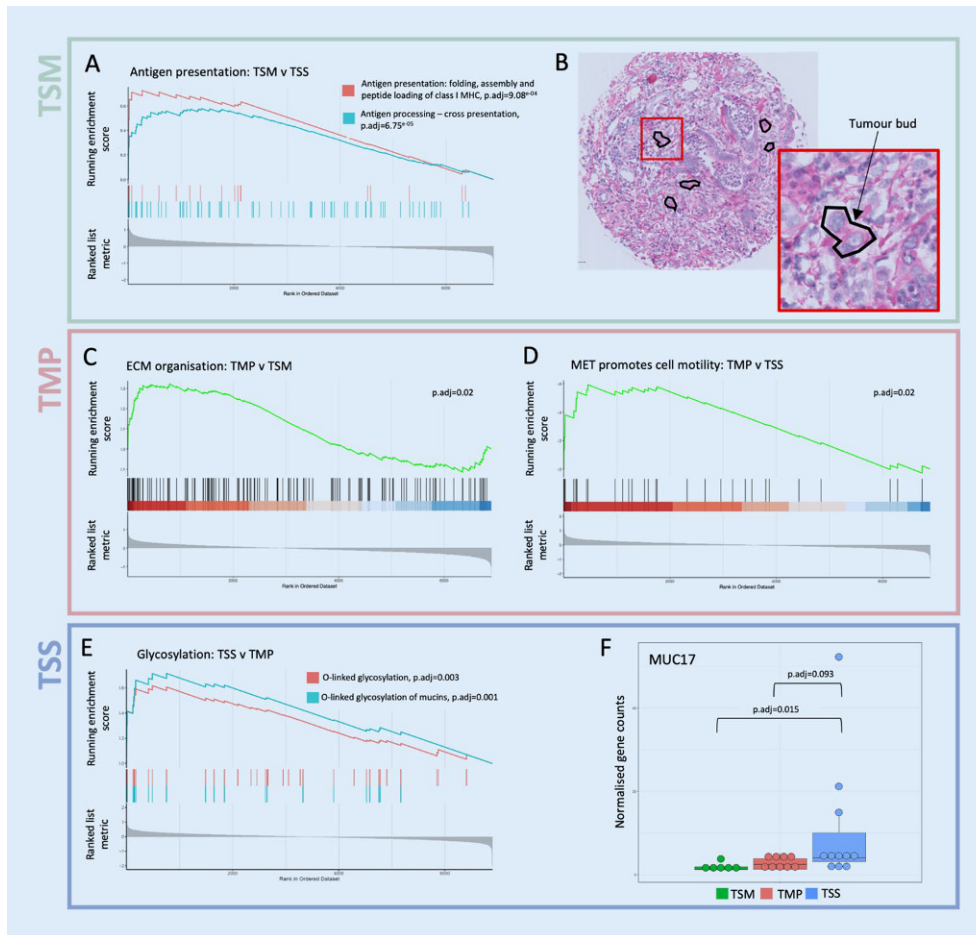
Fig. 2 | A 49 ◄ Gene set enrichment results of tumour budding phenotypes by depth of invasion. TSM (green box): A. Enrichment plot of antigen presentation pathway genes enriched in TSM v TSS (Antigen presentation, p.adj-9.084, Antigen processing, p.adj-6.75). B. Expert pathologist assessment of H&E images derived from the same section as spatial transcriptomics was performed on confirms the absence of significant intra-epithelial immune cells which could pose a source of enriched pathways observed in A. TMP: C. Enrichment plot of ECM organization genes enriched in TMP v TSM (*p*.adj = 0.02). D. Enrichment plot of cell motility genes enriched in TMP v TSS (*p*.adj = 0.02), TSS: E. Enrichment plot of glycosylation pathways enriched in TMP v TSS (0-linked glycosylation, *p*.adj-0.003, O-linked glycosylation of mucins, *p*.adj = 0.001). F. Expression of MUC17 was significantly increased on tumour buds in TSS compared to TSM (Mann-Whitney test, *p*.adj = 0.015)
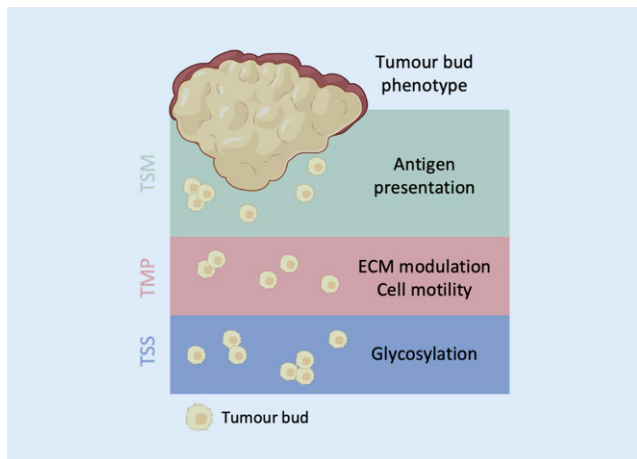
Fig. 3 | A 49 ▲ Summary schematic of study findings. Through spatially resolved transcriptomic profiling of tumour buds at different invasion depths (TSM: tunica submucosa, TMP: tunica muscularis propria, TSS: tunica subserosa) we have resolved distinct tumour bud phenotypes. Tumour buds in the TSM exhibit antigen presentation gene-sets. Tumour buds in the TMP exhibit ECM modulation and cell motility pathways which may reflect movement through the mechanically challenging muscular environment. Tumour buds in the TSS exhibit O-linked glycosylation pathways which have been shown to be associated with invasion and metastatic potential in a variety of cancer types

A 50*
Deep learning-based quantification of immune cells identifies eosinophils as a prognostic factor in colorectal cancer: a retrospective multi-institutional analysis

Mr. Elias Baumann[1]*, Prof. Philippe Krebs[2], Prof. Aurel Perren[2], Dr. Richard Kirsch[3], Prof. Martin D Berger[4], Prof. Alessandro Lugli[2], Prof. Iris Nagtegaal[5], Prof. Inti Zlobec[2]

[1]Institute of Tissue Medicine and Pathology, University of Bern, Bern Switzerland; [2]Institute of Tissue Medicine and Pathology, University of Bern, Bern, Switzerland; [3]Pathology and Laboratory Medicine, Mount Sinai Hospital, University of Toronto, Toronto, Ontario, Canada; [4]Department of Medical Oncology, Inselspital University Hospital, University of Bern, Bern, Switzerland; [5]Department of Pathology, Radboud University Medical Centre, Nijmegen, The Netherlands

Background: The immune infiltrate composition strongly affects colorectal cancer (CRC) prognosis, with lymphocyte presence representing a positive prognostic factor. Eosinophils are also involved in the cancer immune response however it is unclear whether their co-occurrence with lymphocytes potentiates anti-tumor immunity. To investigate this and the potential prognostic role of eosinophils in CRC we developed a deep learning model which automatically detects both cell types in near-tumor areas. We examined the association of derived scores with clinicopathological and outcome data in a large multi-institutional cohort.
Methods: Using an in-house developed nuclei detection model and a tissue segmentation model we quantified lymphocytes and eosinophils within 50 μm of malignant epithelium. We applied this pipeline to H&E scans (0.24mpp) of CRC cohorts from three institutes (Switzerland (n = 202; stage II/III), Netherlands ((n = 571; stage I–IV), and Canada (n = 418; stage I–IV)) and TCGA COAD/READ (n = 463; stage I–IV). Normal-

ized counts were correlated with clinicopathological and outcome data (overall survival (OS), disease-free survival (DFS)).

Results: Eosinophil counts decreased with higher TNM stage and pT classification (2/4 cohorts ($p < 0.05$)). In univariate analysis, eosinophils were prognostic (Canada (OS = 0.015), TCGA (OS: $p < 0.001$, DFS: $p < 0.001$)). Split into tertiles for further investigation, eosinophils stratify all cohorts (Switzerland (OS: $p = 0.07$), Netherlands (DFS: $p = 0.057$), Canada (OS: $p = 0.04$), TCGA (OS: $p < 0.001$, DFS: $p < 0.001$)). We combined cohorts due to sample size limitations, performing percentile normalization per cohort for multivariate analysis (age, sex, location, MMR-Status, stage). Considering only chemotherapy-naïve patients, high eosinophil density was positively associated with survival (OS: $p = 0.0013$, DFS: $p = 0.016$). This indicates a subgroup of patients who may benefit from adjuvant therapy. Eosinophils are positively correlated with lymphocytes (Pearson CC.: 0.64+−0.20) yet remained a significant prognostic feature while additionally including lymphocytes (OS: $p = 0.004$, DFS: $p = 0.09$).

Conclusions: Our multi-institute analysis demonstrates that eosinophils are prognostic specifically in chemotherapy-naive CRCs. However, their functional interaction with lymphocytes warrants further examination.
*Student submission

A 51
Metastatic melanoma immunotherapy response prediction from routine histopathology slides using digital pathology

Mr. Jonatan Bonjour[1]*, Dr. Alexandre Wicky[1], Dr. Amanda Seipel[2], Dr. Sofiya Latifyan[3], Mr. Petros Liakopoulos[4], Mr. Martin Beaussart[4], Dr. Julien Dagher[5], Prof. Olivier Michielin[6], Prof. Michel Cuendet[1], Prof. Andrew Janowczyk[6]

[1]Precision Oncology Center, Department of Oncology, Lausanne University Hospital, Lausanne, Switzerland; [2]Department of Diagnostics, Division of Clinical Pathology, Geneva University Hospital, Geneva, Switzerland; [3]Department of Oncology, Lausanne University Hospital (CHUV) and University of Lausanne, Lausanne, Switzerland; [4]Precision Oncology Center, Department of Oncology, Lausanne University Hospital, Lausanne, Switzerland; [5]Department of Laboratory Medicine and Pathology, Institute of Pathology, Lausanne University Hospital, University of Lausanne, Rue du Bugnon 25, 1011 Lausanne, Switzerland; [6]Precision Oncology Service, Department of Oncology, Geneva University Hospital, Geneva, Switzerland

Background: A clinically actionable biomarker identifying which patients with metastatic melanoma may benefit from immunotherapy is sorely needed. Tumor-infiltrating lymphocyte (TIL) patterns may lead to such a biomarker. Here, we precisely characterized them at scale using digital pathology.

Methods: In $n = 48$ metastatic melanoma biopsies from patients treated with immunotherapy, deep-learning models identified TILs in pre-treatment $40 \times$ magnification Hematoxylin and Eosin (H&E) whole slide images. Hand-crafted TIL spatial organization features were extracted and assessed against overall survival (OS). Using leave-one-out-cross-validation, feature selection using Maximum Relevance Minimum Redundancy (MRMR) led to development of a predictive immunotherapy benefit score via logistic regression.

Results: Several features showed significant OS association: kurtosis of lymphocyte cluster areas (dichotomized at the median: HR = 0.225, $p = 0.001$, 95% CI = 0.089–0.568), fraction of 500×500-pixel tiles with at least one lymphocyte (HR = 0.308, $p = 0.006$, 95% CI = 0.127–0.742), and median distance between non-lymphocyte cells and nearest lymphocyte cluster (HR = 0.390, $p = 0.023$, 95% CI = 0.168–0.907). These computer-only derivable features performed significantly better than those typically assessable visually by pathologists, such as TIL density (HR = 0.500, $p = 0.089$, 95% CI = 0.220–1.130) and TILs to-all-cells ratio (HR = 0.539, $p = 0.133$, 95% CI = 0.238–1.223). In a multivariate setting with clinical characteristics, TIL features remained independently predictive. The logistic regression-based prediction of immunotherapy benefit using six MRMR-selected features yielded an AUC of 0.78 (95% CI = 0.61–0.93).

Conclusion: Initial findings suggest that H&E TIL-based biomarkers hold promise in stratifying patient overall survival after immunotherapy. Computational digital pathology allows precise quantification of complex TIL features inaccessible via visual assessment, offering a novel opportunity for inexpensive, rapid, and non-destructive image-based biomarkers. These promising results indicate that an image-based biomarker using routine histopathology slides may aid in clinical treatment optimization, though further large-scale multi-site validation is necessary.

A 52
Impact of microrna-29a-loxl2 axis on tumor budding in pancreatic ductal adenocarcinoma

Dr. Philipp Zens[1], Dr. Simon April-Monn[1], Ms. Jessica L Rohrbach[1], Dr. José A Galván[1], Mr. Stefan Reinhard[1], Dr. Anna S Wenning[2], Prof. Beat Gloor[2], Prof. Martin D Berger[3], Dr. Martin Wartenberg[1]*

[1]Institute of Tissue Medicine and Pathology, University of Bern, Bern, Switzerland; [2]Department of Visceral Surgery, Inselspital University Hospital, University of Bern, Bern, Switzerland; [3]Department of Medical Oncology, Inselspital University Hospital, University of Bern, Bern, Switzerland

Background: Reduced posttranscriptional microRNA-29a-dependent regulation of stroma-modifying enzyme lysyl oxidase-like 2 (LOXL2) affects the tumor microenvironment (TME) of pancreatic ductal adenocarcinoma (PDAC). Tumor budding (TB) is a suggested morphologic marker of epithelial-mesenchymal transition and biologic aggressiveness in PDAC. In this study, the microRNA-29a-LOXL2 axis was analyzed in PDAC to investigate its potential impact on TB. It is hypothesized that posttranscriptionally deregulated stroma homeostasis locally promotes tumor progression in PDAC.

Methods: MicroRNA-29a (hsa-miR-29a-3p) and lysyl oxidase like 2 (LOXL2) mRNA were visualized by applying miRNAScope™ and RNAscope® chromogenic probes on successively cut tissue micro array (TMA) cohort slides, comprising of 117 cases of curatively resected PDAC. Hybridization signal recognition and quantification in tumor front and tumor center TMA spots were automated by digital image analysis (DIA) algorithms (Random-Forest Pixel classifiers). Statistical correlation of absolute microRNA and mRNA signal counts with TB status (present vs. absent) was performed for the tumor front and tumor center spots separately.

Results: Paired microRNA-29a and LOXL2 mRNA stained TMA cores of the tumor front of 54 PDAC cases, and paired cores of the tumor center of 48 PDAC cases, rendered evaluable hybridization signals (see Table 1). An inverse correlation between tumor suppressive microRNA-29a signal counts and stroma-modifying enzyme LOXL2 mRNA signal counts among the tumor front but not the tumor center was established (see ▪ **Fig. 1**). Among the tumor front spots but not the tumor center spots, presence of TB correlated significantly with low miRNA29a-3p ($p < 0.001$) and high LOXL2 mRNA signal counts ($p = 0.003$), and vice versa (see ▪ **Fig. 2**).

Conclusions: Automated DIA of chromogenic microRNA and mRNA hybridization signals is feasible on PDAC TMA tissue and offers insight into posttranscriptional modes of PDAC progression. The microRNA-29a-LOXL2 axis constitutes specialized, locally distinct stromal niches, that affect tumor morphology and progression.
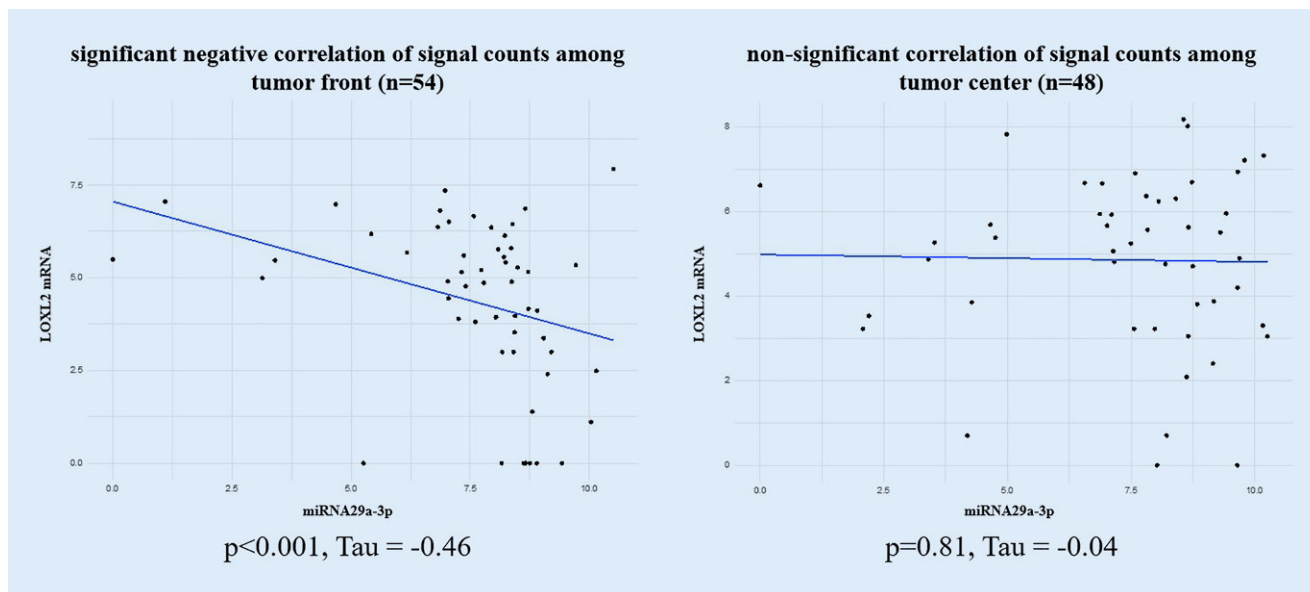
significant negative correlation of signal counts among tumor front (n=54)

p<0.001, Tau = -0.46

non-significant correlation of signal counts among tumor center (n=48)

p=0.81, Tau = -0.04

Fig. 1 | A 52 ▲ miRNA29a-3p LOXL2 mRNA correlation

tumor front

p<0.001   p=0.003

tumor center

p=0.488   p=0.001
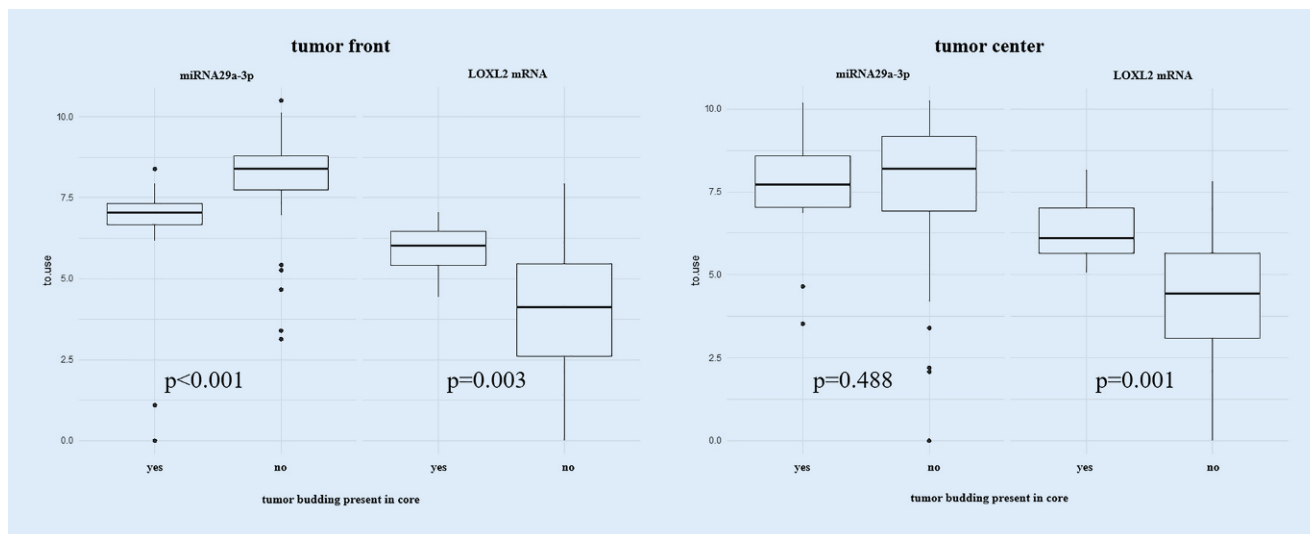
Fig. 2 | A 52 ▲ relation of tumor budding to miRNA29a-3p and LOXL2 mRNA signal counts

	miRNA29a-3p	LOXL2 mRNA
tumor front median signal count (n=54 spots)	3599	141
tumor front front IQR	1221 - 6007	22.2 - 327
tumor center median signal count (n=48 spots)	3098	191
tumor center IQR	994 - 7504	32.3 - 554

Fig. 3 | A 52 ▲ hybridization signal distribution

A 53*
Synergism between epigenomic and genomic alterations in lung cancer brain metastases

Dr. Philipp Zens[1]*, Mr. Benjamin Besson[2], Dr. Elham Kashani[1], Dr. Lorenz Frehner[3], Dr. Philipp Kirchner[1], Dr. Massimo Maiolo[1], Dr. Martina Kirchner[4], Dr. Michael Allgäuer[4], Dr. Albrecht Stenzinger[4], Dr. Tu Nguyen-Ngoc[5], Dr. Sabine Schmid[3], Prof. Erik Vassella[1], Prof. Sabina Berezowska[6]

[1]Institute of Tissue Medicine and Pathology, University of Bern, Bern, Switzerland; [2]Department of Pathology, Centre Hospitalier Universitaire Vaudois and University of Lausanne, Lausanne, Switzerland; [3]Department of Medical Oncology, Inselspital, Bern University Hospital, Bern, Switzerland; [4]Institute of Pathology, University Hospital Heidelberg, Heidelberg, Germany; [5]Department of Medical Oncology, Centre Hospitalier Universitaire Vaudois and University of Lausanne, Lausanne, Switzerland; [6]Department of Laboratory Medicine and Pathology, Institute of Pathology, Lausanne University Hospital, University of Lausanne, Rue du Bugnon 25, 1011 Lausanne, Switzerland

Introduction: Brain metastases (BM) are becoming a focus point in the handling of non-small cell lung cancer (NSCLC) patients due to increasing incidence rates and moderate response to systemic therapy especially in non-oncogene driven cases. Genome-based comparison studies highlight the importance of copy number alterations and *KRAS* activating mutations in NSCLC BM. In this study, we focus on methylation-based heterogeneity between primary lung adenocarcinoma (LUAD) and paired BM.
Methods: A total of 78 patients with paired primary LUAD and BM from three major pathology institutions (Bern, Lausanne and Heidelberg) were used for methylation analysis with the Infinium MethylationEPIC array (Illumina, San Diego, USA). Differentially methylated CpG positions, regions and pathways were identified using a pairwise analysis approach correcting for the patient.

Results: Intrapatient comparison of normal lung, primary LUAD and BM show significantly lower differences in the methylation pattern between the malignant samples than between normal lung tissue and primary LUAD or BM ($p < 0.001$). However, using patient corrected beta values, it was possible to cluster primary LUAD and BM by principal component analysis. We identified a total of 153'239 differentially methylated CpG positions highlighting a global hypomethylation in the BM compared to the paired primary LUAD. The PI3K-Akt and MAPK signaling pathways were the top two differentially methylated pathways. *ERBB2* and *ERBB3* were identified as leading genes in these pathways showing highly differentially methylated CpG positions (absolute logFC ≥ 1). As for other typical NSCLC drivers (e. g., *KRAS*), *ERBB2* and *ERBB3* were hypomethylated especially in promoter regions that showed high DNAse cluster scores.

Conclusion: Our analyses show the epigenetic upregulation of classic oncogenic pathways (PI3K-Akt and MAPK signaling) in LUAD BM and highlight the importance of the EGFR signaling axis through hypomethylation of *ERBB2* and *ERBB3*. This epigenetic activation seem to be synergistic to the described genomic alterations.

*Student submission

A 54*
BRCA promoter methylation in triple negative breast cancer is preserved in xenograft models and represents a potential therapeutic target for PARP inhibitors

Dr. Kavitha Däster[1]*, Dr. Jürgen Hench[2], Dr. Maren Diepenbruck[3], Dr. Katrin Volkmann[3], Dr. Adelin Rouchon[3], Dr. Marta Palafox[3], Dr. Bogdan-Tiberius Preca[3], Prof. Christian Kurzeder[4], Prof. Mohamed Bentires-Alj[3], Prof. Savas Soysal[5], Prof. Simone Muenst[2]

[1]Breast Center Zurich, Zurich, Switzerland; [2]Institute of Medical Genetics and Pathology, University Hospital Basel, Basel, Switzerland; [3]Tumor Heterogeneity Metastasis and Resistance, Department of Biomedicine, University Hospital Basel, University of Basel, Basel, Switzerland; [4]Breast Center, University Hospital Basel, Basel, Switzerland; [5]Praxis Chirurgie im Zentrum, Basel, Switzerland

Background: The majority of *BRCA1* germline mutated breast cancers (BC) are of triple negative subtype, and recent studies have shown that these tumors respond to poly(adenosine diphosphate [ADP]-ribose) polymerases (PARP) inhibitors. However, most triple negative BCs are sporadic in nature and are often associated with silencing or dysfunction of the *BRCA1* or *BRCA2* genes. Since somatic *BRCA* mutations are rare in BC, this dysfunction frequently is the result of *BRCA* promoter methylation. Despite the phenotypic similarities with germline or somatic *BRCA* mutated BC, the evidence of response to PARP inhibitors in these tumors is still lacking.

Methods: We analysed the prevalence of *BRCA* promoter methylation in 28 BC metastases through the well-established Illumina Infinium EPIC Human Methylation Bead Chip. In cases with *BRCA* methylation the xenograft of the same tumor was also tested. Additionally, we compared BC xenografts with an identified *BRCA* methylation to their matched primary tumors. We also subsequently investigated the efficacy of PARP inhibitors on organoids from a *BRCA2* promoter methylated BC.

Results: Methylation analysis showed *BRCA2* promotor hypermethylation in one pleural metastasis of a young patient as well as in the xenograft tissue, which was generated from the breast local recurrence tissue. We also identified 5 more xenograft models with *BRCA2* promotor hypermethylation. Analysis of the matched primary tumor of one of these xenograft models confirmed the same *BRCA2* methylation. PARP inhibitor treatment of organoids derived from the *BRCA2* methylated xenograft tumor tissue of the young patient showed a significant decline in cell viability, similar to organoids with somatic *BRCA1* mutation, while it had no effect on organoids without *BRCA2* methylation.

Conclusions: *BRCA* promotor hypermethylation seems to be a rare event in metastatic BC but is preserved in subsequent xenograft models and might represent an attractive therapeutic target for PARP inhibitors in metastatic BC patients.

*Student submission

A 55
Elaboration of a swiss guideline for next-generation sequencing results reporting

Dr. Yann Christinat[1]*, Dr. Ilaria Alborelli[2], Ms. Valérie Barbié[3], Dr. Bettina Bisig[4], Dr. Milo Frattini[5], Dr. Tobias Grob[6], Prof. Wolfram Jochum[7], Prof. Thomas McKee[1], Dr. Matthias S. Matter[2], Dr. Edoardo Missiaglia[8], Dr. Francesca Molinari[5], Prof. Gad Singer[9], Prof. Erik Vassella[10], Dr. Martin Zoche[11], Prof. Kirsten Mertz[12]

[1]HUG, Service de Pathologie Clinique, Geneva, Switzerland; [2]Institute of Pathology, University Hospital Basel, Basel, Switzerland; [3]Clinical Bioinformatics, SIB, Geneva, Switzerland; [4]Institute of Pathology, Lausanne University Hospital, Lausanne University, Lausanne, Switzerland; [5]Istituto Cantonale di Patologia, Locarno, Switzerland; [6]Universität Bern, Institut für Gewebemedezin und Pathologie, Bern, Switzerland; [7]KSSG, Institut für Pathologie, St-Gallen, Switzerland; [8;1]Institute of Pathology, Lausanne University, Lausanne, Switzerland; [9]KSB, Institut für Pathologie, Baden, Switzerland; [10]Institute of Tissue Medicine and Pathology, University of Bern, Bern, Switzerland; [11]University Hospital Zurich, Department of Pathology and Molecular Pathology, Zurich, Switzerland; [12]Institute of Pathologie, Cantonal Hospital Baselland, Liestal, Switzerland

Background: Mutation analysis through next-generation sequencing (NGS) is well integrated in Swiss molecular pathology laboratories and has become a standard diagnostic analysis for certain indications. Currently, reporting practices differ within the country, and since patients move between hospitals it is becoming increasingly necessary to interpret a NGS report from another laboratory. Furthermore, as many different players have access to the NGS report (oncologists, geneticists, pathologists, patients themselves), it needs to contain broad and detailed information to address the questions of the specialist and to avoid misinterpretation by non-specialist. Two projects with similar aims, one initiated by the Swiss Institute of Bioinformatics and the other by SSMolpath and the SAKK Working Group Molecular Oncology, are now advancing together to address these important issues.

Methods: A first survey was conducted to assess the differences in NGS reporting of ten pathology laboratories located in Basel, Bern, Geneva, Lausanne, Liestal, Zürich, St. Gallen and Locarno. Based on these results, a Delphi method was initiated to reach a consensus on the ideal content of an NGS report.

Results: The first survey identified 48 discrepancies in reporting practices. A second survey, focusing on these items, was sent to all members of SS-MolPath. An expert group was then formed and questioned via a third survey. The expert panel reached a consensus on all but two points (◘ Fig. 1). Outstanding issues are the incidental identification of suspected germline variants and reporting of the actionability of variants.

Conclusion: Comparison of NGS reports revealed many discrepancies in practice. Through several rounds of surveys and discussions, a consensus was reached on all but two points. Once these are resolved, guidelines will be proposed and circulated among SSMolPath members before submission to a scientific journal.
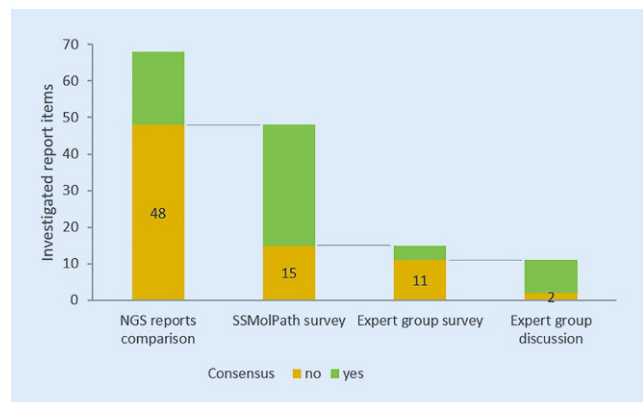
Fig. 1 | A 55 ▲ Identified discrepancies in NGS reports from ten laboratories and their resolution toward a consensus

Abstracts

A 56*
A customized user interface for integration and visualization of AI outcomes via high-performance computing (HPC) in pathology routine

Mr. Chris Rüttimann[1]*, Prof. Inti Zlobec[2], Dr. Amjad Khan[1]

[1]Institute of Tissue Medicine and Pathology, University of Bern, Bern, Switzerland;
[2]Institute of Tissue Medicine and Pathology, University of Bern, Bern, Switzerland

Background: The rise of AI applications in pathology has underscored the need for seamless integration tools, especially for viewing and annotating Whole Slide Images (WSIs). Current tools, tailored for research, often pose challenges for clinicians due to their complex interfaces and additional software requirements. Moreover, they lack compatibility with high-performance computing cluster (HPC) for the integration of AI tools.
Methods: To bridge this gap, we developed a web-based WSI viewer with a user-centric design, operable via a standard web browser, eliminating software installation hassles. The main objective is to display WSIs while highlighting results from machine learning algorithms. The frontend, built using the Vue.js framework, integrates libraries like OpenSeadragon for high-resolution image viewing. The backend manages complex tasks, from data synchronization to secure HPC connectivity via SSH. Communication protocols include HTTP and WebSockets, with SQLite as the current database, though a transition to a more robust system is planned. ◘ **Fig. 1** shows the WSI viewer with an example image overlay with the results of a machine learning algorithm.
Results: Our tool provides efficient access to utilize AI tools by the experts and researchers to visualize outcome and evaluate such models. Initial deployment was stable both for WSI viewing and real time AI model triggering through HPC with results overlays. Despite its success, the project faced challenges like classification mask offsets, connection bottlenecks with storage modules, and limitations in user-initiated classifications. The application's compatibility is also limited to certain scanner types.

Conclusions: The project's future roadmap is promising, encompassing system architecture refinement, a database system upgrade, and a comprehensive user management system introduction. This will be crucial for concurrent usage and facilitating project sharing among users.
*Student submission

A 57*
Impact of computer-aided diagnostic tool on Pathologists' tumor cell fraction estimation–a Swiss national study

Ms. Ana Leni Frei[1]*, Mr. Raphaël Oberson[1], Mr. Elias Baumann[2], Mr. Christian Abbet[3], Prof. Aurel Perren[1], Prof. Alessandro Lugli[1], Dr. Heather Dawson[1], Prof. Rainer Grobholz[4], Prof. Andrew Janowczyk[5], Prof. Inti Zlobec[1]

[1]Institute of Tissue Medicine and Pathology, University of Bern, Bern, Switzerland; [2]Institute of Tissue Medicine and Pathology, University of Bern, Bern, Switzerland; [3]Signal Processing Laboratory 5, Ecole Polytechnique Fédérale de Lausanne, Lausanne, Switzerland; [4]Institute of Pathology Kantonspital Aarau, Aarau, Switzerland; [5]Department of Diagnostics & Department of Oncology, Division of Clinical Pathology & Precision Oncology, Geneva University Hospitals, Geneva, Switzerland

Background: Computer-aided diagnostic (CAD) tools are intended to increase reproducibility and efficiency of routine tasks while reducing inter-observer variability. Here we studied the impact of CAD tool usage by pathologists on the estimation of tumor cell fraction (TCF) in haematoxylin and eosin (H&E) images. Being a routine clinical task, TCF estimation was selected for its well-known large inter-observer variability, making it an ideal scenario to evaluate potential benefits provided by CAD tools.
Design: During a Swiss National Slide Seminar event, pathologists ($n = 69$) estimated TCF in 10 regions of interest (ROIs) from H&E colorectal cancer digital images. ROIs were intentionally selected to display variable tissue
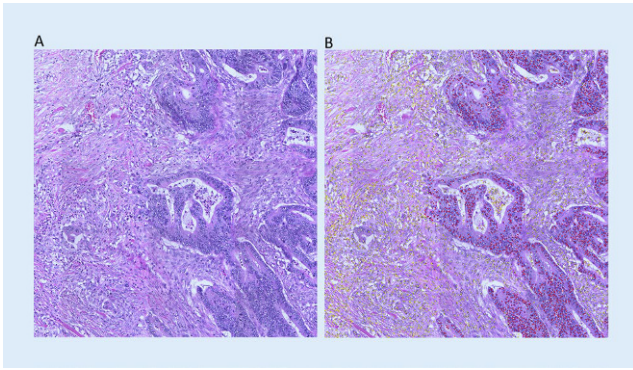
Fig. 1 | A 56 ▲

Fig. 1 | A 57 ▲ H&E ROI and corresponding TCF CAD prediction overlay. (A) Example H&E ROI (1000 × 1000px) at 40X magni- fication (0.25 μm/px) given to pathologists for TCF estimation. (B) Corresponding CAD tool prediction overlay highlighting tumor cells in red and non-tumor cells in yellow

compositions and cellularity. Pathologists then re-evaluated the same ROIs while being provided with computationally created TCF predictions consisting of cells overlays (tumor versus non-tumor cells, ▣ Fig. 1) and the corresponding TCF percentage. Participants' assessments were compared to manual cell counts ground truths (GT) established by experts. Pathologists also reported how confident they felt about their estimations using a 5-tiered scale (no confidence to high confidence).

Results: Inter-observer variability significantly decreased with the CAD tool assistance and scores converged towards the GT (avg. TCF standard deviation to GT was 9.9% vs. 5.8% when assisted, $p < 0.05$), resulting in an increased intraclass correlation coefficient (ICC) from 0.8 to 0.93 (CI95% [0.65, 0.93] vs [0.86, 0.98] with CAD), ▣ Fig. 2. Importantly, the increased scoring accuracy was also observed when CAD tool's predictions slightly deviated from the GT. Overall, pathologists benefited from the CAD tool and felt more confident in their assessment when assisted (3.67 ± 0.81 vs. 4.17 ± 0.82 with CAD).

Conclusion: TCF scoring demonstrated large inter-observer variability which was significantly reduced using CAD. Scoring accuracy, ICC and pathologist's confidence increased with CAD support, suggesting that CAD systems may be able to improve reliability, reproducibility and agreement for tasks involving visual estimations of cell proportions.

*Student submission
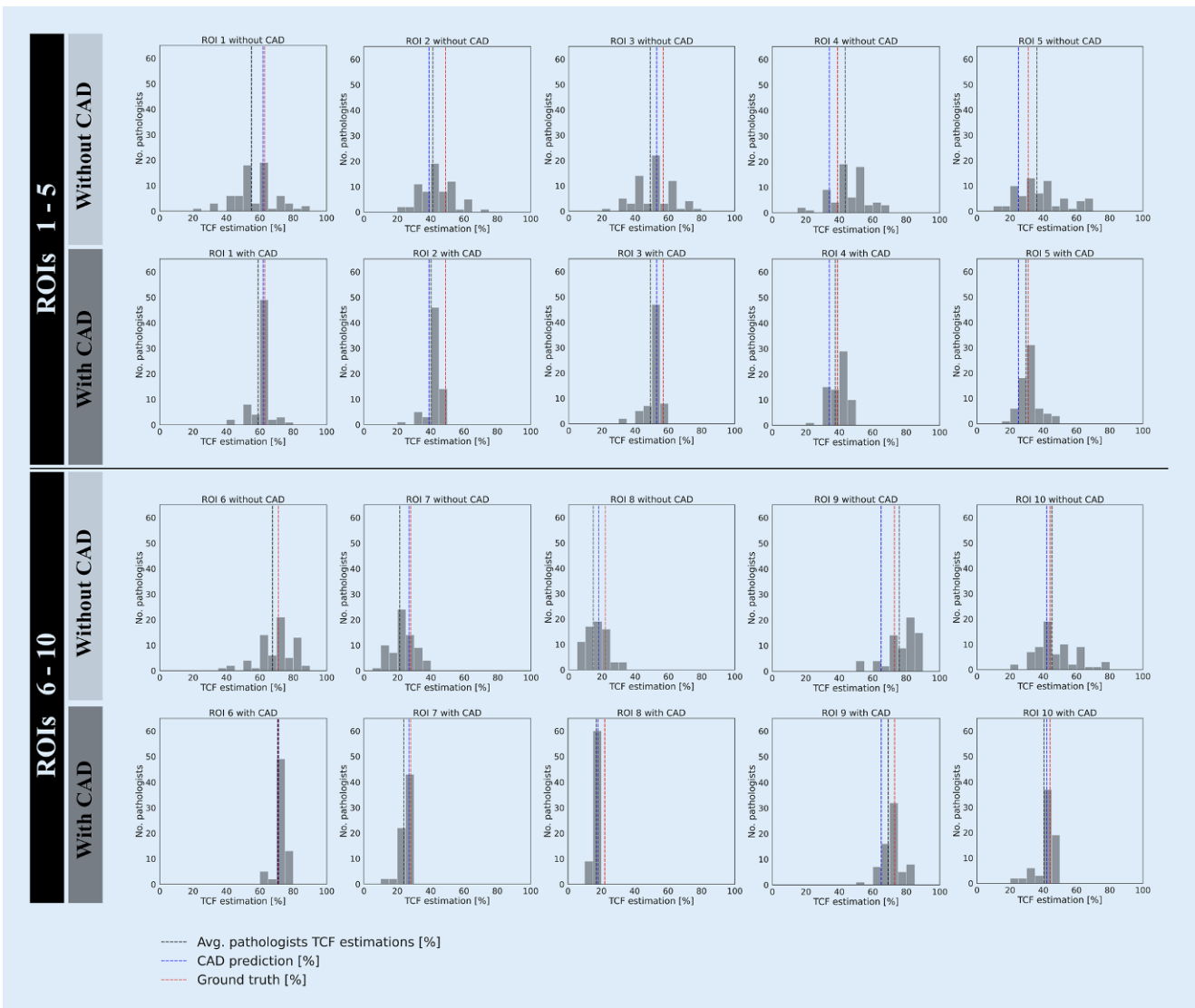
Fig. 2 | A 57 ▲ Dataset scoring by pathologists with and without CAD support. For all 10 ROIS scored, pathologists' TCF estimations are plotted with and without CAD support. Black vertical dashed lines highlight the average score assigned by the pathologists for each ROI, Blue vertical dashed lines show the CAD prediction value that was provided to participants and red vertical dashed lines correspond to the GT value

Abstracts

A 58
Fusion gene landscape of peripheral T-cell lymphomas

Dr. Baptiste Guey[1]*, Dr. David Vallois[1], Dr. Bettina Bisig[1], Dr. Karine Lefort[1], Mr. Vimel Rattina[1], Dr. Olivier Tournilhac[2], Dr. Raphael Koch[3], Dr. Andreas Rosenwald[4], Prof. Philippe Gaulard[5], Dr. Reiner Siebert[6], Prof. Laurence de Leval[1], Dr. Edoardo Missiaglia[1]

[1]Institute of Pathology, Lausanne University Hospital, Lausanne University, Lausanne, Switzerland; [2]Department of Hematology and Cellular Therapy, CHU Hotel Dieu Hématologie, Clermont-Ferrand, France; [3]Department of Hematology and Medical Oncology, University Medical Center Göttingen, Gottingen, Germany; [4]Institute of Pathology, University of Wuerzburg, Wuerzburg, Germany; [5]Faculty of Medicine and Health, Campus Henri Mondor, Paris-Est Créteil University, 94000 Créteil, France; Department of Pathology, Henri Mondor University Hospital, Créteil, France; [6]Institute of Human Genetics, Ulm University and Ulm University Medical Center, Ulm, Germany

Introduction: Fusion genes favor tumorigenesis through promoting gain-of-function of oncogenes or inactivation of tumor suppressor genes. Peripheral T-cell lymphomas (PTCLs) comprise rare and usually aggressive neoplasms, with reported gene fusions involving signaling pathway or tyrosine kinase genes, which could be of diagnostic biological or therapeutic relevance. This study explores the detection of fusion transcripts in routinely processed PTCLs using RNA-seq.

Methods: Strand-specific RNA-seq was performed on 91 PTCL FFPE samples (49 follicular helper T-cell lymphomas (TFHLs), 26 PTCL-not otherwise specified (PTCLs-NOS), 11 ALK-negative anaplastic large cell lymphomas (ALCLs), 5 others) from two European clinical trial cohorts (TRANSCAN project). Gene fusions were detected using both *STAR-Fusion* and *Arriba* tools starting from hg19 human reference-aligned sequences. Fusion candidates were selected using *annoFuse* and internal filtering, including literature-based search. Ten fusions were validated using a custom NGS Archer panel.

Results: Through in-silico steps and prioritization, we identified 26 putative driver fusion candidates across 91 PTCLs. We further confirmed 7 out of 10 tested fusions by NGS. PTCL-NOS subtype exhibited the highest rate of cases harboring fusion (29.2%), followed by ALK-negative ALCL (27.3%) and TFHL (16.3%). We identified recurrent rearrangements involving *IKZF2* or *VAV1* genes, both previously reported in PTCLs. Among others, *VAV1::THAP4, IKZF2::ERBB4, PCM1::JAK2, MKLN1-AS1::DUSP22* corresponding to or resembling known oncogenic fusions were identified in different samples. Additionally, we observed new potential driver fusions not yet described in PTCLs.

Conclusion: This RNA-seq study revealed 26 potential driver fusions across diverse PTCL subtypes. We highlighted recurrent fusions involving *IKZF2*, *PCM1* or *VAV1* previously reported in PTCLs and other cancers along with new candidate fusions. Our findings provide insights into fusion-mediated oncogenesis and potential therapeutic targets in PTCLs.

A 59
Unusual late recurrence of an HPV-associated endocervical adenocarcinoma presenting as pseudomyxoma peritonei: a case report

Mr. Georgios Kitsakis[1]*, Dr. Philip Went[1], Dr. Peter Martin Fehr[2], Dr. Tatjana Vlajnic[1]

[1]Institute of Pathology, Kantonsspital Graubünden, Chur, Switzerland; [2]Frauenklinik Fontana, Kantonsspital Graubünden, Chur, Switzerland

Background: A 59 year-old woman was hospitalized with ascites and suspicion of ovarian carcinoma with peritoneal carcinosis on CT scan. Diagnostic laparotomy revealed pseudomyxoma peritonei and cystic-solid adnexal and appendiceal tumor masses. Intestinal-type adenocarcinoma was diagnosed on intraoperative frozen section, which was considered to be a mucinous neoplasm of the appendix.

Consequently, an appendectomy, bilateral adnexectomy, omentectomy and peritoneal biopsies were performed. Moreover, the patient had a history of an HPV-associated endocervical adenocarcinoma in situ (AIS) 15 years earlier, treated by total hysterectomy with free margins. Follow-up vaginal smears were negative for dysplasia or AIS.

Methods: We performed immunohistochemical analyses for CK7, CK20, CDX2, ER, PAX8 and p16.

Results: Microscopic examination showed an adenocarcinoma with minimally atypical cylindrical cells spreading along the tubal epithelium with only focal infiltration of the tubal wall as well as mass-forming acellular organized mucin in the peritoneum. Surprisingly, the appendix was free of tumor. The morphology and the immunophenotype (PAX8+, p16+, ER–, CDX2–) raised the suspicion of a manifestation of the known AIS, which was proven by detection of HPV genotype 16 by PCR.

Re-evaluation of the hysterectomy specimen revealed an invasive endocervical adenocarcinoma (ECAC), Silva pattern A. The long latency period in this patient reflects the favorable prognosis of this growth pattern. However, the pT category remains unclear. The rpT3b category probably overestimates the current tumor stage. An initial involvement of the tubes by the ECAC with a slow tumor progression cannot be fully excluded.

Conclusion: Retrograde spreading of HPV-associated ECAC as well as AIS to endometrium, ovaries or fallopian tubes rarely occurs. This case raises the awareness of this unusual tumor manifestation and stresses the importance of long-term follow-up of patients with "indolent" ECAC and AIS.

A 60
Optimization by site and time of liquid biopsy for CGP-profiling in early cancer detection: a technical evaluation

Dr. Markus Rechsteiner[1]*, Dr. Michaela Kirschner[2], Dr. Raphael Werner[2], Prof. Alessandra Curioni-Fontecedro[3], Prof. Holger Moch[4], Dr. Bettina Sobottka[5], Dr. Jan Hendrik Rüschoff[6], Prof. Isabelle Opitz[2]

[1]Department of Pathology and Molecular Pathology, University Hospital Zurich, Zurich, Switzerland; [2]Department of Thoracic Surgery, University Hospital Zurich, Zurich, Switzerland; [3]Cantonal Hospital Fribourg, Fribourg, Switzerland; [4]Department of Pathology and Molecular Pathology, University Hospital Zurich, University of Zurich, Zurich, Switzerland; [5]Department of Pathology and Molecular Pathology, University Hospital of Zurich, Zurich, Switzerland; [6]University Hospital Zurich, Department of Pathology and Molecular Pathology, Zurich, Switzerland

Background: Nowadays, liquid biopsies are mainly used in patients with metastatic disease in order to monitor response or to detect emerging resistance mechanisms, while further uses such as early tumor detection are still under investigation. The major difficulty for assays is the low abundance of circulating tumor DNA (ctDNA) in early cancers which comes along with technical limitations. The aim of this study is to assess the technical limits of such an assay and to determine best practices for liquid biopsies concerning input, quality and finally sensitivity and specificity.

Methods: Recently, a new highly sensitive liquid biopsy NGS assay, the Oncomine Precision Assay, was released, which allows for the detection of the most relevant altered genes in cancers, including amplifications, fusions and intra-genic exon skipping, in 24 to 48 h. To optimize the detection of ctDNA, a cohort of stage I–III cancer patients was selected with liquid biopsies at three different time-points: blood from i) peripheral vein at resection, ii) tumor draining vein at resection, iii) peripheral vein at first radiological follow-up.

Results: From a first set of liquid biopsies ($n = 24$) the cfDNA has already been extracted. In average, the cfDNA concentration per ml blood-plasma derived from the peripheral vein at resection 0.91 ng/ul, from the tumor draining vein at resection 24.42 ng/ul, and from the peripheral vein at first radiological follow-up 0.7 ng/ul. Sequencing is ongoing on the Genexus platform using the Oncomine Precision Assay.

Conclusions: The first set of data revealed higher yields of cfDNA derived in liquid biopsies taken from the tumor draining vein compared to peripheral blood. At the venue, we show data evaluating the impact of these sampling strategies on sensitivity and specificity of the results generated by the Oncomine Precision Assay on the Genexus platform.

A 61
Spectrum of histological liver vascular abnormalities in patients with short telomeres

Dr. Chiara Saglietti[1]*, Dr. Alexander Coukos[2], Dr. Gabriela Baerlocher[3], Dr. Monica Haubitz[3], Prof. Darius Moradpour[2], Dr. Montserrat Fraga[2], Prof. Christine Sempoux[1]

[1]Institute of Pathology, Department of Laboratory Medicine and Pathology, Lausanne University Hospital and University of Lausanne, Lausanne, Switzerland; [2]Division of Gastroenterology and Hepatology, Lausanne University Hospital and University of Lausanne, Lausanne, Switzerland; [3]Laboratory for Hematopoiesis and Molecular Genetics, Department of Biomedical Research, University of Bern, Bern, Switzerland

Background: Short telomere syndrome (STS) is a premature aging disorder often caused by inherited gene mutations that result in reduced telomere length (TL) [1]. The liver is affected in up to 40% of patients with STS, often showing features of nodular regenerative hyperplasia [2, 3], a lesion also associated with aging [4]. We characterized in detail the spectrum of histological liver vascular abnormalities in patients with short telomeres, in accordance with the most recent nomenclature [5].

Methods: We reviewed a series of 17 patients for whom TL analysis had been performed, showing short telomeres (STel, 1st–10th percentile for TL) or very short telomeres (VSTel, < 1st percentile for TL) and for whom a liver biopsy reported "vascular abnormalities". Eight additional histopathological parameters were systematically analyzed.

Results: The series consisted in 11 men and 6 women (mean age, 49 years) with STel (11) or VSTel (6). Portal vein stenosis, a lesion associated with non-cirrhotic portal hypertension and previously called obliterative portal venopathy, was seen in 10 patients, nodular regenerative hyperplasia was found in two, and both lesions in three. Portal vein herniation and portal tract hypervascularization were present in 9 and 2 patients, respectively. Portal inflammation, ductular reaction and hepatocyte anisokaryosis were present in half of the patients and fibrosis was seen in four.

Conclusion: Portal vein stenosis is the most frequent histological liver vascular abnormality seen in patients with short telomeres. In the appropriate clinical context, its presence should therefore prompt the pathologist to propose assessing telomere length in the diagnostic process.

References

1. Mangaonkar AA et al (2018) Mayo Clin Proc
2. Kaaipru D et al (2019) Hepatology
3. Patnaik MM et al (2018) J Hepatol
4. Wanless IR (1990) Hepatology. Wanless
5. Guido M et al (2019) Histopathology

A 62
HistoBlur: a deep learning tool for flexible and accurate blur detection on whole slide digital pathology images

Mr. Petros Liakopoulos[1]*, Mr. Sabina Köfler[2], Dr. Laura Padaychy[3], Dr. Mario Kreutzfeldt[4], Dr. Matthieu Tihy[3], Mr. Rahul Nair[5], Prof. Sven Rottenberg[6], Prof. Michel Cuendet[1], Prof. Olivier Michielin[7], Prof. Rupert Langer[2], Prof. Doron Merkler[8], Prof. Andrew Janowczyk[3]

[1]Precision Oncology Center, Department of Oncology, Lausanne University Hospital, Lausanne, Switzerland; [2]Johannes Kepler University Linz, Kepler University Hospital GmbH, Linz, Austria; [3]Department of Diagnostics, Division of Clinical Pathology, University and University Hospitals of Geneva, Geneva, Switzerland; [4]Department of Diagnostics & Department of Pathology and Immunology, Division of Clinical Pathology, Geneva University and Geneva University Hospitals, Geneva, Switzerland; [5]Department of Biomedical Engineering, Case Western Reserve University, Cleveland, Ohio, USA; [6]Department of Infectious Diseases and Pathobiology, Vetsuisse Faculty, University of Bern, Switzerland; [7]Service of Precision Oncology, Department of Oncology, Geneva University Hospital, Geneva, Switzerland; [8]Service of Clinical Pathology, Department of Diagnostics, Geneva University Hospital, Geneva, Switzerland

Background & objectives: Blur artifacts may be introduced by scanners during digitization of histopathology glass slides to whole slide images (WSI). We present an open-source deep learning (DL) tool called HistoBlur that allows for rapid, precise, and annotation-free detection of blurry regions in WSI.

Methods: Two cohorts of $n = 125$ slides (52%/48% blurry vs non-blurry) and $n = 110$ slides (50%/50% blurry vs non-blurry) originating from different sites were analyzed. One non-blurry representative H&E tissue WSI at 20x from each site had low/medium/high levels of Gaussian smoothing applied to yield a supervised training task for blurriness identification ([▶] Fig. 1). The resulting blur score was computed as a percentage of patches predicted as medium/highly blurry. Medium/high blur was defined as levels at which discerning of tissue characteristics by human readers was impeded.

Results: HistoBlur consistently returned higher blur scores for blurry WSIs, with their mean blur score 94.3% and 41.9% for each cohort respectively. For non-blurry WSIs, the mean blur score was 1.6% and 2.0%. With a cutoff blur score of 10%, the sensitivity for the detection of blurry vs. non-blurry slides was 100% and 96% and the specificity was 97% and 100% for each cohort respectively, compared to pathologist annotations. The average throughput was approximately 30 s per slide.

Conclusion: Histoblur is an open-source tool for easily training and employing dl for the detection of blurry regions on WSI via a simple command line interface. Our results suggest that HistoBlur can reliably identify poor-quality scans of histological slides. In a diagnostic workflow setting, HistoBlur could be utilized to automatically identify slides requiring rescanning, substantially reducing human oversight and improving the overall diagnostic efficiency. In addition, blurry regions can be eliminated automatically prior to batch WSI downstream image analyses, thus limiting deleterious effects in image-based biomarker discovery. HistoBlur is freely available at histoblur.com.
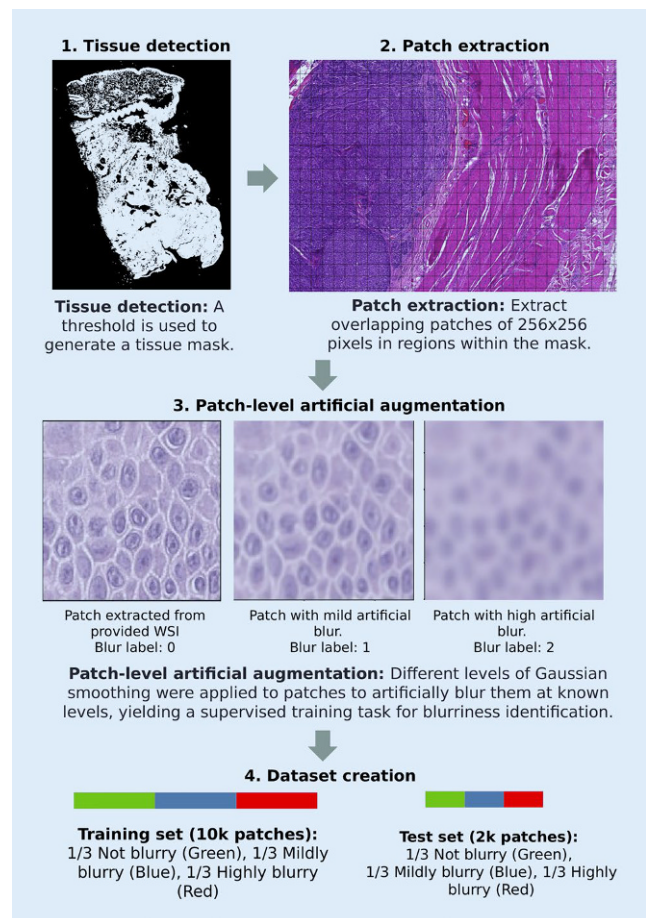
Fig. 1 | A 62 ▲ Overview of dataset preparation. A training and a test set are created. Each contains 1/3 of each class with the corresponding labels of the artificial blur applied

A 63

Spatially resolved transcriptomic profiling: an experimental comparison of GeoMx digital spatial profiling and Visium CytAssist spatial transcriptomics in three cancer types

Dr. Chiara Saglietti[1]*, Dr. Almudena Espín Pérez*[2], Dr. Quentin Bayard*[2], Dr. Sabrina Carpentier*[2], Dr. Daria Buszta[3], Dr. Yixing Dong[3], Dr. Eric Durand[2], Dr. Rémy Dubois[2], Dr. Atanas Kamburov[4], Dr. Senbai Kang[5], Dr. Silvia Lopez Lastra[2], Dr. Nathalie Piazzon[1], Dr. Rita Santos[2], Dr. Katharina von Loga[2], Prof. Raphael Gottardo**[3], Dr. Krisztian Homicsko**[6], Dr. Elo Madissoon**[2], Prof. Laurence de Leval[7]

[1]Institute of Pathology, Department of Laboratory Medicine and Pathology, Lausanne University Hospital and University of Lausanne, Lausanne, Switzerland; [2]Owkin, Paris, France; [3]Biomedical Data Science Center, Lausanne University Hospital and Lausanne University, Lausanne, Switzerland; [4]Owkin; [5]Biomedical Data Science Center, Lausanne University Hospital, Lausanne, Switzerland; [6]Department of Oncology, Lausanne University Hospital and Swiss Cancer Center Leman, Lausanne, Switzerland; [7]Institute of
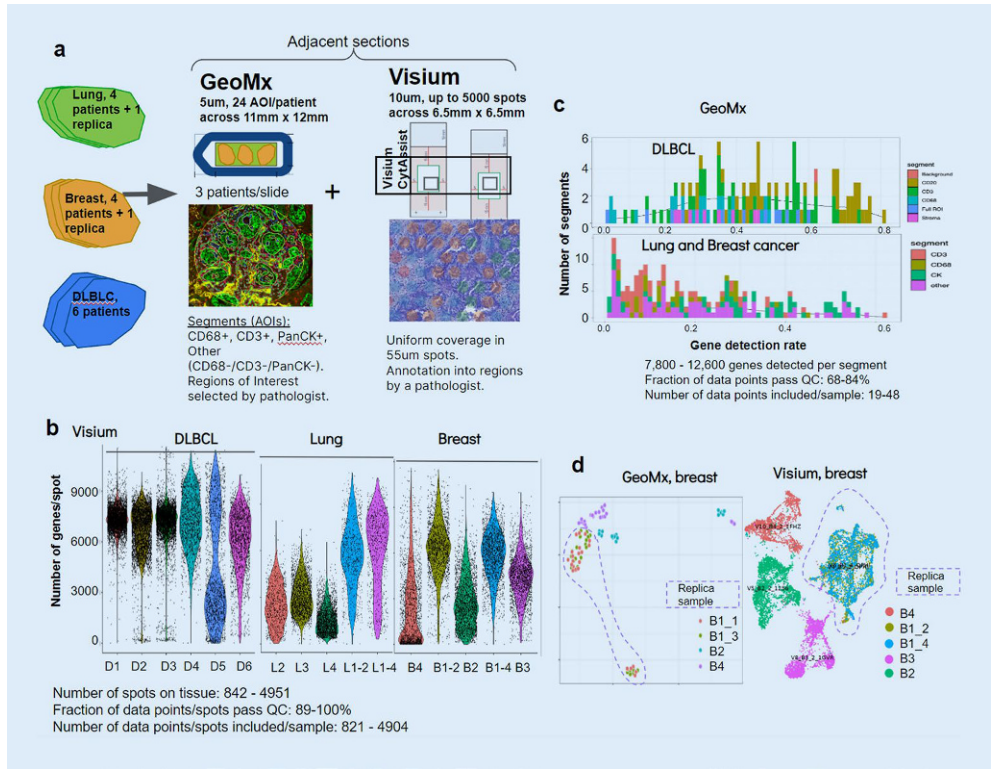
Fig. 1 | A 63 ◄ High quality data was generated with both GeoMx and Visium methods for lung, breast and DLBCL samples. GeoMx and Visium spatial transcriptomics data was generated for three cancer indications across 14 donors and 16 samples (**a**). Gene detection violinplot for all the samples on Visium (**b**). GeoMx data quality is above the recommended thresholds for most AOI-s across all four segments for the gene detection rate (**c**). UMAP plots for breast samples duplicates in GeoMx and Visium show good reproducibility (dashed lines) (**d**)
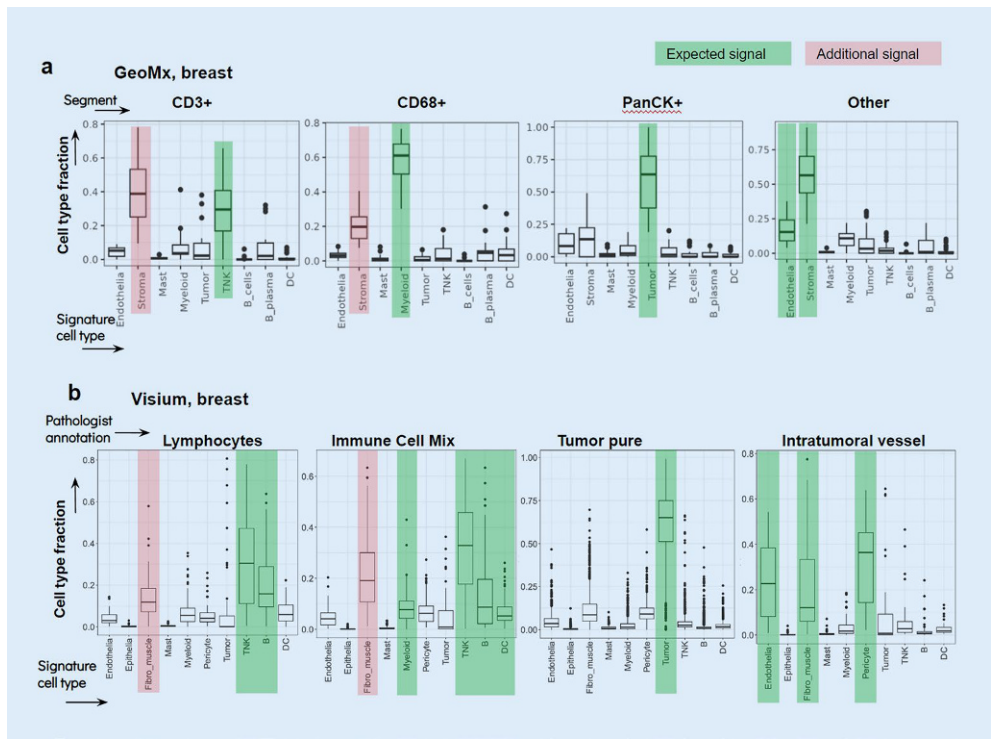
Fig. 2 | A 63 ◄ Data points from both GeoMx and Visium contain signal from mixture of cell types. Cell type deconvolution results for GeoMx AOIs for breast cancer, grouped by the signature cell type signal, separated by the segment type (**a**). Cell type deconvolution results for Visium spots for breast, grouped by the signature cell type signal, separated by the pathologist annotation into groups (**a**). All the data points were compared against the signature cell type matrix to gain cell type fractions

Pathology, Department of Laboratory Medicine and Pathology, Lausanne University Hospital and Lausanne University, Lausanne, Switzerland

Background: Several technologies can characterize spatial heterogeneity of gene expression in tissues. Their relative strengths and weaknesses have been poorly explored. We compared the output of GeoMx DSP (Nanostring) and Visium CytAssist (10x) full transcriptomes in the analysis of human cancers.

Methods: Consecutive sections of archival FFPE blocks (median age 57 months (22–103); median DV200 53.75% (7.2–80.3)) of breast and lung carcinomas (BC/LC; n = 4 each) and diffuse large B-cell lymphomas (DLBCL, n = 6) were profiled with both platforms, in duplicate for one BC and one LC. GeoMx regions of interest (ROIs) were segmented for tumor (CK/CD20+), CD3+, CD68+ and marker-negative areas of illumination (AOIs). Visium capture spots were annotated for majority cell type based on H&E. Sections were aligned to match Visium spots with GeoMx AOI covering > 70% of their areas.

Results: Between 68–84% AOIs (GeoMx) and 89–100% spots (Visium) passed QC, resulting in 376 GeoMx and 36,776 Visium data points. Both methods showed high replicate reproducibility, with strong patient effect. Transcriptomes deconvolution showed a mixture of cell types, enriched in the selected AOI type (GeoMx), and according to pathologists' annotations (Visium). Matching spots/AOIs analysis (598 spots/67 AOIs) showed similar results for capturing cell type mixtures in GeoMx and Visium, with higher variety in stromal compartment for Visium. Independent Differential Expression analysis between biological compartments demonstrated a similar signal in GeoMx and Visium, with higher significance in Visium.

Conclusions: We generated good quality spatial transcriptomics data with GeoMx DSP and Visium CytAssist. Both GeoMx AOIs and Visium spots capture a mixture of cell types, enriched in the expected cell signature. GeoMx enables profiling of expertly selected cell types in predefined tissue areas. Visium offers many more data points that can altogether provide similar cell type enrichments for most cell types based on deconvolution.
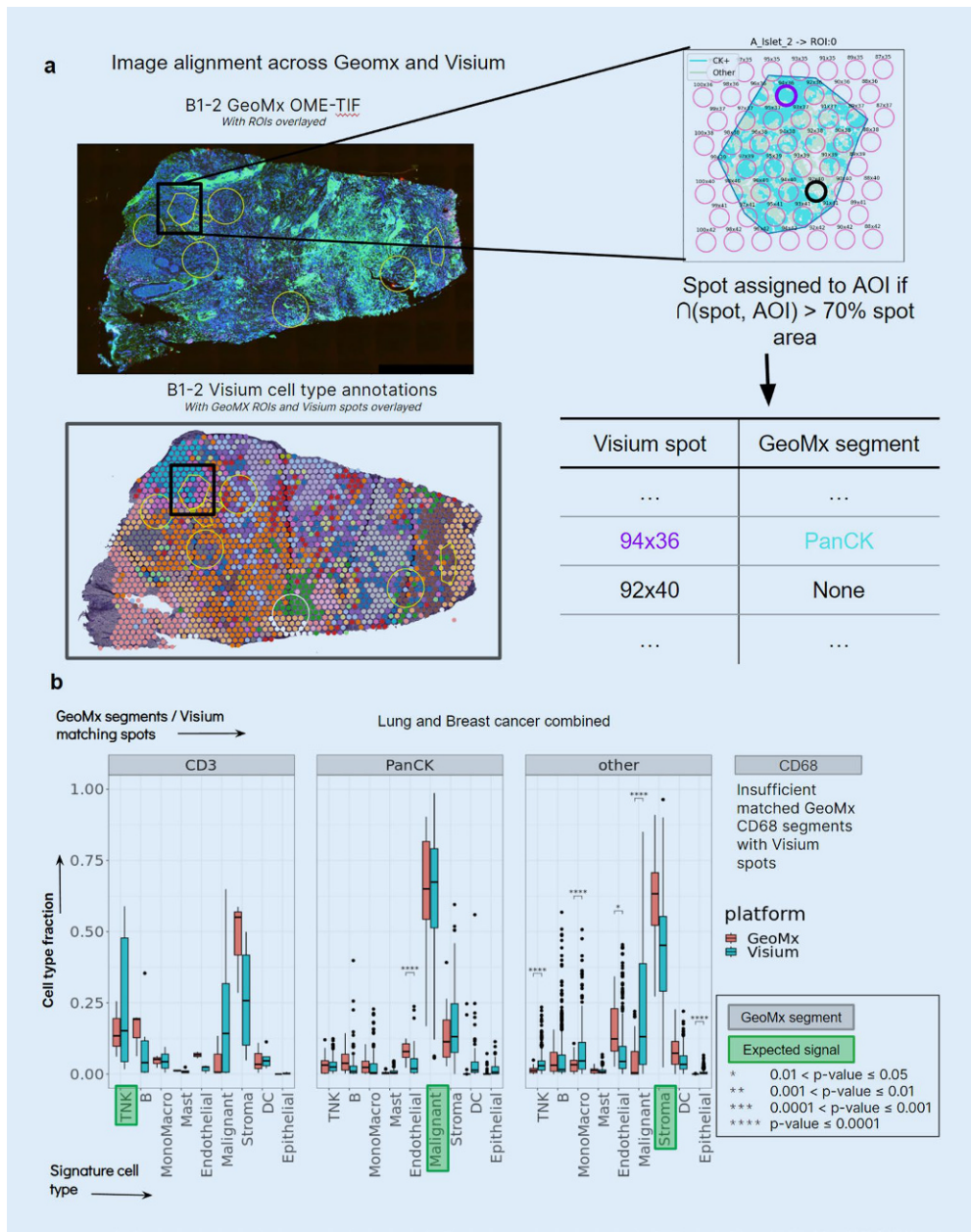
Fig. 3 | A 63 ◄ Direct matching of data unit on tissue show similarities in the cell type composition between GeoMx and Visium. Example of a breast carcinoma sample showing GeoMx ROIs (**a**, top left), overlayed to Visium spots colored by data-driven clustering (**a**, bottom left). Each Visium spot was assigned to a GeoMx AOI if > 70% of spot area was covered by the AOI (a, top and bottom right). Cell type deconvolution results for GeoMx AOIs and 70% matched Visium spots across breast and lung cancers (**b**)

A 64
Detection of large-duct pattern pancreatic ductal adenocarcinoma by artificial intelligence-driven digital image analysis

Mr. Joël Schlegel[1], Ms. Jessica L Rohrbach[2], Mr. Stefan Reinhard[2], Dr. Anna S Wenning[3], Dr. Martin Wartenberg[1]*

[1]Institute of Tissue Medicine and Pathology, University of Bern, Bern Switzerland; [2]Institute of Tissue Medicine and Pathology, University of Bern, Bern, Switzerland; [3]Department of Visceral Surgery, Inselspital University Hospital, University of Bern, Bern, Switzerland

Background: About 7% of pancreatic ductal adenocarcinomas (PDAC) exhibit the "large-duct pattern", a histological growth pattern characterized by cancer glands with diameters larger than 0.5 mm or a microcystic impression on macroscopy in more than 50% of the tumor respectively. Histologically this pattern can be mistaken as intraductal papillary mucinous neoplasia (IPMN) of the pancreas. We hypothesize that automated detection of large-duct pattern cases of PDAC is feasible by means of artificial intelligence (AI) and digital image analysis (DIA) of hematoxylin-eosin (HE) stained whole slide images (WSI), aiding correct tumor classification.

Methods: HALO AI was used to establish a deep learning neural network algorithm on HE stained WSI of ten curatively resected PDAC cases to detect cancer infiltrates. In detail, PDAC infiltrates/glands were annotated, supervised by a pancreato-biliary pathologist, and algorithm training sessions were performed using DenseNet V2. The established algorithm was validated and applied to an existing cohort of 117 PDAC cases. Final HALO markup data was exported to DIA software QuPath to quantify cancer gland diameters and identify large-duct pattern cases (HALO-QuPath-pipeline, see ◘ **Fig. 1**).

Results: By now, based on 599 PDAC cancer infiltrate annotations and 2021 non-cancerous tumor annotations (like pancreatitic areas, vessels and stroma), reliable segmentation of PDAC's epithelial tumor component was achieved (see ◘ **Fig. 2**). The HALO-QuPath-pipeline was able to quantify gland/infiltrate diameters and calcualte proportion of diameters >0.5 mm to total infiltrates on available slides. By now three cases with the large-duct pattern were identified (see ◘ **Fig. 3**).

Conclusions: Automated quantification of cancer infiltrates by AI-driven DIA supports correct classification of large-duct pattern PDAC cases. Correctly diagnosing IPMN and its mimickers/"pseudo-IPMN", such as large duct-pattern PDAC, can support pathologists' day-to-day practice and en-
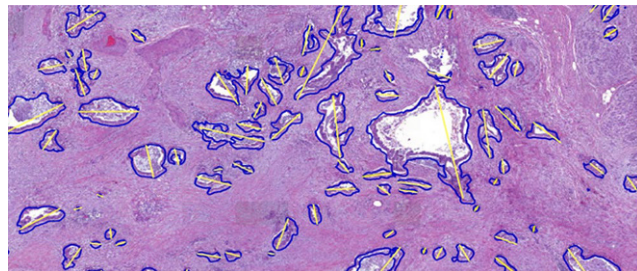
Fig. 2 | A 64 ▲ validation scheme for algorithm performance. Manually annotated tumor gland diameters in yellow & AI-detected tumor annotations in blue to determine sensitivity, speficifity, positive and negative predictive value

sure patient safety. Further, training AI-based recognition of IPMN cases and automated algorithm-driven separation from "pseudo-IPMN cases like large-duct pattern PDAC is warranted.

A 65
Diagnosis of secondary histiocytic sarcoma aided by methylation profiling

Dr. Pierre-Henri Gauthier[1], Dr. Noémie Lang[2], Prof. Jérôme Tamburini[3], Prof. Thomas McKee[4], Dr. Claudio De Vito[1], Dr. Kristof Egervari[5]*

[1]Department of Clinical Pathology, University Hospital Geneva, Geneva, Switzerland; [2]Department of Oncology, University Hospital Geneva, Switzerland; [3]Translational Research Centre in Onco-Hematology, Faculty of Medicine, University of Geneva, and Swiss Cancer Center Leman, Geneva, Switzerland; [4]HUG, Service de Pathologie Clinique, Geneva, Switzerland; [5]Service of Clinical Pathology, Department of Diagnostics, Geneva University Hospital, Geneva, Switzerland

Background: Histiocytic sarcoma (HS) is a rare malignant tumor of the histiocytic-dendritic cell differentiation according to the latest WHO classification. In rare cases, HS has been shown to have a clonal relationship with pre-existing low-grade B cell lymphomas. Here we present two histiocytic sarcomas, one diagnosed with the help of DNA-methylation profiling and describe an epigenetic fingerprint similar to high grade B cell lymphomas.
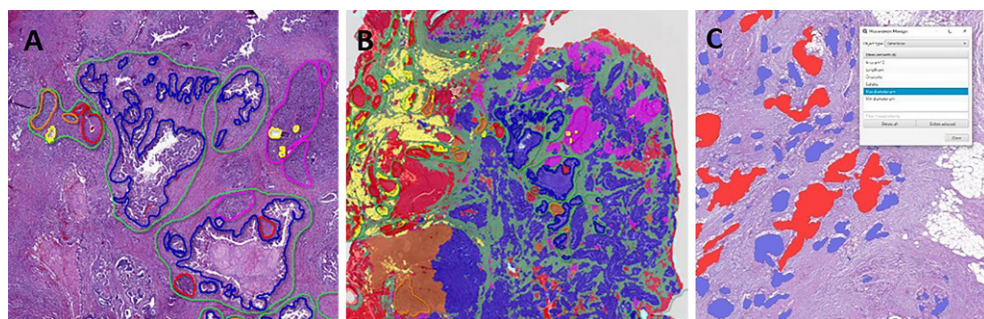
Fig. 1 | A 64 ◄ HALO-QuPath-pipeline. A) Annotation and training of algorithm in HALO AI. B) Application of trained algorithm to established PDAC cohort. C) Exportation of HALO markup data to QuPath and measurement of gland diameters
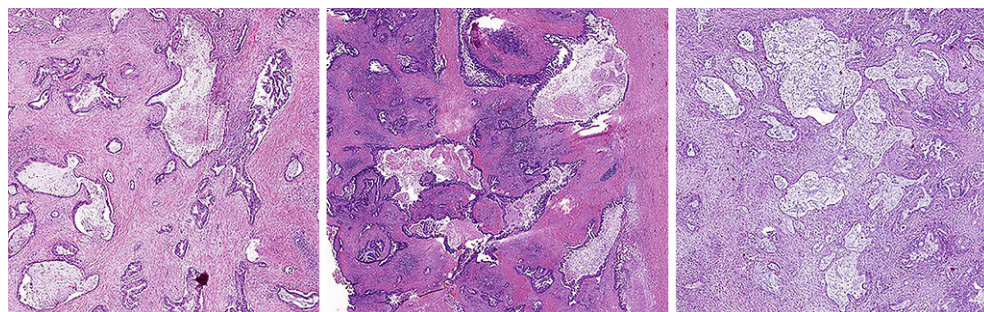
Fig. 3 | A 64 ◄ HALO-QuPath-pipeline-based detected large-duct pattern PDAC. HE stained tissue slides of identified large-duct pattern PDAC cases

Methods: We performed immunohistochemistry, next generation sequencing (Agilent SureSelect), IGH gene rearrangement analysis and DNA methylation profiling with CNV prediction (MethylationEPIC Array, Illumina) on biopsies from two patients. Methylation data was analyzed on the EpiDiP server of the University of Basel.

Results: Patient 1 had a history of chronic lymphocytic leukemia (CLL) was investigated for cervical mass and ulceration at the base of the tongue. Biopsies revealed a poorly differentiated tumor negative for pankeratin and B cell markers. DNA methylation analysis showed an epigenetic similarity with high-grade B cell lymphomas. Additional immunostains, including CD68 and CD163 were positive, supporting the diagnosis of HS.

Patient 2 treated for HIV developed a fulminant acute hepatic failure. Autopsy revealed a massive liver infiltration by a HS. Methylation analysis also showed an epigenetic similarity with high grade B cell lymphoma. Furthermore, in both lesions IGH gene rearrangement was identified supporting the clonal relationship between HS and the CLL in Patient 1 and a possible undiscovered B cell lymphoma in Patient 2. Molecular studies identified alterations of cell-cycle checkpoints (homozygous loss of *RB1* and *CDKN2A* respectively) and the MAPK-pathway (*KRAS* mutation).

Conclusions: Our cases highlight the interest of methylation profiling in classifying rare entities, reinforce the link between HS and B cell lymphomas, and show, for the first time, an epigenetic similarity of HS to high grade B cell lymphomas; to be confirmed by future studies.